Therapeutic Bubbles

Therapeutische bellen

Klazina Kooiman

Paranimfen:

Marjo Kooiman
en
Marcia Emmer

Colophon

Klazina Kooiman

Therapeutic bubbles

Thesis, Erasmus University Medical Center
January 19, 2011.

ISBN 978-94-6108-119-3

Cover design by Anne van der Feest.

Printed in the Netherlands by Gildeprint Drukkerijen.

For a printed version please contact:
Secretary Biomedical Engineering (January 2011: room Ee 2302)
Erasmus Medical Center
P.O. Box 2040
3000 CA Rotterdam
the Netherlands

Therapeutic Bubbles

Therapeutische bellen

Proefschrift

ter verkrijging van
de graad van doctor aan de
Erasmus Universiteit Rotterdam
op gezag van de
rector magnificus

Prof.dr. H.G. Schmidt,

en volgens besluit van het College voor Promoties.

De openbare verdediging zal plaatsvinden op
woensdag 19 januari 2011 om 15:30 uur door

Klazina Kooiman
geboren te Zwijndrecht

Doctoral Committee

Promotors:	Prof.dr.ir. N. de Jong
	Prof.dr.ir. A.F.W. van der Steen
Other members:	Prof.dr.ir. M. de Jong
	Dr. T.L.M. ten Hagen
	Prof.dr. J.R. Lindner

The work described in this thesis was performed at the Department of Biomedical Engineering of Erasmus University Medical Center, Rotterdam, the Netherlands. This work was financially supported by innovation subsidies collaborative projects by the Dutch ministry of economic affairs under nr IS042035 and by NMP-LA-2008-213706 Sonodrugs.

Voor mijn ouders

Financial support

Financial support for the publication of this thesis was kindly provided by:

- Bracco Suisse SA
- Erasmus MC
- Oldelft Ultrasound
- Traskbritt

Contents

1	Introduction	1
2	Vibrating microbubbles poking individual cells: drug transfer into cells via sonoporation	9
3	Ultrasound and microbubble-targeted delivery of macromolecules is regulated by induction of endocytosis and pore formation	23
4	Increasing the endothelial layer permeability through ultrasound-activated microbubbles	43
5	Mechanisms of increased endothelial layer permeability through ultrasound-activated microbubbles	53
6	Sonoporation of endothelial cells by vibrating targeted microbubbles	69
7	Oil-filled polymer microcapsules for ultrasound-mediated delivery of lipophilic drugs	87
8	Therapy with oil-filled polymer microcapsules	109
9	Lipid distribution and viscosity of coated microbubbles	123
10	General discussion and conclusion	137
Summary		155
Nederlandse samenvatting		161
Dankwoord		167
Curriculum vitae Nederlands		171
Curriculum vitae English		172
Publications and presentations		173
PhD portfolio		179
Abbreviations		183

General introduction and outline of thesis

Sound is all around us. We use it daily to communicate and enjoy life. The frequencies we can hear are between 20 and 20,000 Herz [1]. Animals such as cats, bats and dolphins can hear up to higher frequencies. The hearing range for cats is 100 to 60,000 Hz [2], for bats this is 10 to 210,000 Herz [3] and for dolphins this is 200 to 150,000 Herz [2]. Bats use sound for communication but also to localise where they are and to determine where their prey is. They do this by sending sound waves. In an open space the emitted sound will not be reflected but if there are objects or other animals nearby the emitted sound will be reflected and/or scattered and therefore sound will be returned to them. This returned sound is also referred to as an echo and it is this echo that allows them to determine if there are any objects, if they are near or far away, how large the object is, and what kind of object it is. Other animals that also use echolocation are dolphins, whales, seals, moths and even some species of birds [3, 4].

Techniques that use echolocation the way animals do, namely emitting sound and processing the returned echo, are SONAR (SOund NAvigation and Ranging) and echography. SONAR was developed in the early 20th century which allowed detection of submarines. Echography for medical purposes followed shortly after [5-8]. For medical purposes, sound frequencies of around 1,000,000 Herz (1 MHz) and higher are typically used. Because of these high frequencies, this sound is also referred to as ultrasound. Our bodies are comprised of different tissues which scatter and reflect ultrasound differently and it is this difference that gives intensity differences in an ultrasound image. Nowadays, ultrasound is a common diagnostic imaging modality. The advantages over other imaging modalities such as magnetic resonance imaging (MRI) and computed tomography (CT) include portability, cost, and speed of acquisition. In addition, ultrasound uses no harmful radiation [7, 9]. Diagnostic ultrasound imaging is used in for example obstetrics, cardiology and radiology. In obstetrics, it is common use to perform ultrasound imaging to determine the age of the foetus, to monitor foetal development and to detect possible diseases in the foetus. It also allows parents-to-be to take a peek at their unborn child [8]. In Fig. 1.1 an ultrasound image of a 14-week old foetus is shown. The spine and other bone structures of the foetus appear more bright in the ultrasound image as they reflect the ultrasound more than the other structures. The amniotic fluid hardly reflects ultrasound and therefore appears darker in the ultrasound image.

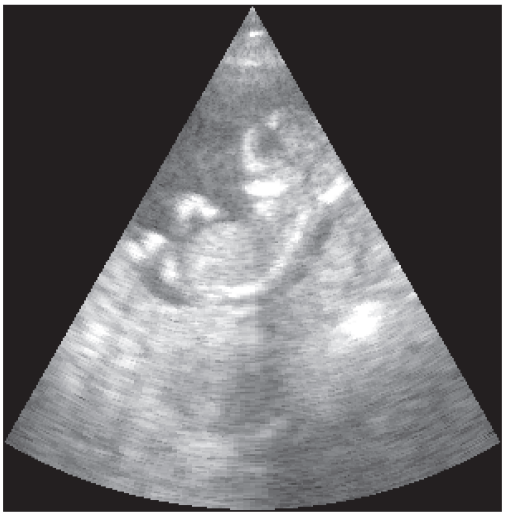

Fig. 1.1. Ultrasound image (2.5 MHz) of a 14-week old foetus.

In cardiology, ultrasound imaging has been used since the 1950s and has evolved from 2-dimensial to real-time 2-dimensional imaging and real time 3-

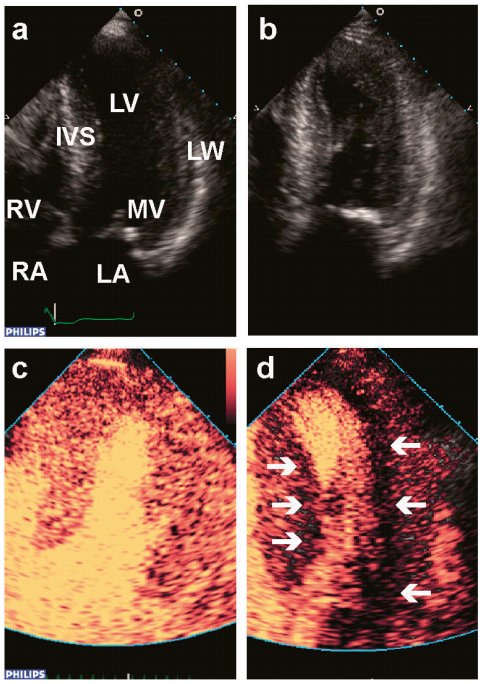

Fig. 1.2. Apical 4-chamber ultrasound image of the heart for two patients with hypertrophic cardiomyopathy. Image a + b): without ultrasound contrast agent. Image c + d): corresponding images to a + b with ultrasound contrast agent. White arrows indicate perfusion defect. IVS = inter-ventricular septum, LA = left atrium, LV = left ventricle, LW = lateral wall, MV = mitral valve, RA = right atrium, RV = right ventricle. Images courtesy of Dr. O.I.I. Soliman and Dr. F.J. ten Cate, Thoraxcenter, Erasmus MC, Rotterdam, the Netherlands.

dimensional imaging [6, 10]. A typical apical 4-chamber view of the heart is shown in Fig. 1.2.a and b. Although the mitral valve (MV) can be clearly detected in the images, the borders of the left ventricle (LV) are not well defined. Also, blood is hardly detected (i.e. appears as black in the images) since it is two to three orders of magnitude less echogenic than the surrounding tissue [11]. However, with the use of an ultrasound contrast agent, the LV borders become well defined as shown in Fig. 1.2.c and 1.2.d. Both ultrasound images are of patients with hypertrophic cardiomyopathy. A thick inter-ventricular septum (IVS) is typical for these patients and the thickness can be accurately determined in the contrast enhanced images. The difference between these patients is that either the contrast is observed throughout the IVS and lateral wall (LW) (Fig. 1.2.c) or is not observed in all parts of the IVS and LW (Fig. 1.2.d; white arrows).

Contrast agents for ultrasound consist of gas microbubbles (see Fig. 1.3) [12-14]. The high scattering of gas microbubbles was accidentally discovered in 1968 when agitated saline was injected during an examination. The gas introduced by agitation appeared as bright

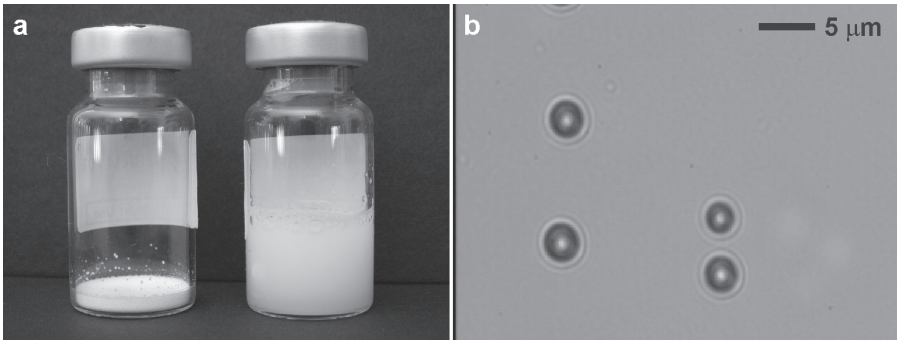

Fig. 1.3. a) Ultrasound contrast agent (UCA) before (left) and after (right) solving in 5 ml sodium chloride solution. After solving, the UCA can be administered. b) UCA consist of microbubbles.

scatterers on the ultrasound image [15]. Since these gas bubbles were short-lived after injection into the bloodstream (less than 0.3 seconds), techniques were developed to coat bubbles so they would have a longer half-life. In the 1990s, Albunex was the first commercially available agent and was produced by sonication of a human albumin solution. Although this agent was safe and effective in enhancing the blood pool, its half-life was still short, namely less than one minute [16-18]. Since then, more agents have been introduced. The current clinically approved ultrasound contrast agents are listed in Table 1.1. The majority of these contrast agents consist of lipid-coated bubbles that contain gasses such as octafluoropropane (Definity), perfluorobutane (Sonazoid), or sulphur hexafluoride (SonoVue). These gasses make the bubbles more stable than normal air since these gasses are hydrophobic and have a low solubility in blood. As a result, the half-life of the agents is increased [12]. Definity and SonoVue [19, 20] have a half-life of ~ 6 minutes while this is

Table 1.1. Overview of current clinically available UCA. USA = United States of America. Table adapted from M. Emmer et al, 20 years of ultrasound contrast agent modelling, submitted review.

Name	Manufacturer	Gas	Coating	Approved	Year
Levovist[1]	Bayer Schering Pharma AG	air	galactose, trace palmitin	worldwide except in USA	1996
Optison[2]	GE Healthcare AS	C_3F_8	human albumin	Europe, USA	1997
Definity	Lantheus Medical Imaging	C_3F_8	phospholipids	USA, Canada, Mexico, Israel, Europe, India, Australia, Korea, Singapore, United Arab Emirates, New Zealand	2001
SonoVue	Bracco	SF_6	phospholipids	Europe, China, South America	2001
Sonazoid	Amersham Health	C_4F_{10}	phospholipids	Japan	2006

[1] expected to discontinue in 2010; [2] temporarily not available from 2006-2010

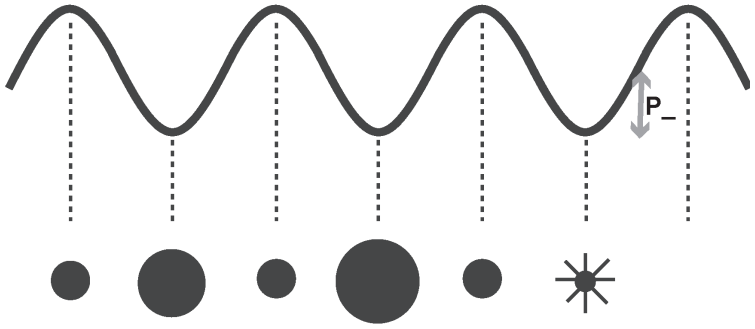

Fig. 1.4. Volume pulsations by microbubbles by ultrasound. When the acoustic pressure is high, the microbubbles compress and when the acoustic pressure is low, the microbubbles expand. If the acoustic pressure is high enough, the microbubble will be destroyed; P_ = peak negative acoustic pressure.

~ 30-40 minutes for Sonazoid [21]. After intravenous administration, microbubbles are carried by the bloodstream through the entire vascular tree. They are too large (1-10 μm) to diffuse through the endothelium and are therefore blood pool agents [14, 18]. If there is an area in the contrast enhanced ultrasound image where the contrast is not observed, as shown in Fig. 1.2.d in parts of the IVS and LW, this indicates a perfusion defect in those parts of the IVS and LW. These perfusion defects would not have been detected without the use of the contrast.

Microbubbles are very effective ultrasound scatterers due to their high compressibility. Upon insonification, they start to vibrate as the gas responds to the pressure change of the ultrasound by volume pulsations as shown in Fig. 1.4 [22, 23]. It is this what makes them unique amongst contrast agents for imaging because the imaging process changes the agent and can even destroy [14, 18, 23].

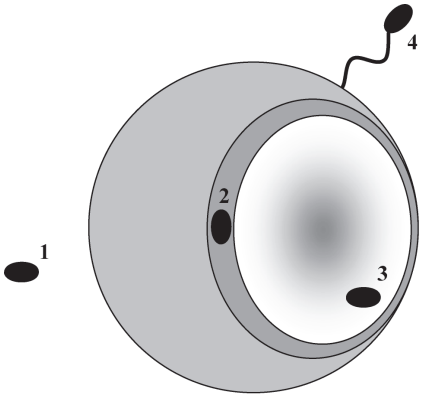

Fig. 1.5. Schematic overview of microbubble for drug delivery (not drawn to scale). A drug can be administered simultaneously with the microbubble (1), or incorporated in the coating (2), the core (3), or attached to the surface (4) of the microbubble.

In the 1990s, the use of ultrasound contrast agents for drug delivery was explored. Nowadays two microbubble-based drug delivery systems are distinguished. In the first system, the therapeutic agent is co-administered with the microbubbles so that the microbubbles circulate through the bloodstream alongside the therapeutic agent (see Fig. 1.5-1). In the second system, the therapeutic agent is attached to or incorporated into the microbubbles (see Fig. 1.5-2 to 4). Hydrophilic as well as lipophilic therapeutic agents can be incorporated. When ultrasound is applied, these microbubbles are triggered to release their payload. Unlike other imaging

modalities, ultrasound can be used to perform triggered, controlled, and local insonifications. Hence, it can be used to trigger drug release only at the region of interest. The benefits are a more controlled biodistribution of the therapeutic agent which will not only reduce side-effects, but also improve therapeutic efficacy. In addition, ultrasound imaging of these microbubble-based drug delivery systems will aid the guidance and monitoring of therapy. The minimally invasive nature of ultrasound may also permit multiple treatments [24-29].

This thesis entitled therapeutic bubbles explores the use of ultrasound contrast agents for local drug delivery. Even though the first therapeutic bubbles were already reported twenty years ago, there remains a lot of room for improvement in terms of amount of drug encapsulation and understanding the mechanisms of improved drug uptake with ultrasound and microbubbles.

For drug delivery via the co-administration route, lipid-coated microbubbles are typically used. Upon insonification, the microbubbles start to vibrate and enhance drug uptake by cells or tissues. This method is also referred to as sonoporation. Although the mechanism of sonoporation remains unclear, a transient increase in the porosity and permeability of the cell membrane is observed [27, 29-31]. The studies described in **Chapter 2 and 3** were set up to give more insight into the mechanism of sonoporation on a single cell level. In **Chapter 4** we explore the possibility of increasing the permeability of an endothelial cell layer, which continues in **Chapter 5** by exploring its mechanism.

Recently, microbubbles have been designed to which a ligand was linked to its coating. These microbubbles, also referred to as targeted or functionalised microbubbles, can be used for molecular imaging. Molecular imaging is defined by the visualization of biological processes at the cellular and molecular level in living systems, with the aim to image molecular changes associated with diseases. Since microbubbles are blood pool agents, targeted microbubbles can therefore be used to image intravascular molecular changes associated with inflammation, ischemia-reperfusion injury, angiogenesis, and thrombi [9, 11, 27, 29, 30, 32]. **Chapter 6** explores whether microbubbles for molecular imaging can also be used for drug delivery. Such a combination could be advantageous because then microbubbles could both detect and treat a disease at the same time.

In **Chapter 7** the development of a new ultrasound contrast agent for lipophilic drug delivery is described. This novel microbubble consists of a polymer shell, a gas core and an oil reservoir. In this oil reservoir, lipophilic drugs can be incorporated such as paclitaxel, which is an anti-tumour agent. Therapeutic efficacy of these polymer microbubbles is shown in **Chapter 8**.

In **Chapter 9** the focus is on the coating of a lipid microbubble. Characteristics such as lipid distribution and viscosity are investigated and related to microbubble behaviour for molecular imaging and drug delivery. Finally, in **Chapter 10**, the experimental results within this thesis as well as the current status of therapeutic bubbles are discussed. In addition, the future of drug delivery with bubbles and ultrasound is discussed.

References

[1] A.C. Guyton, J.E. Hall, Medical Physiology, Elsevier Saunders, London (2006).
[2] Discover Science Almanac, Hyperion, New York (2003).
[3] W. Bogdanowicz, M.B. Fenton, K. Daleszczyk, The relationships between echolocation calls, morphology and diet in insectivorous bats. J. Zool. 247 (1999) 381-393.
[4] W. Metzner, Echolocation Behavior in Bats. Sci. Prog. 75(298) (1991) 453-465.
[5] Handboek Echografie, LOI.
[6] I. Edler, K. Lindstrom, The history of echocardiography. Ultrasound Med. Biol. 30(12) (2004) 1565-1644.
[7] T. Wagai, Studies on the foundation and development of diagnostic ultrasound. P. JPN. Acac. B-Phys. 83(8) (2007) 256-265.
[8] M.B. McNay, J.E. Fleming, Forty years of obstetric ultrasound 1957-1997: from A-scope to three dimensions. Ultrasound Med. Biol. 25(1) (1999) 3-56.
[9] J.R. Lindner, Molecular imaging of cardiovascular disease with contrast-enhanced ultrasonography. Nat. Rev. Cardiol. 6(7) (2009) 475-481.
[10] A.E. Weyman, Future directions in echocardiography. Rev. Cardiovasc. Med. 10(1) (2009) 4-13.
[11] P.A. Dayton, K.W. Ferrara, Targeted imaging using ultrasound. J. Magn. Reson. Imaging 16(4) (2002) 362-377.
[12] S. Kaul, Myocardial contrast echocardiography: a 25-year retrospective. Circulation 118(3) (2008) 291-308.
[13] A.L. Klibanov, Ultrasound Contrast Agents: Development of the Field and Current Status. Top. Curr. Chem. 222 (2002) 73-105.
[14] C. Greis, Ultrasound contrast agents as markers of vascularity and microcirculation. Clin. Hemorheol. Microcirc. 43(1) (2009) 1-9.
[15] R. Gramiak, P.M. Shah, Echocardiography of the aortic root. Invest. Radiol. 3(5) (1968) 356-366.
[16] S.B. Feinstein, J. Cheirif, F.J. Ten Cate, P.R. Silverman, P.A. Heidenreich, C. Dick, R.M. Desir, W.F. Armstrong, M.A. Quinones, P.M. Shah, Safety and efficacy of a new transpulmonary ultrasound contrast agent: initial multicenter clinical results. J. Am. Coll. Cardiol. 16(2) (1990) 316-324.
[17] S. Mayer, P.A. Grayburn, Myocardial contrast agents: Recent advances and future directions. Prog. Cardiovasc. Dis. 44(1) (2001) 33-44.
[18] J.M. Correas, O. Helenon, L. Pourcelot, J.F. Moreau, Ultrasound contrast agents. Examples of blood pool agents. Acta Radiol. Suppl. 412 (1997) 101-112.
[19] M. Schneider, Characteristics of SonoVue™. Echocardiogr.-J. Card. 16(7) (1999) 743-746.
[20] D.W. Kitzman, M.E. Goldman, L.D. Gillam, J.L. Cohen, G.P. Aurigemma, J.S. Gottdiener, Efficacy and safety of the novel ultrasound contrast agent Perflutren (Definity) in patients with suboptimal baseline left ventricular echocardiographic images. Am. J. Cardiol. 86(6) (2000) 669-674.
[21] K.E. Landmark, P.W. Johansen, J.A. Johnson, B. Johansen, S. Uran, T. Skotland, Pharmacokinetics of perfluorobutane following intravenous bolus injection and continuous infusion of sonazoid in healthy volunteers and in patients with reduced pulmonary diffusing capacity. Ultrasound Med. Biol. 34(3) (2008) 494-501.
[22] N. de Jong, M. Emmer, A. van Wamel, M. Versluis, Ultrasonic characterization of ultrasound contrast agents. Med. Biol. Eng. Comput. 47(8) (2009) 861-873.
[23] D. Cosgrove, C. Harvey, Clinical uses of microbubbles in diagnosis and treatment. Med. Biol. Eng. Comput. 47(8) (2009) 813-826.
[24] W.G. Pitt, G.A. Husseini, B.J. Staples, Ultrasonic drug delivery - A general review. Expert Opin. Drug Deliv. 1(1) (2004) 37-56.
[25] J.C. Chappell, R.J. Price, Targeted therapeutic applications of acoustically active microspheres in the microcirculation. Microcirculation 13(1) (2006) 57-70.

[26] A.L. Klibanov, Microbubble contrast agents: targeted ultrasound imaging and ultrasound-assisted drug-delivery applications. Invest. Radiol. 41(3) (2006) 354-362.
[27] S. Hernot, A.L. Klibanov, Microbubbles in ultrasound-triggered drug and gene delivery. Adv. Drug Deliver. Rev. 60(10) (2008) 1153-1166.
[28] K.W. Ferrara, M.A. Borden, H. Zhang, Lipid-Shelled Vehicles: Engineering for Ultrasound Molecular Imaging and Drug Delivery. Accounts Chem. Res. 42(7) (2009) 881-892.
[29] M.R. Böhmer, A.L. Klibanov, K. Tiemann, C.S. Hall, H. Gruell, O.C. Steinbach, Ultrasound triggered image-guided drug delivery. Eur. J. Radiol. 70(2) (2009) 242-253.
[30] M. Schneider, Molecular imaging and ultrasound-assisted drug delivery. J. Endourol. 22(4) (2008) 795-802.
[31] E.C. Pua, P. Zhong, Ultrasound-mediated drug delivery. IEEE Eng. Med. Biol. 28(1) (2009) 64-75.
[32] A.L. Klibanov, Preparation of targeted microbubbles: ultrasound contrast agents for molecular imaging. Med. Biol. Eng. Comput. 47(8) (2009) 875-882.

Vibrating microbubbles poking individual cells: drug transfer into cells via sonoporation

Annemieke van Wamel[1,2], Klazina Kooiman[1], Miranda Harteveld[1], Marcia Emmer[1], Folkert J. ten Cate[3], Michel Versluis[4], Nico de Jong[1,2,4]

[1] Dept. of Biomedical Engineering, Thoraxcenter, Erasmus MC, Rotterdam, the Netherlands
[2] Interuniversity Cardiology Institute of the Netherlands, Utrecht, the Netherlands
[3] Dept. of Cardiology, Thoraxcenter, Erasmus MC, Rotterdam, the Netherlands
[4] Dept. of Applied Physics, Physics of Fluids, University of Twente, Enschede, the Netherlands

Journal of Controlled Release 2006; 112: 149-155

Abstract

Ultrasound contrast microbubbles have the ability to enhance endothelial cell permeability and thus may be used as a new way to deliver drugs. It facilitates the transfer of extracellular molecules into cells activated through ultrasound driven microbubbles. The present study is designed to correlate the relationship between microbubble induced cell deformation and enhanced cell membrane permeability. Propidium Iodide (PI) was used as a membrane integrity probe. Using high-speed imaging of vibrating microbubbles against endothelial cells and imaging of transport of PI into these cells showed a direct correlation between cell deformation and the resulting cell membrane permeability. Membrane permeabilisation lasted for a short period without affecting endothelial cells viability. We identified that microbubbles are crucial for enhancing transient cell membrane permeability. Thus, permeability of individual cells was increased. The roles of ultrasound contrast microbubbles as the trigger for improved drug efficacy are discussed.

2.1. Introduction

Using ultrasound and contrast microbubbles (i.e. ultrasound contrast agents) it is possible to achieve real-time bedside evaluation of myocardial perfusion in coronary artery disease. Furthermore, assessment of myocardial viability, determination of infarction size, and evaluation of reflow and no- or low-reflow after acute myocardial infarction can be studied as well [1, 2]. Another new application of ultrasound contrast agents is controlled local drug delivery [3, 4]. If tissues or cells are subjected to short ultrasound pulses, enhanced local permeability is induced. This effect is enhanced further when contrast microbubbles are present [5].

Based on this local (i.e. increased drug susceptibility) phenomenon, a wide range of practical therapeutic applications of ultrasound in combination with microbubbles are anticipated [3, 4, 6-9]. Takeuchi and colleagues showed that after vascular interventions, simultaneous treatment with ultrasound microbubbles and low doses of C-type natriuretic peptide (CNP) significantly reduced intima media ratio and progression of advanced neointimal development compared to CNP treatment alone [10]. It is intriguing to speculate about the applications in which ultrasound contrast microbubbles can be used for local drug uptake in humans. However, the relation between the physical principles of ultrasound and the cell interactions are unknown and should be studied.

Short ultrasound pulses ($\leq$ 10 ms) are required to avoid negative biological action of ultrasound in relation to the cell cycle [11, 12]. In combination with microbubbles, ultra-short ultrasound pulses ($\leq$ 10 μs) are required to avoid the irreversible membrane poration. In these cases, where the applied stress is below the threshold for irreversible damage, cells will remain viable [13, 14]. The degree of membrane permeabilisation, molecular uptake and cell survival upon membrane poration critically depends on the frequency and duration of the applied ultrasound [15, 16]. Although much progress has been made to elucidate the ultrasound parameter effects, the fundamental physical processes behind the microbubble-

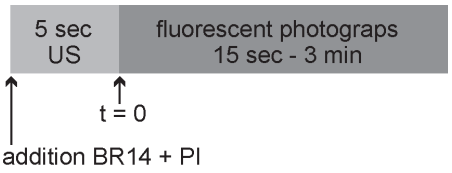

Fig. 2.1. Timetable of sequence of events of sonoporation experiment. US = ultrasound.

induced membrane alterations are not well understood. In today's research, the used conditions of ultrasound microbubble enhanced drug uptake are trial and error based and therefore probably far from optimal.

Although several possible mechanisms may be responsible for the enhanced uptake of extracellular molecules, in this paper we highlighted one mechanism that is most likely to be responsible for instantaneous permeabilisation. This process, which is called sonoporation, is defined as the transfer of extracellular molecules by vibrating or jetting microbubbles [17]. In earlier optical studies we have shown that in the presence of a vibrating microbubble, deformation forces are imposed on a neighbouring cell [18]. Because *in vivo* endothelial cells come into contact with ultrasound contrast microbubbles, we used these cells to investigate the permeability capabilities of vibrating microbubbles *in vitro*. Also, vascular endothelial cells are important in various cardiovascular pathologies and therefore the main target tissue/cells of ultrasound microbubble mediated enhanced drug efficacy.

In the present study, evidence is presented that cells, which experience deformation caused by vibrating microbubbles, become locally permeable to small cell-impermeable extracellular molecules. In addition, we show that permeability lasts only for the short period of the bubble vibration. First, ultrasound driven microbubble induced cell deformation was recorded using high-speed imaging. Secondly, propidium iodide (PI) influx and efflux in the deformed cells was monitored using fluorescent microscopy and conventional photography. Although PI has a relatively small radius (~ 0.5 nm [19]), it does not normally cross the cell membrane. Instead, it permeates when the cell membrane integrity is compromised and labels the genomic material. Binding of PI to double-stranded nucleic acids gives rise to red fluorescence on excitation and is widely used as an indicator for increased permeability of the cell membrane and to show irreversible permeability or cell death [20, 21]. Using this marker molecule, and high speed and conventional imaging modalities, a direct correlation was made between the endothelial cell deformation caused by vibrating microbubbles and the resulting cell membrane permeability.

2.2. Materials and Methods

2.2.1. Cell culture

Bovine endothelial cell cultures (ATCC) were grown in Opticell™ units (Biocrystal, Westerville, OH, USA) and maintained in 10 ml Dulbecco modified Eagle medium supplemented with 10%

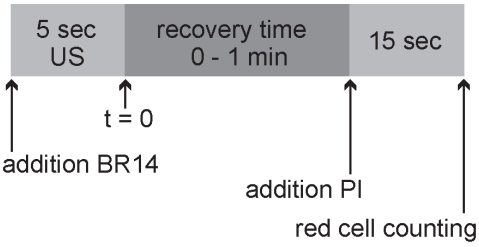

Fig. 2.2. Timetable of sequence of events of recovery time depended PI uptake. US = ultrasound.

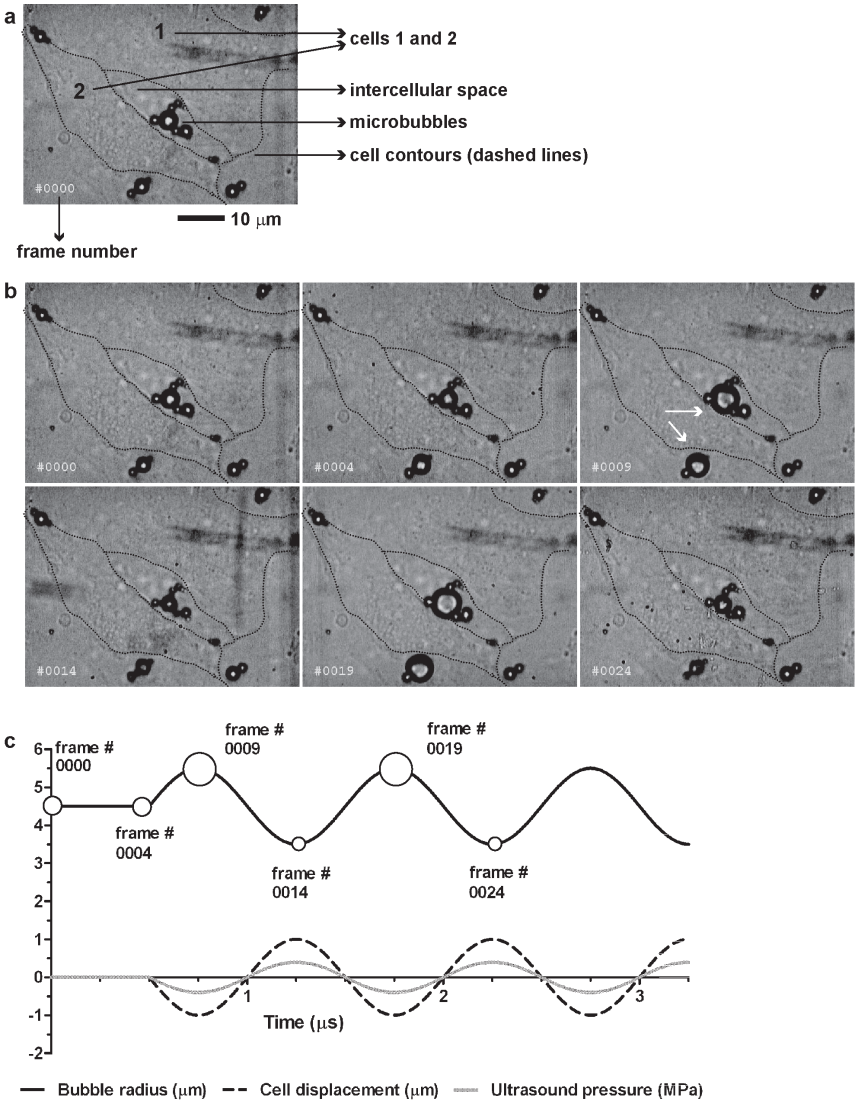

Fig. 2.3. Brandaris-128 high-speed camera recording of insonified microbubbles. a) First out of a total of 128 frames illustrating cell contours, microbubbles and intercellular space. b) Six selected frames out of a total of 128 frames. The vibrating microbubbles deform cell 2, but not cell 1 (arrows in frame # 0009). c) Relation between ultrasound pressure wave, microbubble radius (expansion/compression), and cell no. 2 displacement. Frame numbers correspond to the frame numbers in b.

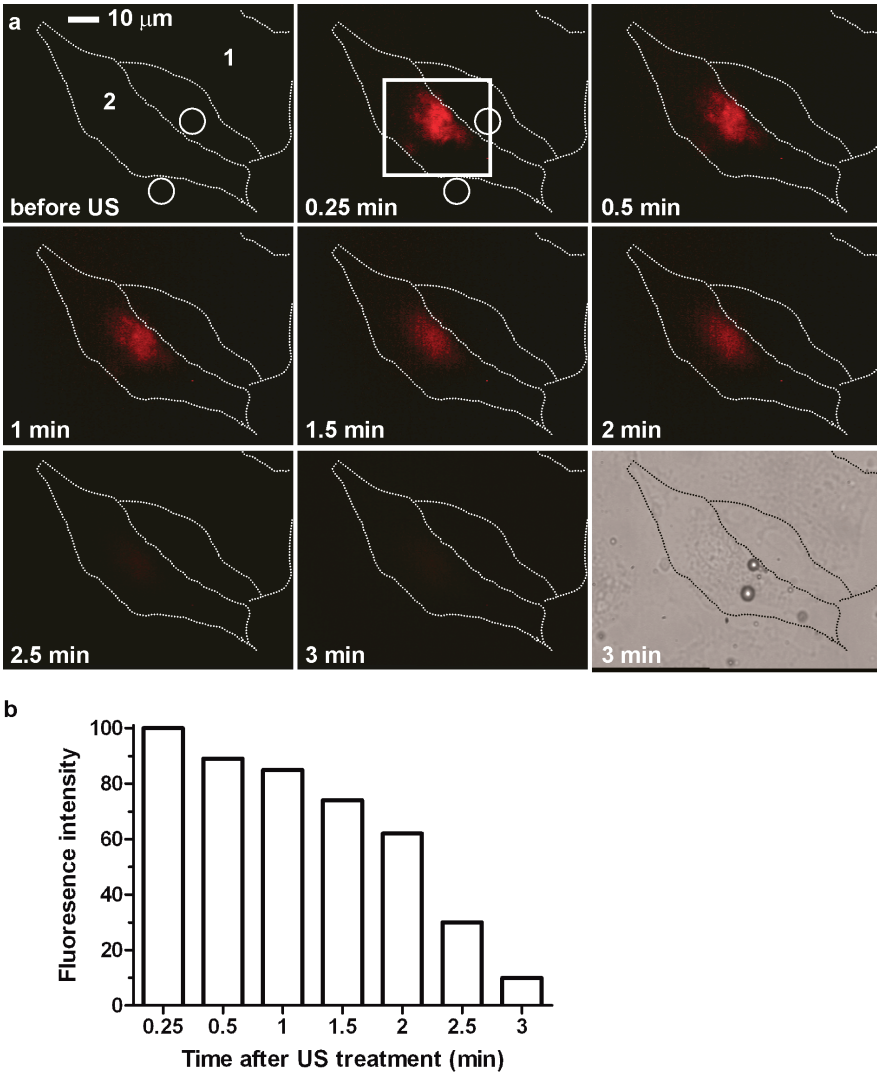

Fig. 2.4. PI uptake. a) Fluorescence and bright field images of PI uptake of two cells before and after insonification; same cells-bubbles as in Fig. 2.3. Circles in fluorescence images indicate position of microbubbles; US = ultrasound. Square in middle top image: region of interest. b) Relative fluorescence intensity after insonification in region of interest of deformed cell 2 as percentage of the first fluorescent image at t = 0.25 min after insonification.

fetal calf serum (Gibco BRL, Invitrogen, Groningen, the Netherlands), penicillin (100 U/ml), and streptomycin (100 µg/ml) in a humidified incubator at 37°C and 5% CO2. At the time of the experiments the cells were sub-confluent.

2.2.2. Ultrasound contrast agent

BR14 (Bracco Suisse SA, Geneva, Switzerland) belongs to the class of second-generation contrast agents. It is composed of perfluorobutane gas microbubbles coated by a phospholipid monolayer shell. The size distribution of microbubbles ranges from below 1 µm to 12 µm (mean diameter of 2.0 - 2.5 µm), with a total number of 5×10^8 microbubbles/ml [22].

2.2.3. Sonoporation of propidium iodide (PI)

Transfer media containing culture media supplemented with $1\text{-}2\times10^5$ microbubbles/ml and 25 µg/ml PI (P-4170; Sigma-Aldrich, Zwijndrecht, the Netherlands) was added to the cell culture just before insonification. The experimental protocol for sonoporation of PI into the endothelial cells included the following steps: (1) adherent cells at a final cell density of $1\text{-}2\times10^5$ cell/cm^2 in transfer media; (2) application of ultrasound field as described below; (3) post-insonification incubation of cells in the transfer medium. After ultrasound application, PI staining of cells was photographed approximately every 15 – 30 seconds for 3 minutes. A timetable of the experiment is depicted in Fig. 2.1. The fluorescence-intensity images were analysed using semi-automated imaging processing tools.

2.2.4. Recovery time dependent PI uptake

The experimental protocol for recovery time dependent uptake of PI into cells included the following steps: (1) adherent cells at a final cell density of $1\text{-}2\times10^5$ cell/cm^2 in culture media; (2) addition of $1\text{-}2\times10^5$ microbubbles/ml; (3) application of ultrasound field as described below; (4) post-insonification incubation of cells in culture medium. PI (25 µg/ml) was added 0, 0.15, 0.5, or 1 minute after insonification; (5) 15 seconds after addition of PI the number of red stained cells were counted (500 cells per time point). A timetable of the experiment is depicted in Fig. 2.2.

2.2.5. Ultrasound exposure protocol

The experimental acoustic set-up consisted of a 1 MHz unfocused single-element transducer (Panametrics, Waltham, MA, USA) mounted in a water tank [18]. The cell culture monolayer was positioned in front of the ultrasound beam at a standoff distance of 6 cm. The peak negative acoustic pressure generated at the region of interest, as measured separately with a calibrated hydrophone (PVDFZ44-0400, Specialty Engineering Associates, Soquel, CA, USA), was 0.4 MPa. This acoustic pressure corresponded to a mechanical index (MI) of 0.4. The microbubbles and cells were exposed to an ultrasonic burst consisting of 10 cycles with a repetition rate of 50 Hz, generated by an arbitrary waveform generator (LeCroy LW 420, Chestnut Ridge, NY, USA) and amplified by a 60-dB linear power amplifier (A-500, ENI, Rochester, NY, USA). The total duration of the ultrasound insonification was 5 seconds.

Using these ultrasound settings, earlier experiments showed that endothelial cells were not destroyed and extracellular uptake occurred [18, 23].

2.2.6. Optical observations

Bovine endothelial cells were grown on the inside of an Opticell™ container and the cell diameter ranged from 10 to 50 μm. A 1:1000 diluted suspension of BR14 microbubbles was added. Optical observations of microbubbles and endothelial cells were done using a fluorescence microscope (Olympus, Zoeterwoude, the Netherlands) mounted in front of the high-speed camera Brandaris-128. After a 120× magnification (60× water-immersed objective (LUMPlanFI, Olympus) and 2× magnifier) of the microbubbles and cells, the image was projected upon the CCD cameras of the Brandaris-128. The Brandaris-128 was built and is located at the Department of Biomedical Engineering of the Erasmus MC in Rotterdam (the Netherlands). Chin et al described the characteristics of this camera to great extend [24]. The Brandaris-128 is capable of recording six sequences of 128 images with a frame rate up to 25 million frames per second. For the experiments described here a frame rate of approximately 10 million frames per second was used. The field of view of the recorded image has a total size of 85 by 62 μm typically covering two to four endothelial cells. Also a high sensitivity CCD camera (LCL-90 2K, Watec America Corp., USA) was mounted on top of the fluorescence microscope. Ultrasound was applied as described above and the interactions between BR14 microbubbles and endothelial cells were recorded. After the Brandaris-128 high-speed camera recordings, the microscope was switched to the fluorescent settings and the red fluorescence images of the PI bound to RNA or DNA in the cells was obtained using the Watec camera. Recordings were taken with a shutter time of 1/100,000 s.

2.2.7. Statistics

Comparisons among fluorescence intensities were performed using a one-way ANOVA followed by Dunnett's multiple comparison test (GraphPad InStat verion 4.0, GraphPad Software, San Diego, CA, USA). Differences were considered significant if $p < 0.05$.

2.3. Results

Vibrating microbubble induced cell deformation was observed in six independent experiments. In these experiments, a total of 18 cells were observed. Of these 18 cells, 12 cells experienced deformation and six cells experienced no deformation. The interaction between oscillating microbubbles and endothelial cells resulted in individual cell deformation. An example is shown in Fig. 2.3.b. In frame 0000 no ultrasound was present. Ultrasound arrived in frame 0004 and reached its peak negative pressure in frame 0009 and peak positive pressure in frame 0014. The burst of ultrasound waves caused the microbubbles to repeatedly oscillate. During insonification, the cell membrane of cell 2 deformed in a smooth curved-shaped manner. Cell 1 did not deform. The cell membrane deformation of cell 2 changed with the oscillating radius fluctuations of the microbubble. Fig. 2.3.c shows the relation between the ultrasound pressure wave, microbubble radius (expansion/compression), and cell

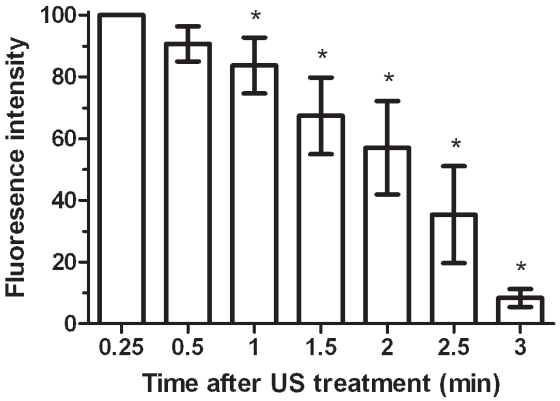

Fig. 2.5. Relative fluorescence intensity up to 3 min after insonification in ten deformed cells; normalised to first fluorescent image taken 0.25 min after insonification; * $p < 0.05$. Columns, means; bars, ± SEM.

displacement. At the highest peak positive pressure, the microbubbles maximally compressed and the cell was maximally outwards deformed. At the lowest peak negative pressure, the microbubbles maximally expanded and the cell was maximally inwards deformed.

After the Brandaris-128 high-speed camera recording, fluorescence images were obtained (see Fig. 2.4). The deformed cell (cell 2) showed PI uptake after insonification, whereas the un-deformed cell (cell 1) showed no PI uptake. The fluorescent signal in the deformed cell decreased over time and was hardly present 3 minutes after insonification (see Fig. 2.4.a). Fig. 2.4.b shows the fluorescent signal in the region of interest of the deformed cell 2 plotted as as relative arbitrary units of the initial intensity (t = 0.25 min).

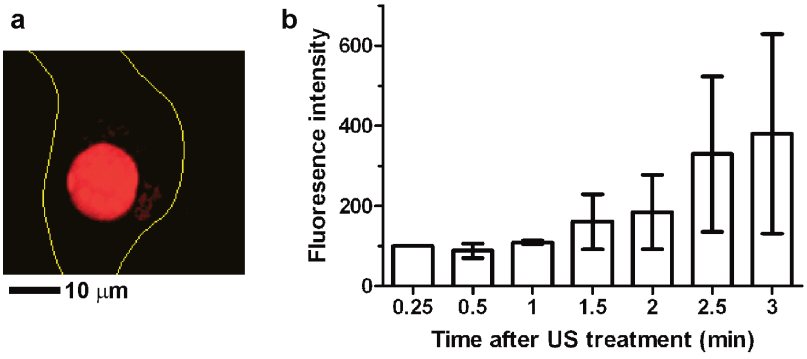

Fig. 2.6. Increase of fluorescence intensity in two deformed cells. a) Fluorescent image of cell 3 min after insonification; nucleus is coloured red from PI uptake. Yellow lines represent contours of cell. b) Relative fluorescence intensity up to 3 min after insonification; normalised to first fluorescent image taken 0.25 min after insonification. Columns, means; bars, ± SEM.

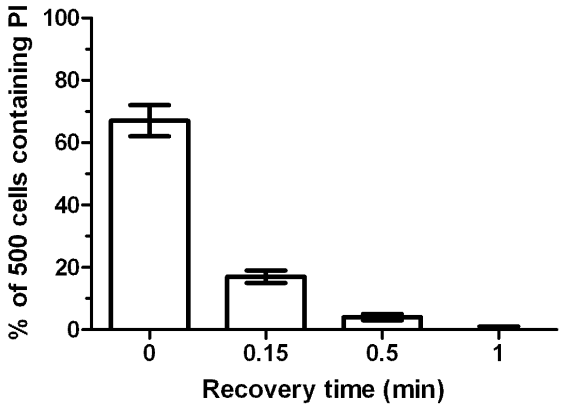

Fig. 2.7. Recovery time depended PI uptake. Columns, means; bars, ± SEM.

The 12 cells that experienced deformation all subsequently showed PI uptake. The six cells that experienced no deformation all showed no PI uptake. In ten out of the 12 cells that showed PI uptake, the PI signal decreased over time and was almost absent 3 minutes after insonification. Fig. 2.5 shows the mean fluorescent signal of these ten cells. The two other deformed cells showed a continuous increase in PI signal, which was mainly localised at the cell nucleus (Fig. 2.6).

Fig. 2.7 shows the recovery time dependent uptake of PI. The mean of four independent experiments for each recovery time is shown. Of the cells to which PI was added directly after insonification, 67% contained PI. When PI was added after a recovery time of 10 seconds, only 17% of the cells contained PI. After a recovery time of 0.5 minute, the percentage of PI containing cells was 4% while this was 0% for a recovery time of 1 minute.

2.4. Discussion

This study was designed to get insight into ultrasound contrast microbubble induced susceptibility for extracellular molecules. Here we show that an ultrasound agent alters the permeability of the membrane of cells *in vitro*. Although the relative expansion of the microbubbles is relatively large, it does not lead to cell lysis. Optical observations 3 minutes after the recordings revealed that no fluorescence signal was observed, suggesting that no cell lysis occurred. The impact on cells of contrast microbubbles in an ultrasound field is a mechanical load and can be used to trigger extracellular uptake. The cells underwent passive oscillations, generated by the oscillating microbubbles. Molecules present in the extracellular matrix could diffuse into the cytoplasm due to a favourable concentration gradient before the membrane resealed.

In our set-up we could distinguish between individual cells that experienced local forces by the vibrating microbubbles and cells that did not. All the observed cells and microbubbles

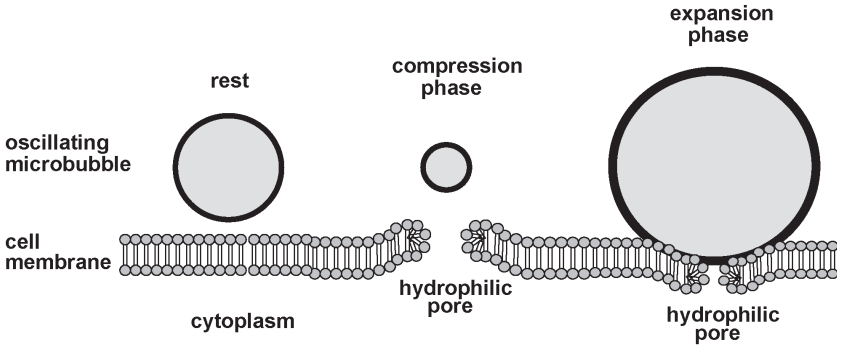

Fig. 2.8. Proposed model of vibrating microbubbles poking cells. The pushing and pulling behaviour of the vibrating microbubble causes rupture of the cell membrane creating a hydrophilic pore that allows trans-membrane flux of extracellular fluid and molecules.

were within the ultrasound field. Thus, every microbubble oscillated but not every cell was close enough to the microbubbles to experience deformation. Only the cells deformed by oscillating microbubbles showed PI internalisation and every deformed cell showed an increase in cell membrane permeability. No correlation between the amount of PI uptake and the magnitude of the microbubble oscillation (i.e. cell deformation) was observed. Most of the permeabilised cells were stained with PI for only a few minutes, indicating that reversible cell membrane permeability is possible. If the permeabilisation was irreversible, an increase in PI signal due to increasing PI diffusion into the cells would have been found. When PI diffuses into a cell, it can bind to RNA in the cytoplasm or diffuse into the nucleus and bind to DNA [21]. Our results indicate that the reversible permeabilised cells breakdown the RNA-PI complexes and transport PI out of the cell. This supports the hypothesis that the time-dependent elimination of PI signal is a result of efflux or metabolism of PI by viable cells [20, 25]. The few cells that showed a continuing increase in PI signal localised at the cell nucleus were permeabilised but unable to transport the PI out of the cell. This does not necessarily mean that the permeabilisation was irreversible. It could also indicate that the permeabilisation site was located close to the nucleus. When the PI diffusion distance to the nucleus is very small, PI can reach the DNA before it is transported out of the cell. However, in the method described here we could not completely discriminate between reversibly and irreversibly permeabilised cells.

Our findings are consistent with the idea that poration of the cell membrane occurs [26]. Poration is a transition of hydrophobic to hydrophilic pores. This transition creates cylindrical pores when a rotation of the polar heads brings a hydrophilic surface to the pore (Fig 2.8). Application of ultrasound in combination with the presence of microbubbles close to cells generates a critical trans-membrane ‘shear’ force, which leads to formation of pores once the membrane breakdown force is exceeded. The rapidly oscillating microbubbles generate a fluid flow over the cell surface. This flow is termed microstreaming and is probably

responsible for the disruption of cell membrane by tearing open the lipid bilayer membrane [27]. Because a cell can withstand compression better than elongation, the elongation phase may act as the main component that determines pore formation. Scanning electron microscopy studies have already shown that membrane poration occurs after ultrasound and microbubbles treatment [28, 29]. Our study suggests that these pores can only exist as long as the vibrating microbubbles and ultrasound field are present, because the percentage of permeabilised cells rapidly decayed once the ultrasound field was switched off. Although Mehier-Humbert et al used larger marker molecules and different cells in their study, they also showed that almost all the routes of entry had closed after termination of ultrasound. Their study showed that this had already occurred 5 seconds after insonification [29]. Both their study and our current study support the general idea that the pores quickly reseal upon termination of the ultrasound.

The action of microbubbles on cells is mechanical and can be as important as chemical stimuli in determining vascular fate or pathological state. Physical stimuli can act in concert with or sometimes override the signals given by proteins and other signal molecules to change cell morphology, growth rate and gene expression [30]. The most important biomedical application of the sonoporation technique is that it allows the introduction of membrane-impermeable xenomolecules such as dyes [29], hormones [31], proteins [32], plasmids [33], etc. into living cells.

In this study ultrasound settings were used that can be reached using current clinical ultrasound equipment. However, to what extent vibrating microbubbles can induce cell deformation within a clinical setting is not known. Sonoporation is a technique that is currently under development and a deeper understanding of the ultrasound contrast agent induced permeabilisation is essential before it can be used as a more controllable, reproducible, and efficient technique compared to alternative chemical or viral methods [34]. Further optimisations of the ultrasound settings and microbubbles are necessary to achieve clinically relevant therapeutic efficacy.

In conclusion, microbubbles in an ultrasound field temporarily inhibit one of the basic membrane functions, namely the selective permeable barrier. Although the optimal clinical settings are not yet known, we believe that by treating tissue with ultrasound contrast microbubbles whilst a drug is administered will improve internalisation and efficiency of that drug. Future research should provide the molecular details of ultrasound contrast agent mediated transmembrane transport of extracellular molecules.

Acknowledgements

This work has been supported by the Technology Foundation STW (RKG.5104). The authors thank Leo Bekkering and Cees Pakvis from the Dept. of Biomedical Engineering, Erasmus MC, for their technical assistance.

References

[1] J.R. Lindner, Microbubbles in medical imaging: current applications and future directions. Nat. Rev. Drug Discov. 3(6) (2004) 527-532.

[2] G.T. Sieswerda, L. Yang, M.B. Boo, O. Kamp, Real-time perfusion imaging: a new echocardiographic technique for simultaneous evaluation of myocardial perfusion and contraction. Echocardiography 20(6) (2003) 545-555.

[3] E.C. Unger, T. Porter, W. Culp, R. Labell, T. Matsunaga, R. Zutshi, Therapeutic applications of lipid-coated microbubbles. Adv. Drug Deliv. Rev. 56(9) (2004) 1291-1314.

[4] P.A. Dijkmans, L.J. Juffermans, R.J. Musters, A. van Wamel, F.J. ten Cate, W. van Gilst, C.A. Visser, N. de Jong, O. Kamp, Microbubbles and ultrasound: from diagnosis to therapy. Eur. J. Echocardiogr. 5(4) (2004) 245-256.

[5] M. Ward, J. Wu, J.F. Chiu, Ultrasound-induced cell lysis and sonoporation enhanced by contrast agents. J. Acoust. Soc. Am. 105(5) (1999) 2951-2957.

[6] R.V. Shohet, S. Chen, Y.T. Zhou, Z. Wang, R.S. Meidell, R.H. Unger, P.A. Grayburn, Echocardiographic destruction of albumin microbubbles directs gene delivery to the myocardium. Circulation 101(22) (2000) 2554-2556.

[7] J.R. Lindner, P.A. Dayton, M.P. Coggins, K. Ley, J. Song, K. Ferrara, S. Kaul, Noninvasive imaging of inflammation by ultrasound detection of phagocytosed microbubbles. Circulation 102(5) (2000) 531-538.

[8] S. Mayer, P.A. Grayburn, Myocardial contrast agents: recent advances and future directions. Prog. Cardiovasc. Dis. 44(1) (2001) 33-44.

[9] S.B. Feinstein, The powerful microbubble: from bench to bedside, from intravascular indicator to therapeutic delivery system, and beyond. Am. J. Physiol. Heart Circ. Physiol. 287(2) (2004) H450-457.

[10] H. Takeuchi, K. Ohmori, I. Kondo, A. Oshita, K. Shinomiya, Y. Yu, Y. Takagi, K. Mizushige, K. Kangawa, M. Kohno, Potentiation of C-type natriuretic peptide with ultrasound and microbubbles to prevent neointimal formation after vascular injury in rats. Cardiovasc. Res. 58(1) (2003) 231-238.

[11] P.R. Clarke, C.R. Hill, Biological action of ultrasound in relation to the cell cycle. Exp. Cell Res. 58(2) (1969) 443-444.

[12] G. Basta, L. Venneri, G. Lazzerini, E. Pasanisi, M. Pianelli, N. Vesentini, S. Del Turco, C. Kusmic, E. Picano, In vitro modulation of intracellular oxidative stress of endothelial cells by diagnostic cardiac ultrasound. Cardiovasc. Res. 58(1) (2003) 156-161.

[13] A.A. Brayman, L.M. Lizotte, M.W. Miller, Erosion of artificial endothelia in vitro by pulsed ultrasound: acoustic pressure, frequency, membrane orientation and microbubble contrast agent dependence. Ultrasound Med. Biol. 25(8) (1999) 1305-1320.

[14] A. van Wamel, A. Bouakaz, F. ten Cate, N. de Jong, Effects of Diagnostic Ultrasound Parameters on Molecular Uptake and Cell Viability. IEEE Ultrasonics Symposium Proceedings 2002, pp. 1387-1390.

[15] H.R. Guzman, D.X. Nguyen, S. Khan, M.R. Prausnitz, Ultrasound-mediated disruption of cell membranes. I. Quantification of molecular uptake and cell viability. J. Acoust. Soc. Am. 110(1) (2001) 588-596.

[16] D.L. Miller, C. Dou, Membrane damage thresholds for 1- to 10-MHz pulsed ultrasound exposure of phagocytic cells loaded with contrast agent gas bodies in vitro. Ultrasound Med. Biol. 30(7) (2004) 973-977.

[17] M. Postema, A. van Wamel, C.T. Lancee, N. de Jong, Ultrasound-induced encapsulated microbubble phenomena. Ultrasound Med. Biol. 30(6) (2004) 827-840.

[18] A. van Wamel, A. Bouakaz, M. Versluis, N. de Jong, Micromanipulation of endothelial cells: ultrasound-microbubble-cell interaction. Ultrasound Med. Biol. 30(9) (2004) 1255-1258.

[19] C. Elfgang, R. Eckert, H. Lichtenberg-Frate, A. Butterweck, O. Traub, R.A. Klein, D.F. Hulser, K. Willecke, Specific permeability and selective formation of gap junction channels in connexin-transfected HeLa cells. J. Cell Biol. 129(3) (1995) 805-817.
[20] C.S. Djuzenova, U. Zimmermann, H. Frank, V.L. Sukhorukov, E. Richter, G. Fuhr, Effect of medium conductivity and composition on the uptake of propidium iodide into electropermeabilized myeloma cells. Biochim. Biophys. Acta 1284(2) (1996) 143-152.
[21] S. Lee, T. Anderson, H. Zhang, T.J. Flotte, A.G. Doukas, Alteration of cell membrane by stress waves in vitro. Ultrasound Med. Biol. 22(9) (1996) 1285-1293.
[22] M. Schneider, A. Broillet, P. Bussat, N. Giessinger, J. Puginier, R. Ventrone, F. Yan, Gray-scale liver enhancement in VX2 tumor-bearing rabbits using BR14, a new ultrasonographic contrast agent. Invest. Radiol. 32(7) (1997) 410-417.
[23] A. van Wamel, A. Bouakaz, N. de Jong, Duration of ultrasound microbubbles enhanced cell membrane permeability. IEEE Ultrasonics Symposium Proceedings 2003, pp. 917-920.
[24] C.T. Chin, C. Lancee, J. Borsboom, F. Mastik, M. Frijlink, N. de Jong, M. Versluis, D. Lohse, Brandaris 128: a 25 million frames per second digital camera with 128 highly sensitive frames. Rev. Sci. Instru. 74(12) (2003) 5026-5034.
[25] N. Kobayashi, M. Nishikawa, K. Hirata, Y. Takakura, Hydrodynamics-based procedure involves transient hyperpermeability in the hepatic cellular membrane: implication of a nonspecific process in efficient intracellular gene delivery. J. Gene Med. 6(5) (2004) 584-592.
[26] K. Tachibana, T. Uchida, K. Ogawa, N. Yamashita, K. Tamura, Induction of cell-membrane porosity by ultrasound. Lancet 353(9162) (1999) 1409.
[27] P. Marmottant, S. Hilgenfeldt, Controlled vesicle deformation and lysis by single oscillating bubbles. Nature 423(6936) (2003) 153-156.
[28] Y. Taniyama, K. Tachibana, K. Hiraoka, T. Namba, K. Yamasaki, N. Hashiya, M. Aoki, T. Ogihara, K. Yasufumi, R. Morishita, Local delivery of plasmid DNA into rat carotid artery using ultrasound. Circulation 105(10) (2002) 1233-1239.
[29] S. Mehier-Humbert, T. Bettinger, F. Yan, R.H. Guy, Plasma membrane poration induced by ultrasound exposure: implication for drug delivery. J. Control. Release 104(1) (2005) 213-222.
[30] D.E. Ingber, Tensegrity II. How structural networks influence cellular information processing networks. J. Cell Sci. 116(Pt 8) (2003) 1397-1408.
[31] A. Van Wamel, A. Bouakaz, B. Bernard, F. Ten Cate, N. De Jong, Radionuclide tumour therapy with ultrasound contrast microbubbles. Ultrasonics 42(1-9) (2004) 903-906.
[32] M. Kinoshita, K. Hynynen, Intracellular delivery of Bak BH3 peptide by microbubble-enhanced ultrasound. Pharm. Res. 22(5) (2005) 716-720.
[33] I. Kondo, K. Ohmori, A. Oshita, H. Takeuchi, S. Fuke, K. Shinomiya, T. Noma, T. Namba, M. Kohno, Treatment of acute myocardial infarction by hepatocyte growth factor gene transfer: the first demonstration of myocardial transfer of a "functional" gene using ultrasonic microbubble destruction. J. Am. Coll. Cardiol. 44(3) (2004) 644-653.
[34] L. Juffermans, P. Dijkmans, R. Musters, A. van Wamel, A. Bouakaz, F. ten Cate, L. Deelman, C. Visser, N. de Jong, O. Kamp, Local drug and gene delivery through microbubbles and ultrasound: a safe and efficient alternative for viral vectors? Neth. Heart J. 12 (2004) 398-403.

Ultrasound and microbubble-targeted delivery of macromolecules is regulated by induction of endocytosis and pore formation

Bernadet D.M. Meijering[1,4], Lynda J.M. Juffermans[2,4], Annemieke van Wamel[3,4], Rob H. Henning[1], Inge S. Zuhorn[5], Marcia Emmer[3], Amanda M.G. Versteilen[2], Walter J. Paulus[2], Wiek H. van Gilst[1,4], Klazina Kooiman[3], Nico de Jong[3,4], René J.P. Musters[2], Leo E. Deelman[1,4], Otto Kamp[2,4]

[1] Dept. of Clinical Pharmacology, University Medical Center Groningen, the Netherlands
[2] Dept. of Cardiology and Physiology, Inst. for Cardiovascular Research, VU University Medical Center, Amsterdam, the Netherlands
[3] Dept. of Biomedical Engineering, Erasmus MC, Rotterdam, the Netherlands
[4] Interuniversity Cardiology Institute of the Netherlands, Utrecht, the Netherlands
[5] Dept. of Cell Biology, University Medical Center Groningen, the Netherlands

Circulation Research 2009; 104: 679-687

Abstract

Contrast microbubbles in combination with ultrasound are promising vehicles for local drug and gene delivery. However, the exact mechanisms behind intracellular delivery of therapeutic compounds remain to be resolved. We hypothesised that endocytosis and pore formation are involved during ultrasound and microbubble-targeted delivery (UMD) of therapeutic compounds. Therefore, primary endothelial cells were subjected to UMD of fluorescent dextrans (4.4 to 500-kDa) using 1-MHz pulsed ultrasound with 0.22-MPa peak-negative pressure, during 30s. Fluorescence microscopy showed homogeneous distribution of 4.4 and 70-kDa dextrans through the cytosol, and localisation of 155 and 500-kDa dextrans in distinct vesicles after UMD. After ATP depletion, reduced uptake of 4.4-kDa dextran and no uptake of 500-kDa dextran was observed after UMD. Independently inhibiting clathrin- and caveolae-mediated endocytosis, as well as macropinocytosis significantly decreased intracellular delivery of 4.4 to 500-kDa dextrans. Furthermore, 3D-fluorescence microscopy demonstrated dextran vesicles (500-kDa) to co-localise with caveolin-1 and especially clathrin. Finally, after UMD of dextran (500-kDa) into rat femoral artery endothelium *in vivo*, dextran molecules were again localised in vesicles that partially co-localised with caveolin-1 and clathrin. Together, these data indicated uptake of molecules via endocytosis after UMD. In addition to triggering endocytosis, UMD also evoked transient pore formation, as demonstrated by the influx of calcium ions and cellular release of pre-loaded dextrans after ultrasound and microbubble-exposure. In conclusion, these data demonstrate that endocytosis is a key mechanism in UMD besides transient pore formation, with the contribution of endocytosis being dependent on molecular size.

3.1. Introduction

Conventional delivery methods for drugs or genes, such as systemic administration via intravenous injection or oral administration, often do not suffice for therapeutic compounds such as peptides, silencing RNAs and genes [1]. A recent development in delivery systems for therapeutic compounds is the microbubble-ultrasound interaction [2,3]. Before its use as a clinical modality, it is of utmost importance to obtain new physiological insights into the mechanisms of uptake by ultrasound and microbubble-exposed cells.

Microbubbles were originally developed as ultrasound contrast agents, and are administered intravenously to the systemic circulation to enhance scattering of blood in echocardiography. They consist of a gas core stabilised with an encapsulation, and range from 1-10 μm in diameter [4]. Nowadays, research focuses on the use of ultrasound and microbubbles for therapeutic applications. It has been demonstrated that ultrasound-exposed microbubbles can achieve safe and efficient local delivery of a variety of drugs [5,6] and genes [7,9]. In an ultrasound field, microbubbles will oscillate, and this may stimulate cells to admit the drug or gene [10]. The advantage of using ultrasound and microbubbles is that only the microbubbles in the ultrasound beam will be activated. In this way, delivery can be

targeted to specific organs or sites by focusing the ultrasound beam on the specific target. This is indicated by the term ultrasound microbubble-targeted delivery (UMD).

However, the exact mechanism of cellular uptake of therapeutics after UMD is not fully understood. One of the principal mechanisms is thought to be induction of cell membrane pores [11,12]. Studies employing scanning-electron microscopy revealed pore-like structures in the cell membrane after treatment by ultrasound either with or without microbubbles [1,8,11,13]. The presence of enhanced transmembrane ion fluxes during ultrasound and microbubble-exposure was also demonstrated [14,15]. Although the hypothesis of pore formation during UMD is supported by these studies, it was recently questioned in studies by Duvshani-Eshet et al [16,17]. In these studies, pore-like structures were found both in ultrasound and microbubble-exposed cells as well as in control cells [16]. Furthermore, atomic-force microscopy studies suggested that these pore-like structures represented depressions in the membrane rather than actual pores. Exposing cells to ultrasound and microbubbles altered both diameter and depth of these depressions [17], indicating that the depressions in the membrane might represent endocytotic invaginations. Interestingly, Juffermans et al recently demonstrated that ultrasound-exposed microbubbles induced formation of hydrogen peroxide (H_2O_2), and an influx of calcium ions, causing local hyperpolarisation of the cell membrane [11,18]. In addition, other studies demonstrated that H_2O_2, as well as a rise in intracellular calcium levels are directly correlated with endocytosis [19-21].

Nevertheless, as there is still no consensus about the internalisation mechanisms involved in UMD, the aim of this study was to examine whether macromolecules enter the cell solely via transient pores, or that endocytosis might also be involved in the uptake during UMD. As a model for drug delivery, uptake of dextrans ranging from 4.4 to 500-kDa in size was studied. Primary endothelial cells and rat femoral artery endothelium, the prime target cells for intravenous microbubbles, were subjected to UMD of differentially sized dextran molecules to study whether the mechanism behind UMD is dependent on molecular size.

3.2. Materials and methods

3.2.1. Cell culture

Primary bovine aortic endothelial cells (BAECs, Cell Applications, San Diego, CA, USA) were cultured as described previously [22]. Cells between passage 3 and 7 were used for UMD experiments. Forty-eight hours prior to UMD, cells were seeded at 33% confluency to one of the two gas-permeable, ultrasound-transparent membranes of an Opticell^{TM} cell culture chamber (Biocrystal, Westerville, OH, USA).

3.2.2. Ultrasound exposure

Prior to UMD, the Opticell^{TM} chamber was mounted in the experimental acoustic set-up, described in detail in [22]. In short, a V303-SU 1-MHz unfocused 14 mm diameter single-element transducer (Panametrics, Waltham, MA, USA) was placed in a water-tank filled with

37°C phosphate-buffered saline (PBS, Invitrogen, Groningen, the Netherlands) at an angle of 45° relative to the cell monolayer. The transducer was connected to an arbitrary waveform generator (33220A, Agilent, Palto Alto, CA, USA) and a linear 60-dB power amplifier (150A100B, Amplifier Research, Bothell, WA, USA). The ultrasound signal was monitored by a synchronised digital oscilloscope (GOULD DSO 465, Valley View, OH, USA). The peak negative acoustic pressure generated at the region-of-interest (ROI) was 0.22 MPa as verified with a calibrated hydrophone (PVDFZ44-0400, Specialty Engineering Associates, Soquel, CA, USA). Cells were exposed to sine-wave ultrasound bursts with a 6.2% duty cycle and a 20-Hz pulse repetition frequency for 30 seconds.

3.2.3. Preparation of microbubbles and dextran suspensions

The ultrasound contrast agent Sonovue™ (Bracco, High Wycombe, UK) was reconstituted in 5 ml of saline solution according to the manufacturer's protocol, resulting in a preparation containing 2-5×10^8 microbubbles/ml. Tetramethylrhodamine isothiocyanate (TRITC)-labeled dextran (4.4, 70 or 155-kDa; Sigma-Aldrich), fluorescein isothiocyanate (FITC)-labeled dextran (500-kDa; Sigma-Aldrich) or lysine-fixable FITC-labeled dextran (500-kDa, Molecular Probes, Invitrogen) was added to 125 µl of Sonovue™, with a final concentration of 2 mg/ml in 10 ml PBS.

3.2.4. Cellular distribution

After the above described microbubble-dextran solution was added to the cells, the ultrasound protocol directly followed. Immediately after UMD, cells were washed with PBS at room temperature and confocal laser microscopy images were taken with a 100× oil-immersion lens (LSM410, Carl-Zeiss, Sliedrecht, the Netherlands) to investigate the cellular distribution and localisation of the dextran.

3.2.5. Inhibition of endocytosis during UMD

To prevent active uptake of extracellular molecules, cells were depleted from adenosine triphosphate (ATP) by incubation with ATP-depletion buffer containing 50 mM NaN_3 and 50 mM deoxyglucose in PBS supplemented with 1.8 mM Ca^{2+}. To test the ATP depletion buffer, cells were pre-incubated with ATP-depletion buffer or with PBS (no depletion) for 30 minutes, followed by 1-hour incubation with Alexa-fluor 488-conjugated transferrin (0.1 mg/ml), or with TRITC-labeled 70-kDa dextran (2 mg/ml), which is specifically taken up via clathrin-coated pits [23] or macropinocytosis [24], respectively. Cells were pre-incubated with ATP-depletion buffer or with PBS for 30 minutes, followed by the UMD protocol. Finally, cells were washed twice in PBS, mounted on a microscope slide, followed by direct acquisition of confocal images using a 40× lens (Carl-Zeiss). SlideBook™ software (Intelligent Imaging Innovations, I.I.I.; www.intelligent-imaging.com, Denver, CO, USA) was used to assess the mean intensity of fluorescence (MIF) per cell. Cells were pre-incubated with ATP-depletion buffer or with PBS for 30 minutes, followed by the UMD protocol.

To study the involvement of three main endocytosis pathways, cells were pre-treated 30 minutes with chlorpromazine (15 μM; Sigma-Aldrich), inhibitor of clathrin-mediated endocytosis; filipin (4 μg/ml; Sigma-Aldrich), inhibitor of caveolin-mediated endocytosis or wortmannin (0.1 μM; Sigma-Aldrich), inhibitor of macropinocytosis prior to UMD of 4.4, 70, 155 and 500-kDa dextrans. Confocal images were acquired directly following UMD using a 40× oil-immersion lens (Carl-Zeiss).

The specificity of the inhibitor was tested in a separate assay, where cells were either not pre-treated or pre-treated for 30 minutes with one of the above mentioned inhibitors. Thereafter, cells were either incubated 1-hour with Alexa-fluor 488-conjugated transferrin (Molecular Probes, Invitrogen), which is specifically taken up by clathrin-coated pits [23] or with Alexa-fluor 488-conjugated cholera toxin subunit-B (Molecular Probes), which is specific for caveolin-mediated endocytosis [24]. To assess the inhibitory effect of the endocytosis inhibitors on macropinocytosis, cells were incubated 1-hour with FITC-labeled 70-kDa dextran [25]. Afterwards, cells were fixed with 4% formaldehyde (Sigma-Aldrich, the Netherlands). Confocal images were taken at 100× magnification using an oil-immersion lens. The number of fluorescent vesicles per cell per image was counted, and expressed as percentage of non-inhibited cells.

3.2.6. Immunostaining for clathrin and caveolin-1

Directly following UMD of lysine-fixable FITC-labeled dextran (500-kDa), ROIs were cut out the Opticell™ (approximately 1.5 cm^2) and placed in PBS. Cells were fixated in 4% formaldehyde 10 minutes at room temperature. Cells were washed three times with PBS, permeabilised for 5 minutes in 0.05% Triton X-100 (Sigma-Aldrich) in PBS, followed by three washes in PBS-Tween (0.5%, Tween 20; Sigma-Aldrich). Cells were incubated with polyclonal goat anti-clathrin heavy chain, a marker for clathrin-mediated endocytosis (Santa Cruz, the Netherlands) or with monoclonal mouse anti-caveolin-1 (Clone C060; BD Biosciences, Breda, the Netherlands), a marker for caveolin-mediated endocytosis; both antibodies were diluted 1:100. No appropriate marker for macropinocytosis is available. Cells were incubated overnight at 4 °C, washed three times with PBS-Tween, and incubated with both Cy3-labeled rat-anti-mouse and Cy5-labeled donkey-anti-goat secondary antibodies (1:100, Molecular Probes) 30 minutes at room temperature in the dark. Cells were washed twice with PBS-Tween, washed once with PBS and mounted on a microscope slide with mounting-medium containing DAPI nuclear stain (Vectashield™, Vector Laboratories, Burlingame, CA, USA). 3-Dimensional (3D) images were acquired using a ZEISS Axiovert 200M Marianas™ inverted microscope (I.I.I) equipped with a motorised stage (stepper-motor z-axis increments: 0.2 micron). Images were taken using a 63× oil-immersion lens (Carl-Zeiss). A cooled CCD camera (C1280x8vb 1024 pixels; Cooke Sensicam, Cooke, Tonawanda, NY) recorded images with true 16-bit capability. The camera is linear over its full dynamic range (up to intensities of over 4000) while dark/background currents (estimated by the intensity outside the cells) are typically <100. The microscope, camera, data viewing/processing were conducted/controlled by SlideBook™. This software was also used

to deconvolve the 3D image stacks in order to remove out-of-focus light, as well as to quantify the extent of co-localisation for dextran with clathrin or caveolin by calculating Pearson's correlation factor. Pearson's correlation factor lies between +1 and –1. A positive value implies a positive correlation, thus co-localisation, '0' implies no correlation, and a negative value implies an inverse correlation. As a control, the correlation factor between clathrin (Cy5)/DAPI and caveolin (Cy3)/DAPI was determined.

3.2.7. In vivo dextran delivery

The animal study was approved by the Animal Research Committee at the VU University Medical Center. Male Wistar rats (n = 4, 400-450g; Harlan, Horst, the Netherlands) were anesthetised with pentobarbital (60 mg/kg intraperitoneal) and ketamine HCl (70 mg/kg intramuscular) with a pentobarbital maintenance dose (30 min/15 mg/kg intraperitoneal). Rats were placed in a supine position on a heating pad maintaining body temperature at 37 ºC. An intraperitoneal catheter was placed to administer pentobarbital. The trachea was intubated with polyethylene tubing to facilitate breathing. The animals received 75 IU/kg heparin (Leo Pharmaceutical Products, Weesp, the Netherlands) intravenously to prevent catheter clotting. Mean arterial pressure (100-120 mm Hg), and heart rate (340-380 bpm) were continuously monitored via a catheter in the carotid artery connected to a pressure transducer. Both femoral arteries were uncovered by opening the skin and cannulated in the common iliac artery, schematically depicted in Fig. 3.1. The internal iliac and deep femoral arteries were closed to optimise microbubble-dextran delivery to the femoral artery. The microbubble-dextran (500-kDa, FITC-labeled, lysine-fixable) saline solution was infused using bifurcated tubing at a constant rate of 4 ml/h. The tip of the ultrasound transducer was fixed at 3 cm distance from the left femoral artery (right femoral artery served as control), with a 2% agarose gel between

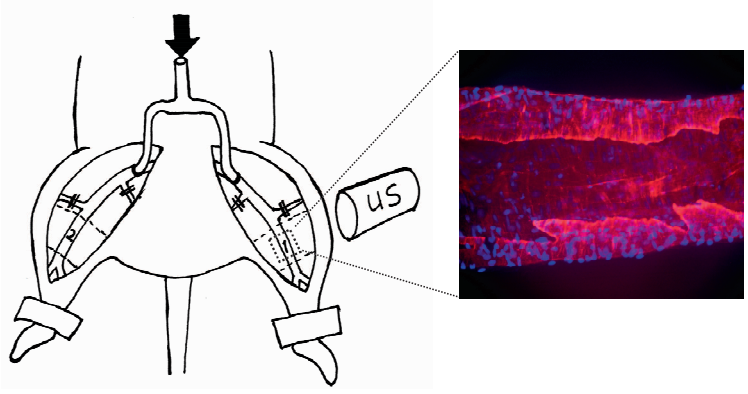

Fig. 3.1. Schematic overview of microbubble-dextran administration to rat femoral arteries. Both femoral arteries were canulated proximal to the aorta and connected with T-tubing to an infusion pump (arrow). The internal iliac and deep femoral arteries were closed to optimise microbubble-dextran delivery to the femoral artery. Area 1 was exposed to ultrasound (US) and area 2 served as control. The area of the artery between the dotted lines was dissected for analysis. An example of the vessel is shown by 10× magnification image, with actin stained red and nuclei blue.

the tip of the transducer and the exposed artery for good ultrasound conductance. The same ultrasound protocol as described above was applied for the *in vivo* situation. Directly after ultrasound exposure, 4% formaldehyde in saline was infused for fixation of the arteries, followed by 5 minute treatment of 0.05% Triton X-100 in saline for permeabilisation of the endothelial cells. Arteries were dissected, cut open longitudinally and fixed on silicone plates. Arteries were stained for clathrin and caveolin-1 as described for BAECs. After staining, arteries were placed on a microscope slide covered with Vectashield™ containing nuclear stain DAPI, and sealed using a cover slip and colourless nail polish. Image acquisition was performed as described in the section above.

3.2.8. Ultrasound and microbubble-induced pore formation

To study pore formation, the influx of calcium ions was measured with the fluorescent probe Fluo-4 (Molecular Probes), a cell-permeant acetoxymethyl ester sensitive for free cytosolic calcium. To acquire time-lapse images during ultrasound exposure the transducer was mounted on the microscope, as described in [15]. To study the effect of inhibitors of endocytosis on the ultrasound and microbubble-evoked calcium influx, cells were pre-incubated 30 minutes with chlorpromazine, filipin and wortmannin at concentrations indicated above prior to the calcium measurements.

To further investigate pore formation, cells were pre-loaded with fluorescent dextrans using the syringe loading protocol of Clarke and McNeil [26], with minor adaptations. In short, 1 ml of DMEM containing 2% PF-68 (Sigma-Aldrich, the Netherlands), 20 mg TRITC-labeled dextran (4.4 or 155-kDa) and 10^6 cells was drawn in and expelled through a 29-gauge needle for four times, using a sterile 1 ml syringe. Subsequently, culture medium was added to the dextran-loaded cell suspension in a 1:1 ratio. This was repeated 5 times for each Opticell™ so a total of 10 ml of the dextran-loaded cells mixture was added to an Opticell™. Cells were allowed to recover overnight. Cells were exposed to ultrasound and microbubbles according to the UMD protocol described above, with the exception that no dextran was incubated with the microbubbles. Immediately after ultrasound and microbubbles exposure, confocal images were taken using a 40× oil-immersion lens (Carl-Zeiss) and dextran release was measured. As positive control, dextran-loaded cells were permeabilised to release all dextran from the cell, using 0.1% triton X-100 PBS solution for 5 minutes. Differences in fluorescence were assessed using ImagePro-plus 5.0. Mean intensity of fluorescence per cell after triton X-100 treatment of the cells was used as baseline.

3.2.9. Statistics

Data are presented as mean ± standard error of the mean (SEM). All experiments were repeated at least three times. Per condition at least six microscopical fields were analysed, containing approximately 10 - 20 cells per field. Groups were tested for normal distribution with one sample Kolmogorov-Smirnov test. Differences between groups were tested using a one-way ANOVA with Bonferroni post-hoc analysis or the non-parametric Kruskal-Wallis test with Dunn's post-hoc test. Differences between groups in the experiment of calcium

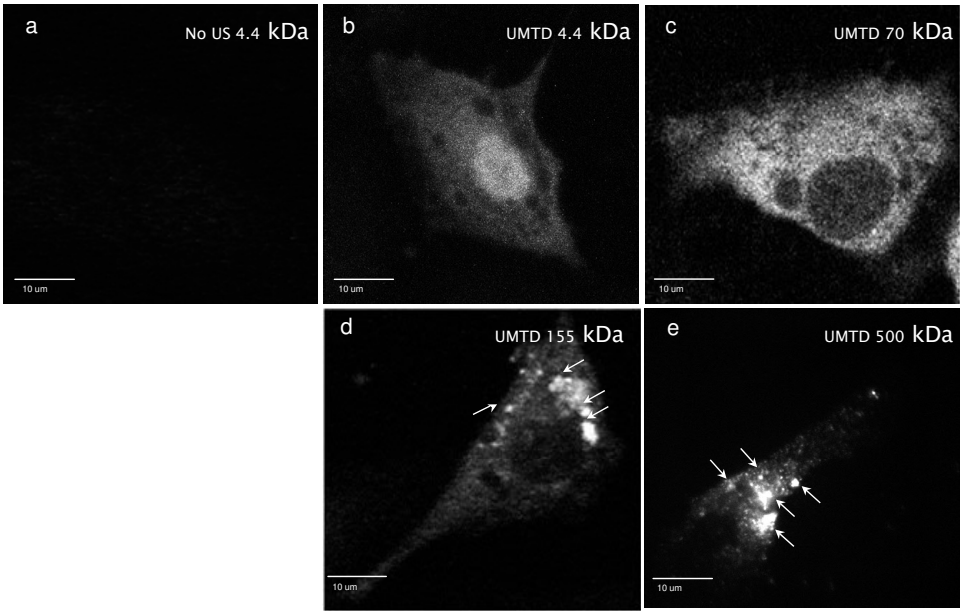

Fig. 3.2. Cellular distribution of fluorescent dextrans after UMD. a) No uptake of 4.4-kDa dextran in the absence of US. b) Homogeneous distribution in the cytosol, and nucleus of 4.4-kDa dextran after UMD. c) Homogeneous distribution in the cytosol of 70-kDa dextran, but absence of nuclear localisation. d) Localisation of 155-kDa mainly in vesicle-like structures. e) Vesicular-like localisation of 500-kDa dextran.

influx were tested using two-way ANOVA with Bonferroni post-hoc analysis. A p-value lower than 0.05 was considered statistically significant.

3.3. Results

3.3.1. Cellular distribution of differently sized dextrans

After UMD dextran molecules of 4.4-kDa showed a homogeneous distribution throughout the cytosol as well as in the nucleus (Fig. 3.2.b). Dextran molecules of 70-kDa showed a similar distribution pattern in the cytosol, but were absent in the nucleus (Fig. 3.2.c). Larger dextrans (155 and 500-kDa) showed a different cytosolic pattern of distribution after UMD, as they were mainly found in vesicle-like structures, but lacked nuclear localisation (Fig. 3.2.d and 3.2.e, respectively). In the absence of ultrasound, no uptake of dextran molecules was found (Fig. 3.2.a, results shown for 4.4-kDa).

3.3.2. Inhibition of endocytosis during UMD

To further investigate whether the found vesicle-like dextran-positive structures after UMD were endocytotic vesicles, UMD of dextran was studied after overall inhibition of endocytosis through ATP depletion of the cells as well as inhibition of specific endocytotic

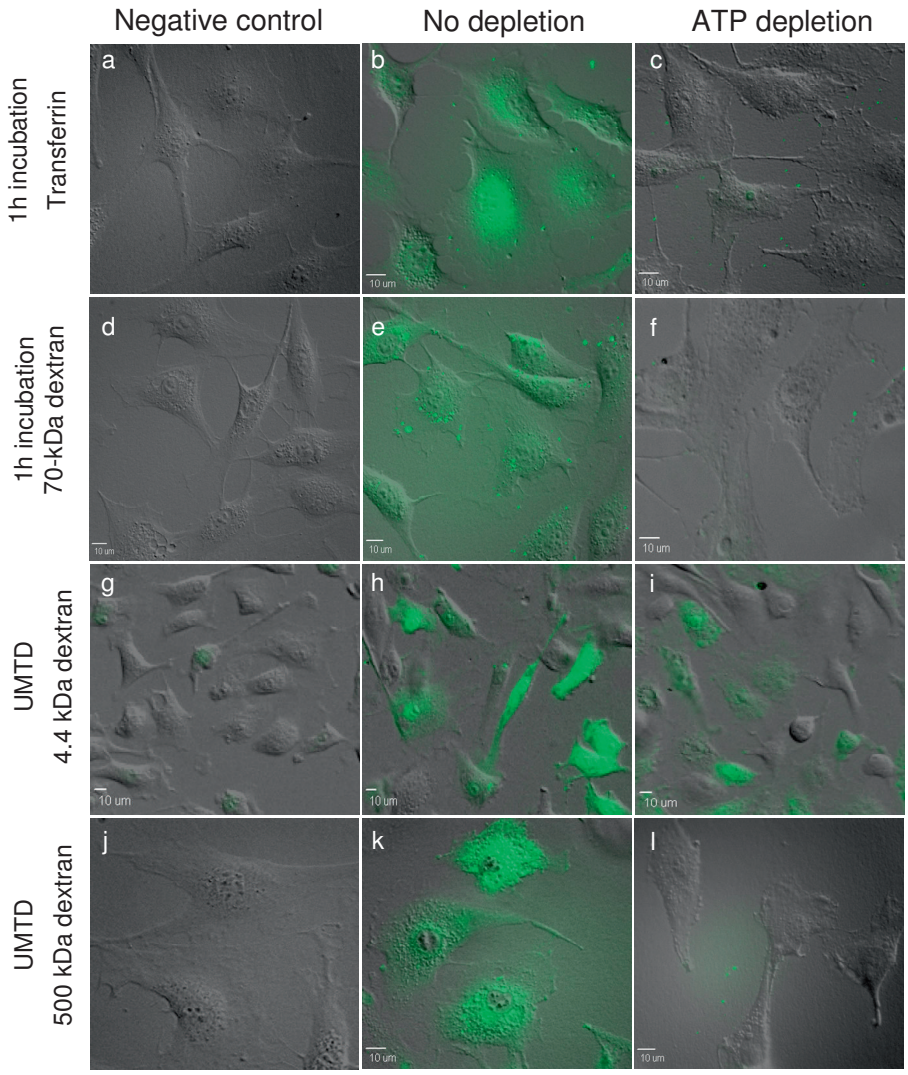

Figure 3.3. ATP depletion. Confocal images demonstrating uptake of transferrin and fluorescent dextrans (4.4 and 500-kDa) in the absence or presence of ATP depletion. Cells were pre-treated with PBS (no depletion) or ATP-depletion buffer for 30 minutes. a,d,g,j) Relative negative controls; a) no transferrin, d) no 70-kDa dextran, g,j) no US. b) Uptake of transferrin after 1-hour incubation in PBS, c) in ATP-depletion buffer. e) Uptake 70-kDa dextran after 1-hour incubation in PBS, f) in ATP-depletion buffer. h) UMD of 4.4 kDa dextran without depletion, i) after ATP depletion. k) UMD of 500-kDa dextran without depletion, l) after ATP depletion.

Table 3.1. Specificity of inhibitors for different routes of endocytosis.

	Clathrin-mediated	Caveolin-mediated	Macropinocytosis
Untreated	100.0 ± 8.4%	100.0 ± 11.3%	100.0 ± 6.7%
Chlorpromazine	**44.3 ± 14.9%**	90.0 ± 6.0%	109.7 ± 14.5%
Filipin	80.3 ± 5.2%	**49.1 ± 11.5%**	123.9 ± 26.5%
Wortmannin	66.4 ± 8.5%	87.5 ± 10.0%	**38.3 ± 7.6%**

pathways. Deprivation of cells from ATP resulted in inactivation of the endocytotic machinery, as these cells were no longer capable to actively internalise transferrin (Fig. 3.3.a-c) or 70-kDa dextran (Fig. 3.3.d-f). Interestingly, UMD of 4.4-kDa dextran was still successful after ATP depletion (Fig. 3.3.g-i). However, mean intensity of fluorescence (MIF ± SEM) decreased by 62% (no depletion: 365.4 ± 15.1, ATP depletion: 138.7 ± 13.3, $p < 0.001$). UMD of 500-kDa dextran was completely inhibited when cells were ATP depleted

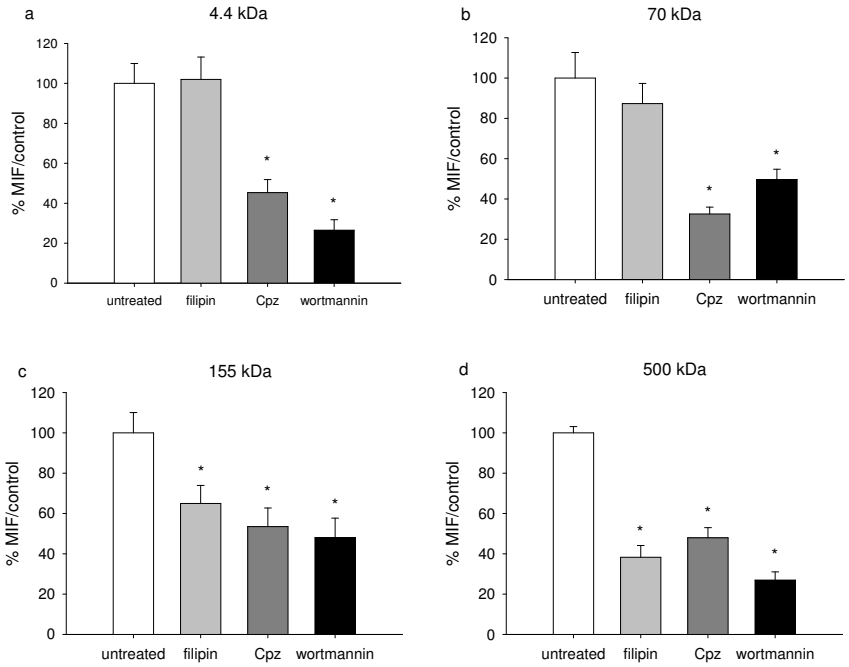

Fig. 3.4. UMD of dextrans in the presence of endocytosis blockers. Graphs show mean intensity of intracellular fluorescence (MIF) ± SEM for UMD of all sizes of dextran, expressed as percentage of control (non-exposed cells). a) Significant reduction in cellular uptake of 4.4, and 70-kDa (b) dextrans in the presence of chlorpromazine (CPZ; clathrin-mediated uptake) and wortmannin (macropinocytosis). Filipin (caveolin-mediated endocytosis) had no significant effect on the uptake of 4.4 and 70-kDa dextrans. c) Significant reduction in cellular uptake of 155-kDa, and 500-kDa (d) dextrans for all blockers.

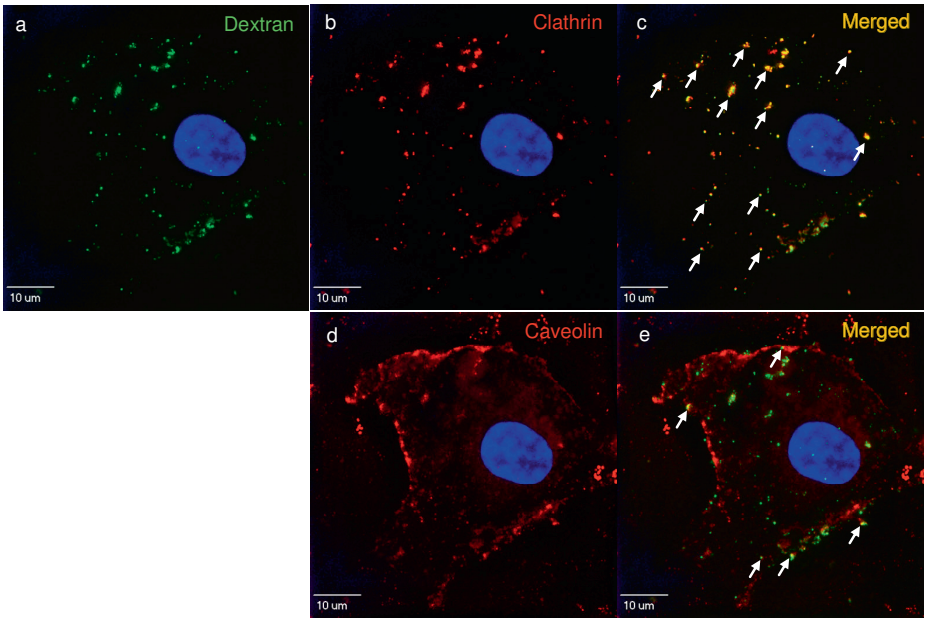

Fig. 3.5. Co-localisation of dextran with endocytosis markers after UMD. One optical section from a 3D-image stack is shown. a) Vesicle-like localisation of 500-kDa dextran in green. b) Immunostaining for clathrin in red. c) Co-localisation of dextran and clathrin, demonstrated by the yellow/orange color (indicated by arrows). d) Immunostaining for caveolin-1 in red. e) Co-localization of dextran and caveolin, demonstrated by the yellow/orange color (indicated by arrows). DAPI was used as nuclear counterstain.

(Figure 3.3.j-l).

Specificity of the inhibitors of endocytosis was evaluated using specific substrates for the three main routes of endocytosis. In BAECs, chlorpromazine inhibited clathrin-mediated endocytosis of transferrin by 55.7 ± 14.9%. Filipin inhibited caveolin-mediated endocytosis of choleratoxin subunit-B by 50.9 ± 11.4%. Macropinocytosis of 4.4-kDa dextrans was inhibited by 61.7 ± 7.6% when cells were pre-treated with wortmannin. Importantly, all three inhibitors were found to have the most pronounced effect on their respective pathway at the concentrations used (Table 3.1).

Blocking macropinocytosis (wortmannin) or clathrin-mediated endocytosis (chlorpromazine) both caused a significant decrease in MIF after UMD of all studied dextran sizes (Fig. 3.4). Filipin, inhibiting caveolin-mediated endocytosis, caused a significant decrease in MIF after UMD of dextrans of 155 and 500-kDa (Fig. 3.4.c-d), but not for 4.4 and 70-kDa dextrans (Fig. 3.4.a-b).

3.3.3. Co-localisation of endocytosis markers and 500-kDa dextran

To further substantiate the role of endocytosis, we investigated whether internalised 500-kDa dextran co-localised with clathrin and/or caveolin-1, which are established markers for two main routes of endocytosis. Fig. 3.5 shows clear co-localisation of dextran with clathrin (Fig. 3.5.b-c) and to a minor extent with caveolin-1 (Fig. 3.5.d-e), as demonstrated by the yellow/orange colour in the merged images of dextran (green) and clathrin/caveolin-1 (red). The extent of co-localisation was determined using Pearson's correlation factor. A positive correlation of 0.35 ± 0.06 ($p < 0.001$, compared to hypothetical value of 0.0) was found for dextran with clathrin, and of 0.19 ± 0.05 ($p < 0.01$) for dextran with caveolin. As control, no correlation was found for DAPI (nuclei) with either Cy3 (0.01 ± 0.01, $p = 0.3$) or Cy5 channel (-0.01 ± 0.02, $p = 0.7$) (both secondary antibodies).

3.3.4. In vivo dextran delivery

Results derived from *in vivo* experiments showed that dextran molecules of 500-kDa were localised in vesicle-like structures in the endothelium of the rat femoral artery after UMD (Fig. 3.6.a-b). No dextran was internalised in the control artery not exposed to ultrasound. The endothelium was stained for clathrin and caveolin-1, and clear changes could be detected in the cellular pattern of both proteins in the ultrasound-exposed artery (Fig. 3.6.d-f) compared to the control artery (Fig. 3.6.c-e). Furthermore, part of the dextran-positive vesicles clearly co-localised with clathrin (Fig. 3.6.d), indicated by the yellow/orange colour. Co-localisation with caveolin-1 was detected to a lesser degree (Fig. 3.6.f). After determining Pearson's correlation factor, results similar to the *in vitro* situation were found. A positive correlation factor of 0.35 ± 0.11 was found for clathrin, as well as for caveolin-1 (0.16 ± 0.04). Both correlations were significantly different from the hypothetical value of 0.0 ($p < 0.05$). As control, no correlation was found for DAPI with either Cy3 (-0.05 ± 0.02, $p = 0.7$) or Cy5 (-0.04 ± 0.02, $p = 0.7$).

3.3.5. Ultrasound and microbubble-induced pore formation

Previously, we ascribed the increase in intracellular calcium levels after ultrasound and microbubbles exposure to transient pore formation in cardiomyoblast cells [15]. Ultrasound and microbubbles also caused influx of calcium ions in BAECs as shown in Fig. 3.7. Fluores-

Fig. 3.6. UMD of 500-kDa dextran *in vivo*. Images are optical sections from 3D-image stacks from the endothelial layer of the femoral arteries. a,c,e) Image from control artery not exposed to US, demonstrating no dextran uptake. b,d,f) Image from artery exposed to US, demonstrating dextran (green) uptake by the endothelium and localisation in vesicle-like structures. c,d) Immunostaining for clathrin in red. Panels demonstrate redistribution of clathrin-positive vesicles, indicated by more and larger clathrin-positive vesicles (possibly late endosomes) after UMD. Arrows indicate co-localisation of a part of the dextran-positive vesicles with clathrin, see arrows. e,f) Immunostaining for caveolin-1 in red. Panels demonstrate redistribution of caveolin-1, indicated by larger internalized caveolin-positive vesicles after UMD, compared to a well-organized pattern on the cell membrane. However, minor co-localisation with dextran is observed (one arrow indicating yellow vesicle) compared to co-localisation of dextran with clathrin.

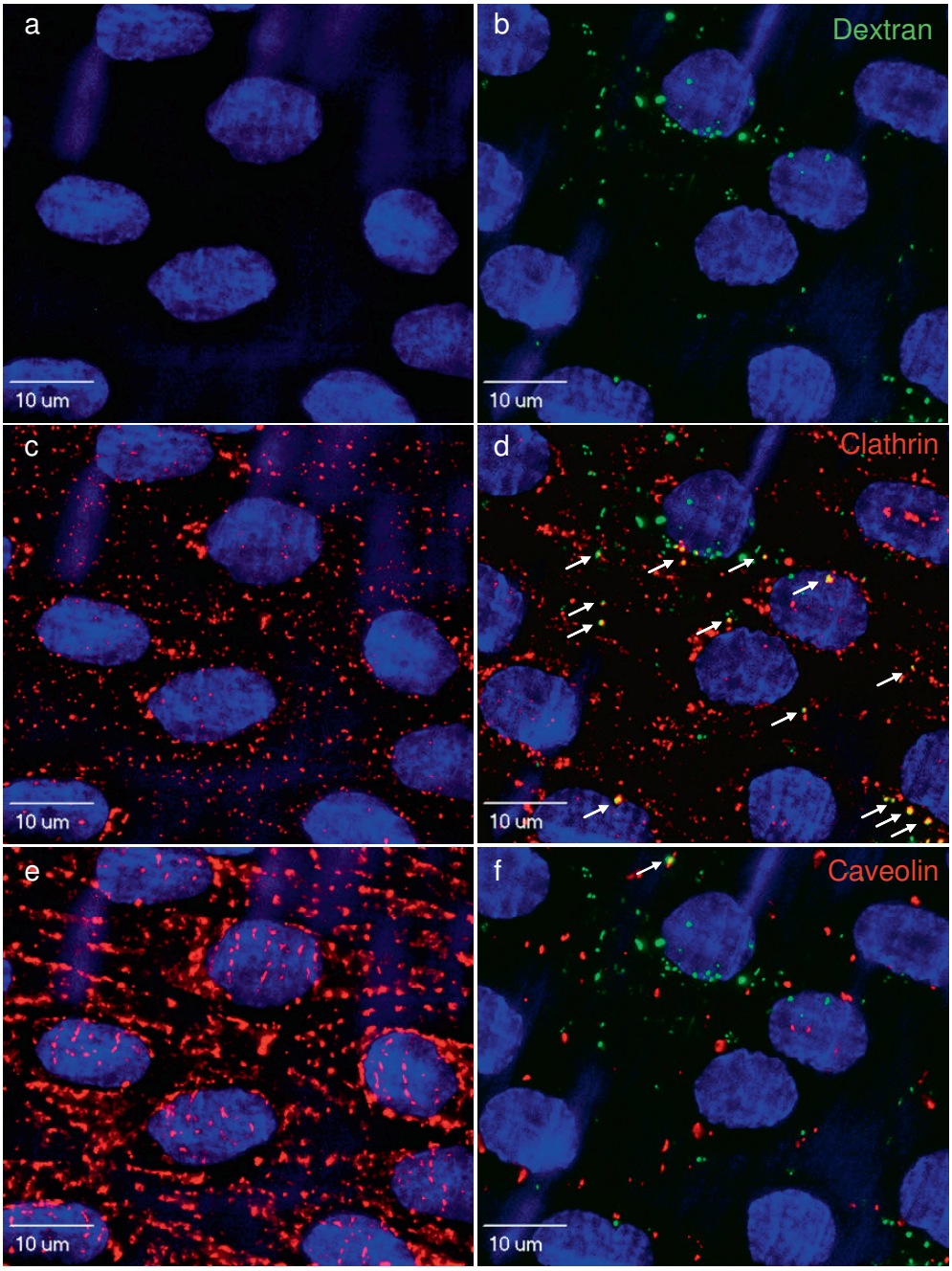
a
10 um
b
Dextran
10 um
c
10 um
d
Clathrin
10 um
e
10 um
f
Caveolin
10 um

cent intensity reached a peak value of 186.4 ± 3.4%, followed by a decrease towards basal levels (Fig. 3.7.a). There was no detectable change in the calcium influx in cells exposed to either ultrasound alone (no microbubbles; 98.2 ± 0.2%) or microbubbles alone (no ultrasound; 97.1 ± 0.3%), or without both ultrasound and microbubbles (94.3 ± 0.3%, Fig. 3.7.b-d). In order to investigate whether the inhibitors of endocytosis affected the calcium influx evoked by ultrasound and microbubbles, the calcium influx was also measured in the presence of chlorpromazine, filipin and wortmannin. It was found that chlorpromazine and wortmannin did not significantly affect the ultrasound and microbubble-evoked influx (Fig. 3.7.e). However, filipin caused a large increase in the ultrasound and microbubble-evoked influx (320.4 ± 7.2%, $p < 0.001$).

Furthermore, formation of transient pores was studied by cellular release of dextran following exposure to ultrasound and microbubbles (Fig. 3.8). Cells were pre-loaded with dextran, and following ultrasound exposure MIF significantly decreased to 63.4 ± 2.1% for 4.4-kDa dextran (Fig. 3.8.a) and to 79.1 ± 2.3% for 155-kDa dextran (Fig. 3.8.b), compared to cells not exposed to ultrasound and microbubbles (100.0 ± 2.7%, $p < 0.05$). Because filipin did not inhibit uptake of 4.4 and 70-kDa dextrans and augmented the ultrasound and microbubble-evoked calcium influx, its influence on dextran release was explored.

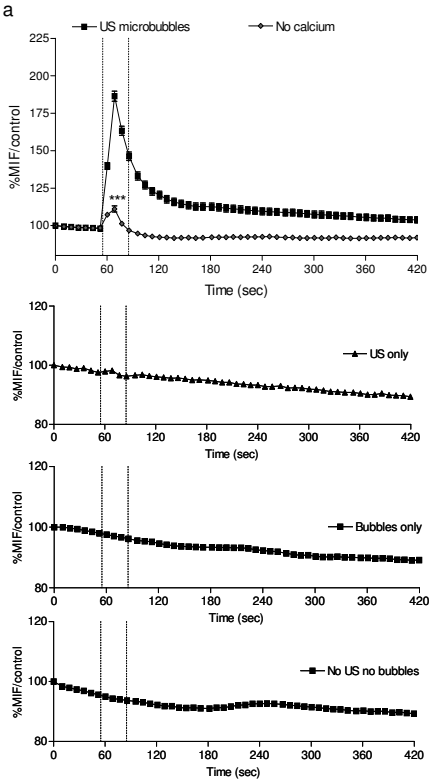

Fig. 3.7. Ultrasound and microbubble-mediated calcium influx. Live-cell measurements of intracellular calcium levels over time. Data shown as mean intensity of fluorescence (MIF) ± SEM, expressed as percentage of MIF on t = 0; *** $p <$ 0.001. Dotted lines represent moments of US on and off-switch, respectively. a) Increase in MIF during US-exposed microbubbles (black squares). Absence of extracellular calcium resulted in a minor increase in MIF, compared to US and microbubbles with calcium. b-d) Calcium influx controls: US alone (b), microbubbles alone (c), or no US and no microbubbles (d). e) Effect of endocytosis inhibitors on the US and microbubble-evoked calcium influx.

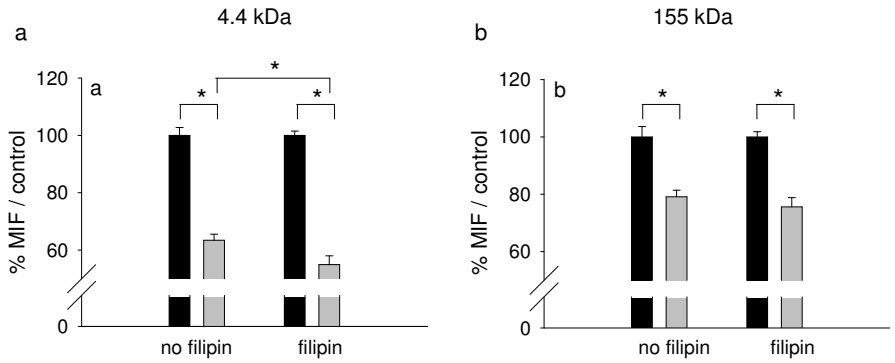

Fig. 3.8. Ultrasound and microbubble-mediated cellular dextran release. a) Mean intensity of fluorescence (MIF) ± SEM of 4.4-kDa dextran-loaded cells after US and microbubble-exposure (grey bars), compared to cells not treated with US and microbubbles (black bars). US-exposed microbubbles resulted in a significant release of dextran ($p < 0.05$). Pre-treatment of cells with filipin prior to US and microbubble-exposure, resulted in significantly more dextran release ($p < 0.05$), compared to cells that only received pre-treatment with filipin (without US and microbubbles) and to cells exposed to US and microbubbles (no filipin). b) 155-kDa dextran loaded cells. Exposure of cells to US and microbubbles (grey bars) resulted in a significant release of dextran ($p < 0.05$), compared to cells not treated with US and microbubbles (black bars). Filipin had no additional effect on release of 155-kDa dextran. Release of 4.4-kDa dextran was significantly higher than release of 155-kDa dextran after US and microbubble-exposure ($p < 0.05$).

Treatment with filipin alone, without ultrasound and microbubbles, did not cause a decrease in MIF (100.0 ± 1.5%, Fig. 3.8). However, exposure of filipin-treated cells to ultrasound and microbubbles caused significantly more release of the 4.4-kDa dextrans (54.9 ± 3.1%, $p < 0.05$), compared to non-filipin-treated cells exposed to ultrasound and microbubbles (63.4 ± 2.1%; Fig. 3.8.a). Filipin-treatment of cells did not significantly alter the release of 155-kDa dextran (75.6 ± 2.3%) after ultrasound and microbubble-exposure (Fig. 3.8.b).

3.4. Discussion

This is, to the best of our knowledge, the first study demonstrating that endocytosis plays a key role in UMD of macromolecules sized between 4 and 500-kDa besides transient pores. The role of endocytosis was established by studying cellular localisation of dextrans after UMD, uptake of dextrans during ATP depletion, and the effect of individual blockers of the three main routes of endocytosis on dextran uptake. Furthermore, co-localisation of 500-kDa dextran with markers for different endocytosis pathways was demonstrated *in vitro* as well as *in vivo*. In addition to endocytosis, we demonstrated the occurrence of transient pores in the cell membrane by showing both influx of calcium ions and cellular release of pre-loaded dextrans.

Studying cellular localisation of fluorescent dextrans after UMD, we found that the smaller dextran molecules of 4.4 and 70-kDa were homogeneously distributed throughout the cytosol. This is similar to the cellular distribution found after micro-injection of dextran molecules from 3-70-kDa into the cytosol [27,28], indicating that during UMD the small dextran molecules enter cells via transient pores in the cell membrane. In contrast, dextran molecules of 155 and 500-kDa were mainly localised in vesicle-like structures after UMD, indicating that the larger dextrans might be taken up via endocytosis [29]. When these dextran molecules had entered via pores, a homogeneous cytosolic distribution would be expected, comparable to the distribution of these dextran molecules after micro-injection [27,28]. Therefore, uptake of larger dextrans through UMD appears to be mediated through other pathways than pore formation. After this first indication of endocytosis, these experiments were repeated while depriving the cell from ATP. Depleting the cells from ATP did not stop the 4.4-kDa from entering the cell, but did significantly block the uptake by 62%. This decrease in fluorescence may be explained by either a 62% contribution of the endocytotic pathway or by a (partial) wash-out of the dextrans taken up via pores as these pores might not have resealed, as this is also - like all cellular processes - an energy-dependent process [30]. Interestingly, UMD of 500-kDa dextran was completely blocked after ATP depletion, suggesting endocytosis as a route of entry during UMD. Endocytosis is further evidenced as an important mechanism of UMD by the decrease in cellular uptake of dextran molecules after inhibition of clathrin-mediated endocytosis, caveolin-mediated endocytosis and macropinocytosis. Interestingly, not only the uptake of larger dextrans was inhibited by the endocytosis inhibitors, but also the smaller dextrans showed a similar decrease after inhibiting clathrin-mediated endocytosis and macropinocytosis, although the confocal images of the smaller dextrans indicated uptake via pores. This discrepancy might be explained by the high level of fluorescence in the cytosol masking seperate vesicles. Finally, co-localisation of 500-kDa dextran with clathrin, and to a lesser degree caveolin-1, further supported the role of endocytosis during UMD.

Importantly, the *in vitro* findings pointing to the involvement of endocytosis were extended to the *in vivo* situation. Using the same ultrasound parameters, 500-kDa dextrans were delivered into endothelium of the rat femoral artery. Confocal images of the ultrasound and microbubble-exposed artery showed conspicuous changes in the cellular pattern of caveolin-1 and clathrin, compared to the artery not exposed to ultrasound, indicating translocation of caveolin and clathrin upon UMD. It has been described in literature that *in vitro* for example shear stress can induce translocation of caveolin-1 [31,32]. Furthermore, the dextran was clearly localised in vesicle-like structures that partially co-localised with both clathrin, and to a lesser degree caveolin-1, comparable to the *in vitro* data. These *in vivo* data further substantiated the role of endocytosis in UMD of macromolecules to endothelial cells.

All three main routes of endocytosis were involved in UMD of dextran molecules of 155 and 500-kDa, as demonstrated by the effect of the inhibitors of these routes of endocytosis. Caveolin-mediated endocytosis did not seem to be involved in UMD of dextran molecules of 4.4 and 70-kDa, as filipin was not able to block the uptake of these smaller dextrans.

However, it is known that filipin disrupts formation of caveolae by altering the distribution of cholesterol in the membrane [33], thereby changing the physical properties of the membrane. This is confirmed by pre-treating the cells with filipin, followed by exposure to ultrasound and microbubbles. Under these conditions, filipin enhanced the ultrasound and microbubble-induced calcium influx three-fold. Secondly, filipin augmented the loss of cytosolic small fluorescent dextrans following UMD, but did not affect the loss of larger dextrans. Together, these data suggest that filipin increased vulnerability of the cell membrane, and enhanced pore formation during exposure to ultrasound and microbubbles. Thus, caveolin-mediated endocytosis is also likely to play a role in UMD of molecules $\leq$ 70-kDa. Unfortunately, replacing filipin with another inhibitor of caveolin-mediated endocytosis would most likely also result in increased formation of transient pores as these inhibitors all interfere with the physical properties of the cell membrane [34].

We previously demonstrated the occurrence of transient pores evoked by ultrasound and microbubbles in cardiomyoblast cells. We showed that an increase in intracellular calcium was caused by the influx of calcium ions from the extracellular environment through transient pores in the cell membrane [15]. In the present study it was found that also in BAECs, ultrasound and microbubbles evoked a calcium influx. Pore formation caused by ultrasound and microbubbles is further supported by the cellular release of fluorescent dextrans. Cells pre-loaded with 4.4-kDa dextran (diameter of 2.8 nm) showed a decrease in cytosolic fluorescence down to 63.4% after UMD compared to only a small decrease down to 79.1% for 155-kDa dextran (diameter of 17 nm). This indicates that the contribution of transient pores is less important for UMD of macromolecules $\geq$ 155-kDa using our ultrasound parameters. These data are in contrast with the study of Mehier-Humbert et al who suggested that dextran molecules with a diameter between 11.6 and 37.0 nm were able to enter the cell via pores, and no differences were found between molecule sizes [13]. However, the role of endocytosis in cellular entry of these molecules was not excluded in that study.

It remains unclear how UMD induces endocytosis. It has been demonstrated that ultrasound-exposed microbubbles may cause a rise in temperature, which might affect membrane permeability and endocytosis. However, the rise in temperature has only been demonstrated for cavitating microbubbles [35]. Exposing microbubbles to ultrasound with our parameters does not cause inertial cavitation and most likely also no increase in temperature. Several studies demonstrated that shear stress induces endocytosis in endothelial cells [36-38]. Flow of extracellular fluid induced by oscillation of microbubbles in an ultrasound field may cause shear stress and subsequent activation of endocytotic pathways. Furthermore, ultrasound and microbubble-evoked generation of H_2O_2, as well as a rise in intracellular calcium levels are involved in inducing endocytosis [15,18-21,39]. Another recent publication showed that resealing of pores in the cell membrane, induced by a bacterial toxin, requires calcium-dependent endocytosis to remove the pores from the plasma membrane. They also found that this calcium-dependent endocytosis is required in a similar way to repair lesions formed in mechanically porated cells [40], which may be comparable with ultrasound and microbubble-porated cells. Besides ultrasound and microbubble-induced

uptake via endocytosis, another route of uptake that has been proposed is fusion of microbubble shell components with the cell membrane, especially in the case of lipid microbubbles. However, fusion has not yet been demonstrated experimentally, only suggested [4,41]. Furthermore, if fusion does take place, it is to be expected that this will lead to a homogeneous distribution of the dextran in the cytosol. In this study, we found a vesicular localisation of the larger dextrans and a key role for endocytosis, arguing against an important role for fusion.

To summarise, UMD provides opportunities for new therapies due to its low toxicity, low immunogenicity, non-invasive nature, local application and its cost-effectiveness. Another advantage over other targeted delivery systems for therapeutic compounds is that molecular imaging and therapeutic compound delivery can be performed simultaneously [42]. The finding that the contribution of endocytosis and pore formation to intracellular delivery and subsequent subcellular localisation of the therapeutic compound is dependent on the molecular size, should be taken into account when designing new effective therapies using UMD. Pharmaceutical chemical compounds are generally smaller than 4-kDa and may have their target in the cytosol or nucleus, as they are small enough to pass the nuclear pore. Proteins may range from 4 to 500-kDa. DNA, which needs to enter the nucleus for effective therapy, often exceeds 500-kDa and is likely to be trapped in endosomes. This compartmentalisation of therapeutic compounds, and most importantly genes, may affect therapy efficiency and should be taken into consideration when measuring drug action following UMD. On the other hand, as many crucial signalling events are known to occur in these endosomes [43], the endocytotic mechanism could also be exploited for therapy.

In conclusion, endocytosis plays a key role in UMD of molecules sized between 4 and 500-kDa besides transient pore formation. The contribution of transient pores as a mechanism of UMD decreases when molecule size increases. These findings provide important new insight in the mechanisms of UMD and will lead to the rational design of new drug or gene therapies involving UMD.

References

[1] Schlicher RK, Radhakrishna H, Tolentino TP, Apkarian RP, Zarnitsyn V, Prausnitz MR. Mechanism of intracellular delivery by acoustic cavitation. Ultrasound Med. Biol. 32 (2006) 915-924.

[2] Newman CM, Bettinger T. Gene therapy progress and prospects: Ultrasound for gene transfer. Gene Ther. 14 (2007) 465-475.

[3] Mayer CR, Bekeredjian R. Ultrasonic gene and drug delivery to the cardiovascular system. Adv. Drug Deliv. Rev. 60 (2008) 1177-1192.

[4] Dijkmans PA, Juffermans LJM, Musters RJP, van Wamel A, ten Cate F, van Gilst W, Visser CA, de Jong N, Kamp O. Microbubbles and ultrasound: from diagnosis to therapy. Eur. J. Echocardiography 5 (2004) 245-256.

[5] Unger EC, McCreery TP, Sweitzer RH, Caldwell VE, Wu Y. Acoustically active lipospheres containing paclitaxel: a new therapeutic ultrasound contrast agent. Invest. Radiol. 33 (1998) 886-892.

[6] Bekeredjian R, Chen S, Grayburn PA, Shohet RV. Augmentation of cardiac protein delivery using ultrasound targeted microbubble destruction. Ultrasound Med. Biol. 31 (2005) 687-691.
[7] Chen S, Ding JH, Bekeredjian R, Yang BZ, Shohet RV, Johnston SA, Hohmeier HE, Newgard CB, Grayburn PA. Efficient gene delivery to pancreatic islets with ultrasonic microbubble destruction technology. Proc. Nat. Acad. Sci. USA 103 (2006) 8469-8474.
[8] Taniyama Y, Tachibana K, Hiraoka K, Namba T, Yamasaki K, Hashiya N, Aoki M, Ogihara T, Yasufumi K, Morishita R. Local delivery of plasmid DNA into rat carotid artery using ultrasound. Circulation 105 (2002) 1233-1239.
[9] Leong-Poi H, Kuliszewski MA, Lekas M, Sibbald M, Teichert-Kuliszewska K, Klibanov AL, Stewart DJ, Lindner JR. Therapeutic arteriogenesis by ultrasound-mediated VEGF165 plasmid gene delivery to chronically ischemic skeletal muscle. Circ. Res. 101 (2007) 295-303.
[10] van Wamel A, Bouakaz A, Versluis M, de Jong N. Micromanipulation of endothelial cells: ultrasound-microbubbles-cell interaction. Ultrasound Med Biol. 30 (2004) 1255-1258.
[11] Tachibana K, Uchida T, Ogawa K, Yamashita N, Tamura K. Induction of cell-membrane porosity by ultrasound. Lancet 353 (1999) 1409.
[12] van Wamel A, Kooiman K, Harteveld M, Emmer M, Ten Cate FJ, Versluis M, de Jong N. Vibrating microbubbles poking individual cells: Drug transfer into cells via sonoporation. J. Control. Release 112 (2006) 149-55.
[13] Mehier-Humbert S, Bettinger T, Yan F, Guy RH. Plasma membrane poration induced by ultrasound exposure: Implication for drug delivery. J. Control. Release 104 (2005) 213-222.
[14] Deng CX, Sieling F, Pan H, Cui J. Ultrasound-induced cell membrane porosity. Ultrasound Med. Biol. 30 (2004) 519-526.
[15] Juffermans LJ, Dijkmans PA, Musters RJ, Visser CA, Kamp O. Transient permeabilization of cell membranes by ultrasound-exposed microbubbles is related to formation of hydrogen peroxide. Am. J. Physiol. Heart Circ. Physiol. 291 (2006) H1595-601.
[16] Duvshani-Eshet M, Machluf M. Therapeutic ultrasound optimization for gene delivery: A key factor achieving nuclear DNA localization. J. Control. Release 108 (2005) 513-528.
[17] Duvshani-Eshet M, Baruch L, Kesselman E, Shimoni E, Machluf M. Therapeutic ultrasound-mediated DNA to cell and nucleus: bioeffects revealed by confocal and atomic force microscopy. Gene Ther. 13 (2006) 163-172.
[18] Juffermans LJ, Kamp O, Dijkmans PA, Visser CA, Musters RJ. Low-intensity ultrasound-exposed microbubbles provoke local hyperpolarization of the cell membrane via activation of BK(Ca) channels. Ultrasound Med. Biol. 34 (2008) 502-508.
[19] Sundqvist T, Liu SM. Hydrogen peroxide stimulates endocytosis in cultured bovine aortic endothelial cells. Acta Physiol. Scand. 149 (1993) 127-131.
[20] MacDonald PE, Eliasson L, Rorsman P. Calcium increases endocytotic vesicle size and accelerates membrane fission in insulin-secreting INS-1 cells. J. Cell Sci. 118 (2005) 5911-5920.
[21] Saliez J, Bouzin C, Rath G, Ghisdal P, Desjardins F, Rezzani R, Rodella LF, Vriens J, Nilius B, Feron O, Balligand JL, Dessy C. Role of caveolar compartmentation in endothelium-derived hyperpolarizing factor-mediated relaxation: Ca2+ signals and gap junction function are regulated by caveolin in endothelial cells. Circulation 117 (2008) 1065-1074.
[22] Meijering BD, Henning RH, van Gilst W, Gavrilovic I, van Wamel A, Deelman LE. Optimization of ultrasound and microbubbles targeted gene delivery to cultured primary endothelial cells. J. Drug Target. 15 (2007) 664-671.
[23] Zuhorn IS, Kalicharan R, Hoekstra D. Lipoplex-mediated transfection of mammalian cells occurs through the cholesterol-dependent clathrin-mediated pathway of endocytosis. J. Biol. Chem. 277 (2002) 18021-18028.
[24] Li H, Brodsky S, Basco M, Romanov V, De Angelis DA, Goligorsky MS. Nitric oxide attenuates signal transduction: possible role in dissociating caveolin-1 scaffold. Circ. Res. 88 (2001) 229-236.
[25] Falcone S, Cocucci E, Podini P, Kirchhausen T, Clementi E, Meldolesi J. Macropinocytosis: regulated coordination of endocytic and exocytic membrane traffic events. J. Cell Sci. 119 (2006) 4758-4769.

[26] Clarke MS, McNeil PL. Syringe loading introduces macromolecules into living mammalian cell cytosol. J. Cell Sci. 102(Pt 3) (1992) 533-541.
[27] Perez-Terzic C, Gacy AM, Bortolon R, Dzeja PP, Puceat M, Jaconi M, Prendergast FG, Terzic A. Structural plasticity of the cardiac nuclear pore complex in response to regulators of nuclear import. Circ. Res. 84 (1999) 1292-1301.
[28] Seksek O, Biwersi J, Verkman AS. Translational diffusion of macromolecule-sized solutes in cytoplasm and nucleus. J. Cell Biol. 138 (1997) 131-142.
[29] Miller DL, Quddus J. Sonoporation of monolayer cells by diagnostic ultrasound activation of contrast-agent gas bodies. Ultrasound Med. Biol. 26 (2003) 661-667.
[30] Bement WM, Yu HY, Burkel BM, Vaughan EM, Clark AG. Rehabilitation and the single cell. Curr. Opin. Cell Biol. 19 (2007) 95-100.
[31] Sun RJ, Muller S, Stoltz JF, Wang X. Shear stress induces caveolin-1 translocation in cultured endothelial cells. Eur. Biophys. J. 30 (2002) 605-611.
[32] Fawzi-Grancher S, Sun RJ, Traore M, Stoltz JF, Muller S. Role of Ca2+ in the effects of shear stress and TNF-alpha on caveolin-1 expression. Clin. Hemorheol. Microcirc. 33 (2005) 253-261.
[33] Orlandi PA, Fishman PH. Filipin-dependent inhibition of cholera toxin: evidence for toxin internalization and activation through caveolae-like domains. J. Cell Biol. 141 (1998) 905-915.
[34] Byfield FJ, Aranda-Espinoza H, Romanenko VG, Rothblat GH, Levitan I. Cholesterol depletion increases membrane stiffness of aortic endothelial cells. Biophys. J. 87 (2004) 3336-3343.
[35] Hilgenfeldt S, Lohse D, Zomack M. Sound scattering and localized heat deposition of pulse-driven microbubbles. J. Acoust. Soc. Am. 107 (2000) 3530-3539.
[36] Apodaca G. Modulation of membrane traffic by mechanical stimuli. Am. J. Physiol. Renal Physiol. 282 (2002) F179-F190.
[37] Niwa K, Sakai J, Karino T, Aonuma H, Watanabe T, Ohyama T, Inanami O, Kuwabara M. Reactive oxygen species mediate shear stress-induced fluid-phase endocytosis in vascular endothelial cells. Free Radic. Res. 40 (2006) 167-174.
[38] van Bavel E. Effects of shear stress on endothelial cells: possible relevance for ultrasound applications. Prog. Biophys. Mol. Biol. 93 (2007) 374-383.
[39] Wu LG. Kinetic regulation of vesicle endocytosis at synapses. Trends Neurosci. 27 (2004) 548-554.
[40] Idone V, Tam C, Goss JW, Toomre D, Pypaert M, Andrews NW. Repair of injured plasma membrane by rapid Ca2+-dependent endocytosis. J. Cell Biol. 180 (2008) 905-914.
[41] Hernot S, Klibanov AL. Microbubbles in ultrasound-triggered drug and gene delivery. Adv. Drug Deliv. Rev. 60 (2008) 1153-1166.
[42] Schneider M. Molecular imaging and ultrasound-assisted drug delivery. J. Endourol. 22 (2008) 795-802.
[43] Xu Y, Buikema H, Van Gilst WH, Henning RH. Caveolae and endothelial dysfunction: filling the caves in cardiovascular disease. Eur. J. Pharmacol. 585 (2008) 256-260.

Increasing the endothelial layer permeability through ultrasound-activated microbubbles

Klazina Kooiman[1], Marcia Emmer[1], Miranda Foppen-Harteveld[1], Annemieke van Wamel[1], Nico de Jong[1]

[1] Dept. of Biomedical Engineering, Erasmus MC, Rotterdam, the Netherlands

IEEE Transactions on Biomedical Engineering 2010; 57(1): 29-32

Abstract

Drug delivery to diseased tissue will be more efficient if the vascular endothelial permeability is increased. Recent studies have shown that the permeability of single cell membranes is increased by ultrasound in combination with contrast agents. It is not known whether this combination can also increase the permeability of an endothelial layer in the absence of cell damage. To investigate the feasibility of controlled increased endothelial layer permeability, we treated monolayers of human umbilical vein endothelial cells with ultrasound and the contrast agent BR14. Barrier function was assessed by measuring transendothelial electrical resistance (TEER). Ultrasound-activated BR14 significantly decreased TEER by 40.3 ± 3.7 % ($p < 0.01$). After treatment, no cell detachment or damage was observed. In conclusion, ultrasound-activated BR14 microbubbles increased the endothelial layer permeability. This feature may be used for future ultrasound-guided drug delivery systems.

4.1. Introduction

The vascular endothelium maintains the barrier between the blood and the extravascular tissues. It does not form a passive barrier but actively controls the extravasation of fluids, solutes, and cells into the surrounding tissues [1, 2]. Its integrity depends largely upon the presence of specialised junctions between adjacent endothelial cells [3]. On the other hand, the endothelial layer forms a major barrier for drug delivery into the extravascular tissue. A local increase in permeability of the endothelial layer may have important clinical implications as a more efficient delivery of drugs to a diseased tissue would be expected [1-3]. To enhance drug delivery to extravascular tissues, a controlled, temporal and local increase in endothelial layer permeability is needed. At the same time, transient opening of the vascular barrier should also make it possible to reduce drug doses and side effects.

Recent studies have established that ultrasound, when combined with a contrast agent, locally and transiently increases the permeability of membranes of single cells *in vitro* as well as *in vivo* [4-7]. *In vivo* drug delivery to the extravascular tissue of non-blood brain barrier (BBB) has also been reported but mostly with hemorrhage as a bioeffect [8, 9]. This study focuses on increasing the endothelial layer permeability of non BBB by means of ultrasound-activated microbubbles in the absence of cell damage. Permeability was determined by TEER which is a sensitive measure of endothelial layer integrity which effectively reflects rapidly occurring changes in endothelial permeability well ahead of any measurable changes in macromolecular transport across the monolayer [10].

4.2. Materials and Methods

4.2.1. Endothelial monolayers

Primary human umbilical vein endothelial cells (HUVECs; C2519A; Lonza, Verviers, Belgium) were cultured in EGM-2 medium (CC-3162; Lonza) and maintained at 37°C in a

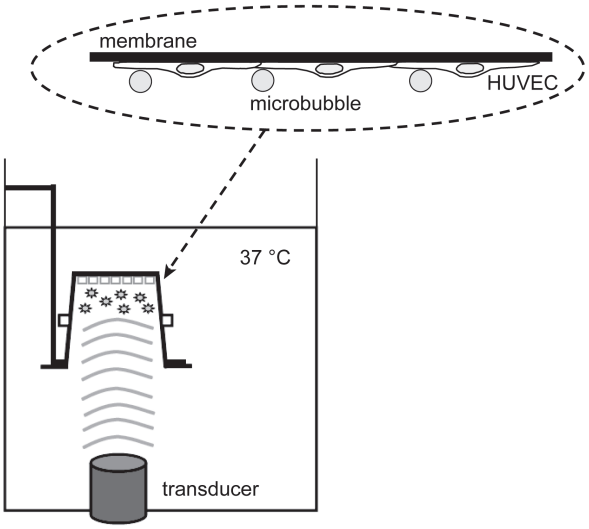

Fig. 4.1. Experimental set-up (not drawn to scale).

humidified incubator with 5% CO_2. HUVECs (passages 2-9) were detached by 0.25% trypsin in EDTA (Lonza) and replated onto ultrasound transparent membranes of cell culture inserts (23.1 mm diameter, PET membrane; 353090; BD Falcon, Alphen aan den Rijn, the Netherlands). Membranes were pre-treated with 1 ml Biomatrix I (90 µg/ml; Biomedical Technologies Inc., Stoughton, MA, USA) and left to air-dry overnight on a rotating shaker (250 rpm; LaboTech RS 300, Ochten, the Netherlands). EGM-2 was added to both inserts (i.e. apical; 2 ml) and wells (i.e. basolateral; 3 ml), and the membrane was equilibrated for 5 hours in the incubator before adding 1.25×10^6 cells per insert. Fluid volumes were selected to yield no hydrostatic pressure gradient across the cells.

4.2.2. Treatment of endothelial monolayer

Before treatment, culture medium was replaced with an equal volume of Krebs (in mM: NaCl 118, KCl 4.8, $CaCl_2$ 2.5, $MgSO_4$ 1.2, KH_2PO_4 1.2, $NaHCO_3$ 2.4, D-glucose 5 and HEPES 5; at pH 7.4), and monolayers were allowed to equilibrate in the incubator. Endothelial monolayers were treated by positioning the inserts upside down in a custom made micro-positioner in front of the ultrasound beam at a standoff distance of 60 mm in a 4 liter Krebs-filled tank (Fig. 4.1). The experimental ultrasound contrast agent BR14 (Bracco Suisse SA, Geneva, Switzerland) was added to the monolayer with a 1 ml syringe and customly curved blunt 19 gauge needle. BR14 is composed of perfluorobutane-containing microbubbles stabilised by a phospholipid monolayer coating. It was added in a microbubble-cell ratio of 1:1. To determine the number of microbubbles needed, cells of three inserts were counted in a haemacytometer before each experiment. After addition of the BR14, ultrasound (1 MHz) was given for 30 sec. Thereafter, BR14 was added to the monolayer again and

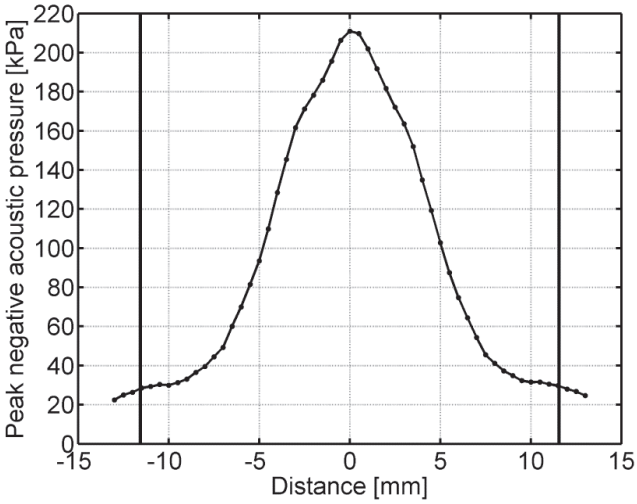

Fig. 4.2. Lateral beam profile of the 1 MHz unfocused single-element transducer at a standoff distance of 60 mm, i.e. where the endothelial monolayer was positioned. The two vertical lines represent the border of the insert, 23.1 mm in diameter.

ultrasound was given for another 30 sec. As this was repeated another two times, BR14 was added a total of four times and ultrasound was given a total of two minutes. The unfocused single-element transducer (1.27 cm in diameter; V303SU; Panametrics, Waltham, MA, USA) was driven by an arbitrary waveform generator (Agilent 33220A; Agilent Technologies, Amstelveen, the Netherlands) connected to a 60 dB power amplifier (model 150A100B; emv Benelux, Nieuwkoop, the Netherlands). The peak negative acoustic pressures (P_) distribution at the endothelial monolayer, as verified with a calibrated hydrophone (0.2 mm PVDF needle hydrophone, Precision Acoustics Ltd, Dorchester, UK), are given in Fig. 4.2. The highest peak negative acoustic pressure was 210 kPa, which corresponded to a mechanical index (MI) of 0.21. BR14 and monolayers were exposed to an ultrasonic burst consisting of 10,000 cycles of a sine wave with a repetition rate of 20 Hz.

Sham, ultrasound alone and BR14 alone were used as control treatments. After treatment, the inserts were taken out of the tank and Krebs was re-applied apically. As a positive control, 12 mM EDTA (apically only) was used as it increases endothelial layer permeability [11].

4.2.3. TransEndothelial Electrical Resistance (TEER)

Electrical resistances were measured by transferring the inserts to an Endohm-SNAP chamber (World Precision Instruments, Berlin, Germany). The chamber, filled with 5 ml of EGM-2 (during growth) or Krebs (during treatment), was coupled to an EVOMX resistance meter (World Precision Instruments). TEER, in $\Omega \cdot cm^2$, was calculated using (resistance of experimental insert - resistance of corresponding blank insert) × 4.2, where 4.2 is the area (in cm^2) of the insert membrane. After plating the HUVECs, TEER was monitored daily (n = 18 inserts; resistances of corresponding blank inserts were measured just before plating). During

treatments, TEER was determined after pre-incubation in Krebs and immediately after treatment. Resistances of corresponding blank inserts were measured at the end of the treatment by scraping off the cells with a rubber policeman (VWR, Amsterdam, the Netherlands). TEER was reported as percentage of the TEER measured after pre-incubation in Krebs.

4.2.4. Determination of cytotoxicity

To determine the cytotoxic effect of treatment, release of lactate dehydrogenase (LDH) was measured. Immediately after treatment and TEER measurement, EGM-2 medium was added to the cells. At 15, 30, 60, 90 and 120 minutes, 50 µl medium was taken from the apical chamber and replaced by an equal volume of pre-warmed EGM-2 to maintain fluid volumes. Samples were diluted 1:1 with EGM-2 without fetal bovine serum (FBS) to get a 1% FBS concentration, which was required for the LDH diagnostic kit (Roche Diagnostics, the Netherlands). LDH release was measured according to the manufacture's instructions. Absorbance was measured at 490 and 655 nm in a Model680 microplate reader (Bio-Rad, Veenendaal, the Netherlands). Released LDH was expressed as a percentage of sham treatment and corrected for repetitive sampling. Monolayers treated with 1% Triton X-100 (Sigma, Zwijndrecht, the Netherlands) in EGM-2 were used as positive controls. Experiments were done twice in triplicate.

4.2.5. Morphology

Immediately after treatment EGM-2 medium was added to the cells and morphology was studied up to three hours after treatment. Pictures were taken using a Zeiss AxioVert 100M inverted microscope with an Epiplan NeoFluar 10× lens and AxioCam camera (Carl Zeiss, Sliedrecht, the Netherlands).

4.2.6. Statistical analysis

Results were expressed as mean ± SEM. Comparisons among multiple groups were performed using a one-way ANOVA followed by Dunnett's multiple comparison test (GraphPad InStat verion 4.0, GraphPad Software, San Diego, CA, USA). Differences were considered significant if $p < 0.05$.

4.3. Results

After plating, TEER was used to assess the integrity of the endothelial monolayer and the formation of tight junctions. TEER reached maximum values 3 days post-plating, stabilised for 2 days and then decreased daily as previously reported by others [12]. Maximum TEER at day 3 was 23.1 ± 0.2 $\Omega \cdot cm^2$, indicating that this time was required for monolayers to develop well-formed intercellular junctions as established by others [12, 13]. Accordingly, all experiments were performed on inserts 3 days post-plating. Three days post-plating the monolayer consisted of 0.61 ± 0.02 $\times 10^6$ cells (n=15 inserts), which is 49% of the initially

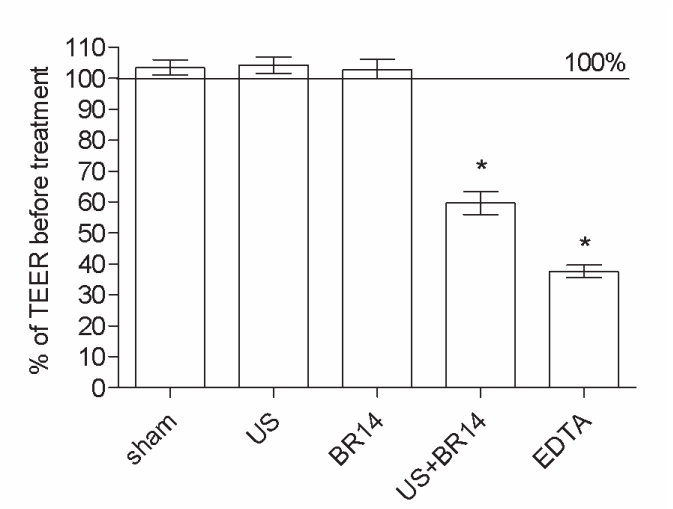

Fig. 4.3. TEER expressed as percentage of TEER after 30 min pre-incubation in Krebs for sham, ultrasound (US), BR14, US in combination with BR14, and EDTA treatment (*: significantly lower than sham, $p < 0.01$). Columns, means; bars, ± SEM; n = 15-22 inserts.

plated amount. Plating fewer cells however, did not result in a visible confluent monolayer nor were maximum TEER values reached.

On the day of the experiments (i.e. 3 days post-plating), culture medium was replaced with Krebs, and monolayers were allowed to equilibrate 30 min in the incubator. This was found to be sufficient to re-establish baseline TEER.

Ultrasound in combination with the contrast agent BR14 decreased TEER significantly to 59.7 ± 3.7 % ($p < 0.01$) (Fig. 4.3). Sham, ultrasound alone and BR14 treatment alone did not significantly change TEER. As expected, EDTA significantly decreased TEER to 37.6 ± 2.0 % ($p < 0.01$).

LDH release measurements were done to define whether direct cytotoxicity contributed to the lower TEER. No significant differences from sham-treated monolayers were found for monolayers treated with ultrasound in combination with BR14, ultrasound alone or BR14 alone, indicating that these treatments had no toxic effect on the HUVECs. Monolayers treated with 1% Triton X-100 showed a 4.3-fold increase in LDH release compared to sham treatment.

Microscopic examinations revealed no apparent cell loss directly after treatment and up to 3 hours after treatment for all treatment groups, except for the EDTA positive control group (Fig. 4.4). Three hours after EDTA treatment, cells rounded up and detached from the insert, indicating loss of contact and initiation of intercellular gap formation.

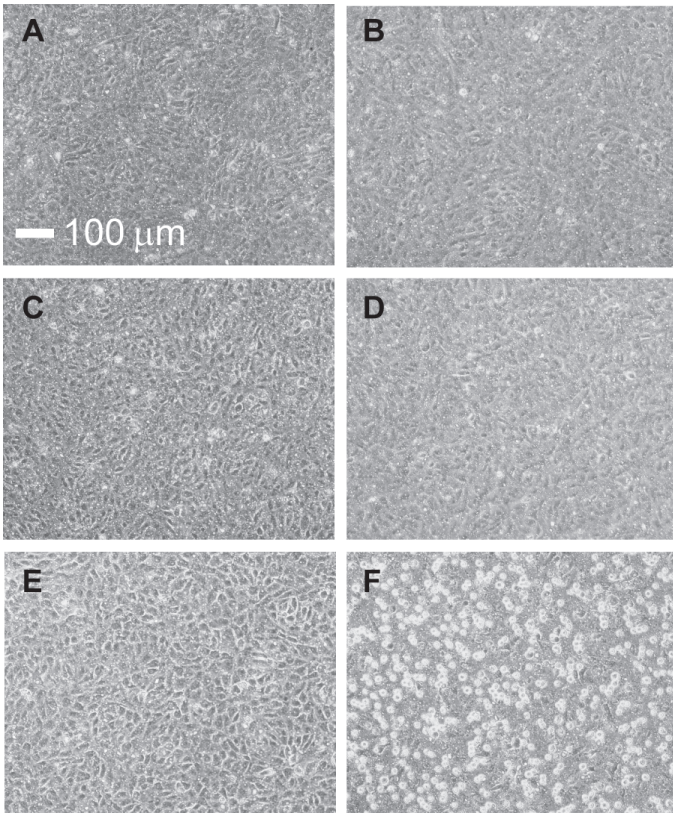

Fig. 4.4. Microscopic examination of monolayers directly after treatment (a, c, e) and 3 hours after treatment (b, d, f) for sham (a, b), ultrasound and BR14 (c, d), and EDTA (e, f) treated endothelial monolayers.

4.4 Discussion

Endothelial monolayers treated with the combination of ultrasound and BR14 significantly decreased TEER values to 59.7 ± 3.7% of initial values. This was not a consequence of cell loss or direct cytotoxicity. In addition, ultrasound or BR14 treatments alone were not able to decrease TEER.

HUVECs are widely used to study endothelial barrier function [10, 12-14]. In our study we used these cells as an *in vitro* model system to simulate microbubble interactions with the vessel wall and to study effects of ultrasound-activated microbubbles on endothelial barrier function. EDTA treatment resulted in a lower TEER than treatment with ultrasound-activated BR14. Whereas EDTA chelates all Ca^{2+} and can thereby open all cell-cell junctions [11], only BR14 present within the ultrasound beam may have been able to affect cells. In addition, the lateral beam profile of the transducer used in this study (Fig. 4.2) indicates that different parts of the monolayer were insonified at different P_. Not all microbubbles may therefore have

been activated by the ultrasound nor might their oscillation amplitude have been the same [15]. The range of pressures at which ultrasound-activated microbubbles influence endothelial layer permeability and whether there may be a threshold needs further investigation.

It is known that ultrasound facilitates the delivery of drugs and genes through a complex interplay of the therapeutic agent, microbubble characteristics, target tissue, and ultrasound energy [16]. Our study revealed that ultrasound-activated BR14 increased endothelial layer permeability without cell loss or cytotoxicity. This is in contrast to another *in vitro* study which showed disruption of HUVEC monolayers using Definity as the contrast agent [17]. The difference may be explained by the ultrasound energy (continuous wave at MI of 0.4 versus pulsed wave at MI of 0.2 in our study) and the use of different ultrasound contrast agents (Definity versus BR14 in our study).

The mechanism by which ultrasound-activated BR14 increase endothelial layer permeability will be the subject of our future studies and may involve opening of the cell-cell junctions, just as reported for *in vivo* BBB opening using ultrasound-activated Optison microbubbles [18], although the BBB has much tighter cell-cell junctions than other parts of the vasculature [19]. We will also study whether permeability is transient and assess whether drug delivery is increased. Further studies may also enable us to understand the complex interplay of microbubbles and the endothelial layer. These findings are important for agents that have difficulty crossing the endothelial barrier. An example is chemotherapeutic drugs as a high interstitial fluid pressure and a chaotic vasculature hinders the traverse of chemotherapeutic drugs from the bloodstream into the tumour tissue. Ten Hagen et al. [20] use vasoactive compounds, like tumour necrosis factor alpha, histamine and interleukin-2 to increase permeability of the tumour-associated vasculature resulting in an increased accumulation of chemotherapeutic drug in the tumour tissue. They have recently called this process tumour vessel abnormalisation [20, 21]. With the use of locally applied ultrasound in combination with a contrast agent that manipulates the vasculature to become more permeable, we may also be able to deliver drugs more efficiently to tumours.

Acknowledgement

This project is supported by innovation subsidies collaborative projects by the Dutch Ministry of Economic Affairs under number IS042035. The authors want to thank Bracco Suisse SA, Geneva, Switzerland for kindly providing the BR14 samples. The authors thank Leo Bekkering (Dept. Biomedical Engineering, Erasmus MC) for his technical assistance and Dr. Ann L.B. Seynhaeve (Dept. Surgical Oncology, Erasmus MC) for her assistance with the morphology studies and insightful suggestions.

References

[1] J.R. Gudgeon, W. Martin, Modulation of arterial endothelial permeability: studies on an in vitro model. Br. J. Pharmacol. 98(4) (1989) 1267-1274.

[2] G.P. van Nieuw Amerongen, V.W. van Hinsbergh, Targets for pharmacological intervention of

endothelial hyperpermeability and barrier function. Vasc. Pharmacol. 39(4-5) (2002) 257-272.
[3] P. Telo, S. Lostaglio, E. Dejana, Structure of intercellular junctions in the endothelium. Therapie 52(5) (1997) 395-398.
[4] S. Mehier-Humbert, T. Bettinger, F. Yan, R.H. Guy, Plasma membrane poration induced by ultrasound exposure: Implication for drug delivery. J. Control. Release 104(1) (2005) 213-222.
[5] H. Pan, Y. Zhou, O. Izadnegahdar, J. Cui, C.X. Deng, Study of sonoporation dynamics affected by ultrasound duty cycle. Ultrasound Med. Biol. 31(6) (2005) 849-856.
[6] A. van Wamel, K. Kooiman, M. Harteveld, M. Emmer, F.J. ten Cate, M. Versluis, N. de Jong, Vibrating microbubbles poking individual cells: drug transfer into cells via sonoporation. J. Control. Release 112(2) (2006) 149-155.
[7] B.D. Meijering, L.J. Juffermans, A. van Wamel, R.H. Henning, I.S. Zuhorn, M. Emmer, A.M. Versteilen, W. Paulus, W.H. van Gilst, K. Kooiman, N. de Jong, R.J. Musters, L.E. Deelman, O. Kamp, Ultrasound and microbubble-targeted delivery of macromolecules is regulated by induction of endocytosis and pore formation. Circ. Res. 104(5) (2009) 679-687.
[8] D.L. Miller, J. Quddus, Diagnostic ultrasound activation of contrast agent gas bodies induces capillary rupture in mice. Proc. Natl. Acad. Sci. USA 97(18) (2000) 10179-10184.
[9] R.J. Price, D.M. Skyba, S. Kaul, T.C. Skalak, Delivery of colloidal particles and red blood cells to tissue through microvessel ruptures created by targeted microbubble destruction with ultrasound. Circulation 98(13) (1998) 1264-1267.
[10] N. Gautam, P. Hedqvist, L. Lindbom, Kinetics of leukocyte-induced changes in endothelial barrier function. Br. J. Pharmacol. 125(5) (1998) 1109-1114.
[11] W. Tschugguel, Z. Zhegu, L. Gajdzik, M. Maier, B.R. Binder, J. Graf, High precision measurement of electrical resistance across endothelial cell monolayers. Pflugers Arch. 430(1) (1995) 145-147.
[12] P.G. Bannon, M.J. Kim, R.T. Dean, J. Dawes, Augmentation of vascular endothelial barrier function by heparin and low molecular weight heparin. Thromb. Haemost. 73(4) (1995) 706-712.
[13] M.H. Ali, S.A. Schlidt, N.S. Chandel, K.L. Hynes, P.T. Schumacker, B.L. Gewertz, Endothelial permeability and IL-6 production during hypoxia: role of ROS in signal transduction. Am. J. Physiol. 277(5 Pt 1) (1999) L1057-1065.
[14] A.L. Seynhaeve, C.E. Vermeulen, A.M. Eggermont, T.L. ten Hagen, Cytokines and vascular permeability: an in vitro study on human endothelial cells in relation to tumor necrosis factor-alpha-primed peripheral blood mononuclear cells. Cell Biochem. Biophys. 44(1) (2006) 157-169.
[15] M. Emmer, A. van Wamel, D.E. Goertz, N. de Jong, The onset of microbubble vibration. Ultrasound Med. Biol. 33(6) (2007) 941-949.
[16] J.M. Tsutsui, F. Xie, R.T. Porter, The use of microbubbles to target drug delivery. Cardiovasc. Ultrasound 2(1) (2004) 23.
[17] N.R. Soman, J.N. Marsh, M.S. Hughes, G.M. Lanza, S.A. Wickline, Acoustic activation of targeted liquid perfluorocarbon nanoparticles does not compromise endothelial integrity. IEEE T. Nanobiosci. 5(2) (2006) 69-75.
[18] N. Sheikov, N. McDannold, S. Sharma, K. Hynynen, Effect of focused ultrasound applied with an ultrasound contrast agent on the tight junctional integrity of the brain microvascular endothelium. Ultrasound Med. Biol. 34(7) (2008) 1093-1104.
[19] G. Bazzoni, O. Martinez Estrada, E. Dejana, Molecular structure and functional role of vascular tight junctions. Trends Cardiovasc. Med. 9(6) (1999) 147-152.
[20] T.L. ten Hagen, A.L. Seynhaeve, A.M. Eggermont, Tumor necrosis factor-mediated interactions between inflammatory response and tumor vascular bed. Immunol. Rev. 222 (2008) 299-315.
[21] A.L. Seynhaeve, A.M. Eggermont, T.L. ten Hagen, TNF and manipulation of the tumor cell-stromal interface: "ways to make chemotherapy effective". Front. Biosci. 13 (2008) 3034-3045.

Mechanisms of increased endothelial layer permeability through ultrasound-activated microbubbles

Klazina Kooiman[1], Geerten P. van Nieuw Amerongen[2], Victor W.M. van Hinsbergh[2], Nico de Jong[1,3,4]

[1] Dept. of Biomedical Engineering, Thoraxcenter, Erasmus MC, Rotterdam, the Netherlands
[2] Dept. of Physiology, Institute for Cardiovascular Research, VU University Medical Center, Amsterdam, The Nethelands
[3] Interuniversity Cardiology Institute of the Netherlands, Utrecht, the Netherlands
[4] Physics of Fluids Group, University of Twente, Enschede, the Netherlands

Based on unpublished results

Sonoporation of endothelial cells by vibrating targeted microbubbles

Klazina Kooiman[1], Miranda Foppen-Harteveld[1],
Antonius F.W. van der Steen[1,2], Nico de Jong[1,2,3]

[1] Dept. of Biomedical Engineering, Thoraxcenter, Erasmus MC, Rotterdam, the Netherlands
[2] Interuniversity Cardiology Institute of the Netherlands, Utrecht, the Netherlands
[3] Physics of Fluids Group, University of Twente, Enschede, the Netherlands

Submitted

Oil-filled polymer microcapsules for ultrasound-mediated delivery of lipophilic drugs

Klazina Kooiman[1], Marcel R. Böhmer[2], Marcia Emmer[1], Hendrik J. Vos[1], Ceciel Chlon[2], William T. Shi[3], Christopher S. Hall[3], Suzanne H.P.M. de Winter[2], Karin Schroën[4], Michel Versluis[5], Nico de Jong[1,5,6], Annemieke van Wamel[1]

[1] Dept. of Biomedical Engineering, Erasmus MC, Rotterdam, the Netherlands
[2] Philips Research Laboratories Eindhoven, Eindhoven, the Netherlands
[3] Philips Research Laboratories North America, Briarcliff Manor, NY, USA
[4] Food and Bioprocess Engineering Group, Dept. of Agrotechnology and Food Sciences, Wageningen University, Wageningen, the Netherlands
[5] Physics of Fluids Group, University of Twente, Enschede, the Netherlands
[6] Interuniversity Cardiology Institute of the Netherlands, Utrecht, the Netherlands

Journal of Controlled Release 2009; 133: 109-118

Abstract

The use of ultrasound contrast agents as local drug delivery systems continues to grow. Current limitations are the amount of drug that can be incorporated as well as the efficiency of drug release upon insonification. This study focuses on the synthesis and characterisation of novel polymeric microcapsules for ultrasound-triggered delivery of lipophilic drugs. Microcapsules with a shell of fluorinated end-capped poly(L-lactic acid) were made through pre-mix membrane emulsification and contained, apart from a gaseous phase, different amounts of hexadecane oil as a drug-carrier reservoir. Mean number weighted diameters were between 1.22 μm and 1.31 μm. High-speed imaging at ~10 million fames per second showed that for low acoustic pressures (1 MHz, 0.24 MPa) microcapsules compressed but remained intact. At higher diagnostic pressures of 0.51 MPa, microcapsules cracked, thereby releasing the encapsulated gas and model lipophilic drug. Using conventional ultrasound B-mode imaging at a frequency of 2.5 MHz, a marked enhancement of scatter intensity over a tissue-mimicking phantom was observed for all differently loaded microcapsules. The partially oil-filled microcapsules with high drug loads and well-defined acoustic activation thresholds have great potential for ultrasound-triggered local delivery of lipophilic drugs under ultrasound image-guidance.

7.1. Introduction

Ultrasound contrast agents (UCA) are routinely used to enhance diagnostic ultrasound (US) imaging. Nowadays, their potential as local drug delivery systems is widely recognised and their use for this purpose continues to expand [1-4]. UCA contain gas microbubbles that are coated by a lipid, protein, sugar, or polymer shell. The diameter of the microbubbles is in the range of 1 to 10 μm [5-7]. The advantage of using them as a drug delivery system is the ability to trigger drug release only at the region of interest. In addition, US imaging of these UCA-based drug delivery systems will aid the guidance and monitoring of therapy [2, 4, 8].

As with all local drug delivery systems, the aim is to achieve a specific pharmacological response of a therapeutic agent at a particular diseased site in the body. The benefits are a more controlled biodistribution of the therapeutic agent which will not only reduce side-effects, but also improve therapeutic efficacy. This is especially important for therapeutic agents that are very toxic, lack a specific affinity toward a pathological site, or have a low bioavailability because they are rapidly cleared or inactivated by blood components and detoxifying systems [9-12].

In general, two UCA-based drug delivery systems are distinguished. In the first system, the therapeutic agent is co-administered with the UCA so that the UCA circulates through the bloodstream alongside the therapeutic agent. When US is applied locally, endothelial cell membrane permeability will locally and transiently increase and the therapeutic agent will be taken up by the cell or tissue [6, 13, 14]. In the second system, the therapeutic agent is attached to or incorporated into the microbubbles. Microbubbles of different composition have been designed to carry hydrophilic as well as lipophilic therapeutic agents. When US is

applied locally, these microbubbles are triggered to locally release their payload [1, 2, 4, 6, 7]. For this type of UCA-based drug delivery system, it is important that the microbubbles: (1) incorporate an efficient payload of the drug; (2) can be triggered to release the drug with diagnostic US; (3) can be imaged under non-destructive conditions so that US can be used for guidance and monitoring of therapy [2, 4, 7, 14, 15]. Loading a sufficient amount of therapeutic agent onto or into a microbubble as well as its efficient release are current limitations for these UCA-based drug delivery systems [7, 15].

Instead of incorporating a therapeutic compound into or onto the shell of a microbubble, an additional oil-phase can be incorporated into the microbubbles which increases their lipophilic drug-carrier reservoirs considerably. For lipid-coated microbubbles, this approach has been reported and US-triggered release of the chemotherapeutic drug paclitaxel was demonstrated [16, 17]. Using a similar approach, we incorporated an oil-phase in a polymer-shelled UCA. Fluorinated end-capped polymer poly(L-lactic acid), abbreviated as pLA-pFO, was chosen as the shell material. The fluorinated end groups of the pLA-pFO change the surface properties of this biodegradable polymer and make the shell hydrophobic, thereby improving water resistance [18, 19]. Hexadecane oil was chosen as drug-carrier reservoir not only because it is non-polar which makes it ideal to solve lipophilic (model) drugs in [20, 21], but also because it is a poor solvent for poly(L-lactic acid) [22]. In addition, hexadecane hardly lyophilises during freeze-drying, making it easy to control the amount of oil and drug encapsulation. The aim was to use diagnostic US to release the oil so that the incorporated drug is released from a solution or a fine dispersion rather than through diffusion from the shell of the polymer microbubbles, as the latter has been shown to be inherently slow [23]. Preliminary *in vitro* and *in vivo* studies only suggested the potential of half oil-filled microcapsules as a UCA-based drug delivery system [24]. Important characteristics, such as the acoustic response, the mechanism of US-triggered drug release, and the effect of the amount of encapsulated oil on the acoustic properties were not investigated yet. In this study, we investigate the potential of partially oil-filled microcapsules as UCA-based drug delivery system for lipophilic drugs based on the efficiency to incorporate oil in the microcapsules, the particle size distribution, morphology, acoustic properties, US-triggered drug release, and US imaging capacity.

7.2. Materials and methods

7.2.1. Microcapsule preparation

For the polymer microcapsule shell, poly(L-lactic acid) terminated with 1H-1H perfluoro-octan-1-ol (MW 3,000), abbreviated as pLA-pFO, was used [18]. The microcapsules were prepared from a 5% (w/w) solution of pLA-pFO in dichloromethane (DCM; Merck, Schiphol, the Netherlands; 1.06050.1000). To 250 mg of this solution, a total of 100 mg of cyclodecane (Fluka, Buchs, Switzerland; 28699) and hexadecane (Sigma-Aldrich, Zwijndrecht, the Netherlands; H6703) were added at a ratio of 1:0 for the production of completely gas-filled microcapsules (S_c), at a ratio 1:1 for the production of half oil-filled microcapsules (S_{ch}), and

at a ratio 0:1 for the production of almost completely oil-filled microcapsules (S_h). As a reference sample, solid polymer particles were prepared from the 5% pLA-pFO solution in DCM without the addition of alkanes. The DCM-based solutions were emulsified with 20 g of 0.3% (w/w) poly-vinylalcohol (PVA; Fluka, Buchs, Switzerland; 81383) in water. First, the mix was shaken manually to prepare a premix and then pressed 10 times through an Acrodisk glass filter (1 µm pore size; Gelman, Ann Arbor, MI, USA) for the formation of emulsion droplets. Subsequently, the emulsion was stirred for one hour to remove the DCM by dissolution in the aqueous phase and subsequent evaporation. After removal of the DCM, a 20% (w/w) poly(ethylene glycol) (PEG, MW 3,000; Sigma-Aldrich, Zwijndrecht, the Netherlands; 20,244-4) solution was added to obtain a total PEG concentration of 5% (w/w) in the suspension. The sample was centrifuged at 3,000 rpm (~ 968 *g*) for 30 minutes (Biofuge Stratos, Heraeus, Hanau, Germany). The top fraction was collected and washed two more times in the presence of PEG, after which the sample was filtered over a 13 µm fiber cloth (Kabel Metaal, Zaandam, the Netherlands) and rapidly frozen at – 80 °C in a pre-cooled glass vial. To remove the ice and the cyclodecane fraction, freeze-drying took place in an Epsilon 2-6 freeze drier (Martin Christ, Osterode am Harz, Germany) at 1.98 mbar for 20 hours and then at 0.03 mbar for another 20 hours. After freeze-drying, the apparatus was filled with nitrogen. Lyophilised microcapsules were stored at 4 °C until use, and re-dispersed in 5 ml deionised water for all studies unless mentioned otherwise. The absorbing dye Sudan Black (Sigma-Aldrich, Zwijndrecht, the Netherlands; 199664) is a hydrophobic molecule and was chosen to mimic a lipophilic model drug. For specific experiments, Sudan Black was incorporated into the microcapsules by adding 0.52 mg (S_c and S_h) or 0.26 mg (S_{ch}) Sudan Black to the 5% (w/w) solution of pLA-pFO in DCM during the microcapsule preparation.

7.2.2. Composition of microcapsules

7.2.2.1. Modulated Differential Scanning Calorimetry (MDSC)

For the determination of the microcapsule composition by MDSC, the microcapsule preparation was carried out without PEG since it affects the MDSC analysis. As the only function of PEG is to get rapid re-dispersion of the microcapsules, it is not needed for the MDSC analysis. MDSC experiments were performed using a Q1000 calorimeter (TA-instruments, New Castle, DE, USA). For the analysis, lyophilised microcapsules and the pLA-pFO polymer were weighed (~ 0.5 mg) on an MX5 precision balance (Mettler Toledo, Tiel, the Netherlands) and then packed in Perkin-Elmer aluminium pans (Groningen, the Netherlands). Empty reference pans were included. A modulated heating program was used. The temperature of the pans was first equilibrated at -50 °C. The heating cycle started from this point until 200 °C at a rate of 5 °C/min. The amplitude of the modulation was 1 °C at a period of 60 sec. The MDSC program used here is similar to other programs found in the literature for the analysis of poly(lactic acid) microspheres [25, 26] and fibers [27].

7.2.2.2. Gas Chromatography/Mass Spectrometry (GC/MS)

To quantify hexadecane inclusion in the microcapsules, GC/MS was performed. For this analysis, the microcapsule preparation procedure was carried out without the addition of PEG, as in the MDSC experiments. An Agilent 6890 Gas Chromatograph with a 5973N quadrupole Mass Spectrometer (Amstelveen, the Netherlands) was used. Lyophilised microcapsules dissolved in DCM (at a concentration of ~ 0.5 mg/ml) were injected, using a CTC CombiPAL sample robot (Zwingen, Switzerland), into a split/splitless injector. In split mode, 1 µl was injected (1:150) at 300 °C. Compounds were separated on a Varian-Chrompack VF1-MS column (30 m x 0.25 mm I.D. x 0.25 µm film). The carrier gas was helium at a flow rate of 1.0 ml/minute. The oven temperature of 80 °C was ramped to 240 °C at 20 °C/minute, followed by a ramp of 10°C/minute to 300 °C, and held at 300 °C for 2 minutes. Spectra were recorded using electron impact (EI) ionisation with nominal electron energy of 70 eV. The scan range was m/z 29-400. The temperature of the mass spectrometer source was set at 230 °C and the quadrupole was set at 150 °C. Measurements were done in triplicate. Calibration curves (n = 3) were prepared with known concentrations of cyclodecane and hexadecane diluted in DCM, yielding linear regression coefficients of $R^2 > 0.999$.

7.2.2.3. Gas encapsulation

The amount of encapsulated gas in the microcapsules was determined with oscillating U-tube densitometry with a DMA 5000 (Anton Paar, Graz, Austria) as reported previously [28, 29]. First, the density of the re-dispersed microcapsules was measured in triplicate (microcapsule concentration was ~ 1 % v/v). Then, 5 ml of re-dispersed microcapsules were sonicated for 30 seconds with a Sonifier 250 (microtip, output level 5; Branson, Danbury, CT, USA) to destroy the microcapsules and thereby remove the encapsulated gas. Thereafter, density was measured again in triplicate. The encapsulated gas fraction (% v/v) was calculated using $(\rho_{\text{after sonication}} - \rho_{\text{before sonication}}) / (\rho_{\text{after sonication}} - \rho_{\text{air}})$. The encapsulated gas fraction per microcapsule (in %) was calculated by dividing the encapsulated gas fraction by the volume of the microcapsules: $\frac{4}{3}\pi N \sum_{i=1}^{k} x_i r_i^3$, where x_i is the number fraction, r_i the radius of that fraction, and k the number of bins (as determined with the Coulter Counter).

7.2.2.4. Microcapsule size distribution

Microcapsule size distributions were measured (n = 3) on a Coulter Counter Multisizer 3 (Beckman Coulter, Mijdrecht, the Netherlands). A 20 µm aperture tube was used, allowing quantification between 0.40 and 12 µm using a linear spacing between the 256 channels. Size distributions were determined before and after the microcapsules were freeze-dried. To assess the polydispersity of the samples the SPAN was calculated, which illustrates the width of the distribution, by using (d90%-d10%)/d50% where d90, d10 and d50 are the microcapsule diameters below which 90, 10, and 50% of the cumulative amount of microcapsules is found.

7.2.2.5. Transmission Electron Microscopy (TEM) and Scanning Electron Microscopy (SEM)

TEM was used to obtain an impression of microcapsule shell thickness and to determine whether they contained gas and/or oil. Samples were prepared by applying lyophilised microcapsules onto standard TEM grids (C foil on Cu grid; Agar formvar/carbon films, Stansted, UK). TEM studies were performed using a CM12 system (Philips, Eindhoven, the Netherlands), operating at 120 kV in low-dose mode. SEM was used to evaluate the surface structure of the microcapsules. Samples were prepared by applying a drop of re-dispersed microcapsules on a silica substrate. Samples were dried and SEM studies were performed using a SEM XL 40 FEG system (Philips, Eindhoven, the Netherlands).

7.2.3. Acoustic properties of the microcapsules

7.2.3.1. Attenuation

Ultrasonic properties of the microcapsules and solid polymer particles were determined *in vitro* by measuring the attenuation as a function of frequency. A pulse-echo set-up was employed using the back wall of the sample chamber as a reflector. In a water tank, four focused single element transducers (V305, centre frequency of 2.5 MHz; V308, centre frequency of 5 MHz; V319, centre frequency of 15 MHz; and V317, centre frequency of 20 MHz; Panametrics-NDT^{TM}, Olympus NDT, Waltham, MA, USA) were mounted in parallel to allow attenuation measurements from 0.3-22 MHz on the same sample. The back wall of the sample chamber was positioned in the focus of the transducers. To obtain sufficient attenuation of the microcapsules and solid polymer particles, different dilutions in deionised water were applied. S_c and S_{ch} microcapsules were diluted 1:3,000 in the 430 ml sample chamber, the S_h microcapsules were diluted 1:1,000, and the solid polymer particles were diluted 1:300. A magnetic stirrer was used to ensure a homogeneous distribution of microcapsules. The input of the transducers was 1 cycle of a sine at the centre frequency, which resulted in short pulses with a mechanical index (MI) of 0.033, as was verified by a calibrated hydrophone (0.2 mm PVDF needle hydrophone for the 2.5-15 MHz transducer, 0.075 mm PVDF needle hydrophone for the 20 MHz transducer; both Precision Acoustics Ltd, Dorchester, UK). The difference in received energy before and after the addition of microcapsules or solid polymer particles determined the attenuation by the microcapsules or solid polymer particles. For each transducer, the attenuation was calculated at –20 dB bandwidth around the centre frequency and divided by the acoustic path length. Because attenuation is linearly dependent on the concentration of microbubbles [30], the attenuation could be normalised to a microcapsule or solid polymer particle concentration of 3.5×10^5/ml. Data were smoothed using a power spectral density estimate via Welch's method (8192-point FFT, 64 segments, 70% overlap) (pwelch function in Matlab, Mathworks, Natick, MA, USA).

7.2.3.2. Event counts

Single microcapsule activation as a function of peak negative acoustic pressure (P_) was determined using event counts. A description and schematic overview of the set-up is given in reference [31]. Briefly, when the P_ was increased above a certain threshold value, the

insonified microcapsules disrupted, which released their gas content. Free gas microbubbles resonate when exposed to US and at the P_ applied, they radiated significant harmonic energy. A microcapsule disruption event was detected and counted when the harmonic energy increased above a defined level (RMS amplitude higher than 2.0 mV). To ensure single microcapsule detection, the microcapsule concentration in the 3.4 l water tank was ~17 microcapsules/ml. For each acoustic pressure, a percentile event count was determined by dividing the number of counted events by the total number of insonifications (n = 300). Each percentile event count measurement was repeated independently for at least three times.

7.2.3.3. Scattering

To determine scattering as function of insonification amplitude in P_ of escaped gas bubbles when single microcapsules cracked upon insonification, the same data as for the event count measurements were used. Scattering, relative to the incident intensity, was calculated by dividing the power of the averaged receive transducer output (in mV) by the power of the transmit transducer input (in mV), which was then normalised to the highest scattering intensity.

7.2.4. Characterisation of microcapsule behaviour and drug release

7.2.4.1. Microcapsule behaviour during insonification

Microcapsule behaviour during insonification was studied using the Brandaris-128 high-speed camera system [32]. The experimental set-up was described by for example Emmer et al. [33]. A 1.0 MHz single element transducer (V302; Panametrics-NDT^{TM}, Olympus NDT, Waltham, MA, USA) transmitted 10-cycle-sine wave bursts, with P_ ranging from 0.17 to 0.51 MPa (MI = 0.17 to 0.51), as verified with a calibrated 0.2 mm PVDF needle hydrophone (Precision Acoustics Ltd, Dorchester, UK). Images of insonified microcapsules were recorded using a 60× water-immersed objective (LUMPlanFI, Olympus, Zoeterwoude, the Netherlands) and 4× magnifier, and recorded in six sequences of 128 image frames at a speed near 10 million frames per second. The time between the sequences was 80 ms. An area-time curve was extracted from the recorded images according to the procedure described in [34]. Images were processed through contrast stretching in Matlab (Mathworks, Natick, MA, USA).

7.2.4.2. Drug release

Sudan Black release relative to the amount encapsulated was quantified in triplicate for S_c and S_{ch} microcapsules. Lyophilised microcapsules were re-dispersed in 4 ml deionised water and put into a 10 ml syringe. Until the opaqueness markedly changed, microcapsules were compressed by applying pressure to the piston whilst blocking the opening of the syringe by parafilm [29]. The sample was then centrifuged at 500 rpm (Biofuge Stratos, Heraeus, Hanau, Germany). The top fraction (i.e. released fraction) was retrieved (~ 1 ml), to which 4 g of dodecane (Fluka, Buchs, Switzerland; 44020) was added. Water was added to the remaining fraction to obtain a total volume of 10 ml, and this was centrifuged at 4000 rpm. The bottom fraction (i.e. non-released fraction) was now retrieved, to which 4 g of dodecane was added.

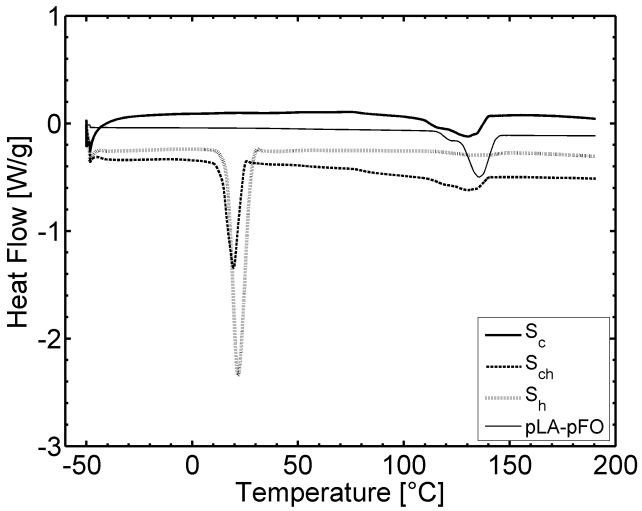

Fig. 7.1. MDSC thermogram of pLA-pFO and microcapsules re-dispersed after freeze-drying. Given is the heat flow during the heating cycle. The melting peak of hexadecane (18°C) is clearly visible in the S_{ch} and S_h microcapsules, indicating that these were filled with hexadecane. No melting peak of cyclodecane (9.5°C) was visible in all three differently loaded microcapsules, indicating that it had successfully been removed in the freeze-drying process.

Sudan Black was extracted to the dodecane phase for 72 hours and absorbance at 560 nm was measured on a FLUOstar microplate reader (BMG Labtech, Offenburg, Germany). As a reference, microcapsules were not compressed. Drug release from a single microcapsule was also studied using optical recording at video frame rate. The experimental set-up was similar to the one described in section 7.2.4.1. However, instead of the Brandaris-128 high-speed camera, a high sensitivity CCD camera (LCL-902K, Watec, Orangeburg, NY, USA) was mounted on top of the microscope. Recordings were taken at 30 frames/sec, using a 60× water-immersed objective lens (for S_h microcapsules) (LUMPlanFI, Olympus, Zoeterwoude, the Netherlands) and 2× magnifier (for S_c and S_{ch} microcapsules). Microcapsules were insonified with one burst of a 10 cycle-sine wave at a P_ of 0.51 MPa (MI = 0.51). Images were processed through contrast stretching in Matlab (Mathworks, Natick, MA, USA) and minor pieces of dust on the CCD, not overlapping the microcapsule before and after insonifaction, were removed with the clone brush in Paint Shop Pro 8.

7.2.5. Ultrasound imaging

To determine the imaging capacity of the microcapsules, *in vitro* diagnostic US imaging was performed. A 2.2 l water tank was filled with water, and a magnetic stirrer was used to ensure a homogeneous distribution of the microcapsules. An acoustic absorbing pad was placed on the bottom of the tank to reduce reflections. On top of this pad, a tissue-mimicking phantom (TMP) was placed (7 cm in diameter, 7 cm in height) that was made of 2% (w/w)

agar (CMN 50048, Boom, Meppel, the Netherlands) and 0.2% (w/w) scattering particles (Carborundum No. 600, Cats, Hoogvliet, the Netherlands). Microcapsule suspensions with a final concentration of 1×10^5 capsules/ml, were imaged using a phased array transducer (FPA 2.5 MHz) connected to an echocardiography US system (VingMed System 5; GE, Hoevelaken, the Netherlands). The centre frequency of the transmitted pulses was 2.5 MHz, and the pulse duration was 1.1 μs [35]. Fundamental B-mode images were recorded at two applied power levels: –30 dB and –4 dB. A 0.2 mm PVDF needle hydrophone (Precision Acoustics Ltd, Dorchester, UK) was used to verify that these applied powers corresponded to a P_ of 0.03 MPa (MI = 0.02) and a P_ of 0.53 MPa (MI = 0.51).

7.3. Results

7.3.1. Composition of microcapsules

We prepared microcapsules with a cyclodecane to hexadecane ratio of 1:0 for the production of completely gas-filled microcapsules (S_c), at a ratio 1:1 for the production of half oil-filled microcapsules (S_{ch}), and at a ratio 0:1 for the production of almost completely oil-filled microcapsules (S_h). After freeze-drying, the composition of these three differently filled microcapsules were analysed with MDSC, GC/MS and densitometry. The MDSC thermogram is shown in Fig. 7.1. The absence of a melting peak for cyclodecane at 9.5°C indicated that cyclodecane had successfully been removed in the freeze-drying process. For the microcapsules filled with hexadecane, a peak was observed at 18ºC, the melting point of hexadecane. This indicated that hexadecane still remained inside these microcapsules after freeze-drying. As the thermal contact for intact gas-filled microcapsules will not be optimal, truly quantitative measurements with MDSC are subject to debate, albeit that we did observe that the hexadecane melting-peak was smaller for the S_{ch} than for the S_h microcapsules. In the thermogram, a melting peak was also observed at 140ºC, which is attributed to melting of crystalline pLA-pFO. This suggested that the shell was at least partly crystalline. This observed peak, however, was much smaller for S_h than for S_c and S_{ch} microcapsules, suggesting that the presence of hexadecane influences the crystallinity of pLA-pFO. To

Table 7.1. GC/MS analysis of three types of differently loaded microcapsules when they are re-dispersed after freeze-drying. Mean values of analysis in triplicate; % m/m are the mass percentages of cyclodecane (CD) or hexadecane (HD) compared to the mass of the whole microcapsule. Encapsulated gas per microcapsule (% v/v) was determined with densitometry in triplicate.

	CD to HD ratio	% m/m CD		% m/m HD		HD encapsulation efficiency (%)	Calculated fill of micro-capsule	Encapsulated gas per microcapsule (% v/v)
		Theory	GC/MS	Theory	GC/MS			
S_c	1:0	0	0 ± 0	0	0 ± 0	-	0% oil	88.8 ± 9.2
S_{ch}	1:1	0	0 ± 0	80	64 ± 4	80 ± 5	40-42% oil	34.9 ± 0.7
S_h	0:1	0	0 ± 0	88	85 ± 1	97 ± 1	97-100% oil	9.7 ± 0.6

quantitatively determine the amount of hexadecane incorporated in the microcapsules, we performed GC/MS analysis (Table 7.1). The GC/MS analysis confirmed that cyclodecane was completely removed during the freeze-drying process, while hexadecane was substantially retained. For the S_{ch} microcapsules, which were prepared with a cyclodecane to hexadecane ratio of 1:1, the measured percentage of encapsulated hexadecane was 20% lower than theoretically predicted based on the initial composition. One possible factor for the lowered hexadecane encapsulation efficiency is that during freeze-drying, some of the hexadecane might have sublimed from the microcapsules. Another contributing factor may be that the stabilizer (PVA) was not completely removed during the washing steps, resulting in underestimation of the encapsulation efficiency. If the latter factor is not taken into account, GC/MS revealed that the microcapsules were completely gas-filled (S_c), half-filled with oil (S_{ch}), or almost completely filled with oil (S_h) (Table 7.1). Density measurements confirmed that the microcapsules contained different amounts of gas (Table 7.1). Based on these data and a polymer to alkane ratio of 1:8, it could be concluded that the inner core of S_c microcapsules contained ~ 100 ± 10% gas, for S_{ch} this was 39 ± 1 %, and for S_h this was 11 ± 1%.

Fig. 7.2. shows the size distributions of the S_c, S_{ch}, and S_h microcapsules and the solid polymer particles when they were re-dispersed after freeze-drying. The typical microcapsule concentration was in the order of 1×10^9 per ml. For all three differently loaded microcapsules at least 99% of the microcapsules were less than 3.04 μm in diameter. The number weighted mean diameter of the microcapsules ranged between 1.21 and 1.31 μm (Fig. 7.2), and the volume weighted mean diameter ranged between 2.02 and 2.67 μm, indicating some but limited variation between S_c, S_{ch}, and S_h microcapsules and within batches. This observation was also reflected in the SPAN, as the SPAN was 1.20 for the S_c microcapsules, 1.36 for the S_{ch} microcapsules, and 1.29 for the S_h microcapsules. The size of the microcapsules and the width of the distribution were not altered by the freeze-drying process, indicating that the microcapsules were not altered by processing and can be re-dispersed.

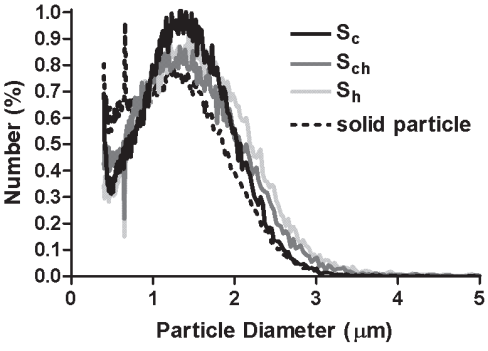

Fig. 7.2. Coulter counter size distribution measurements of microcapsules and solid polymer particles when re-dispersed after freeze-drying. Number weighted mean diameter (in μm) is 1.21 for S_c, 1.22 for S_{ch}, 1.31 for S_h, and 1.07 for solid polymer particle. More than 99% of capsules have smaller diameter than (in μm): 2.60 for S_c, 2.88 for S_{ch}, 3.04 for S_h, and 2.57 for solid polymer particle.

Morphology of the microcapsules was studied using electron microscopy. TEM studies revealed that S_c microcapsules were hollow, and had a thin shell of about 40 nm (Fig. 7.3.a). SEM analysis showed that these microcapsules had a spherical shape

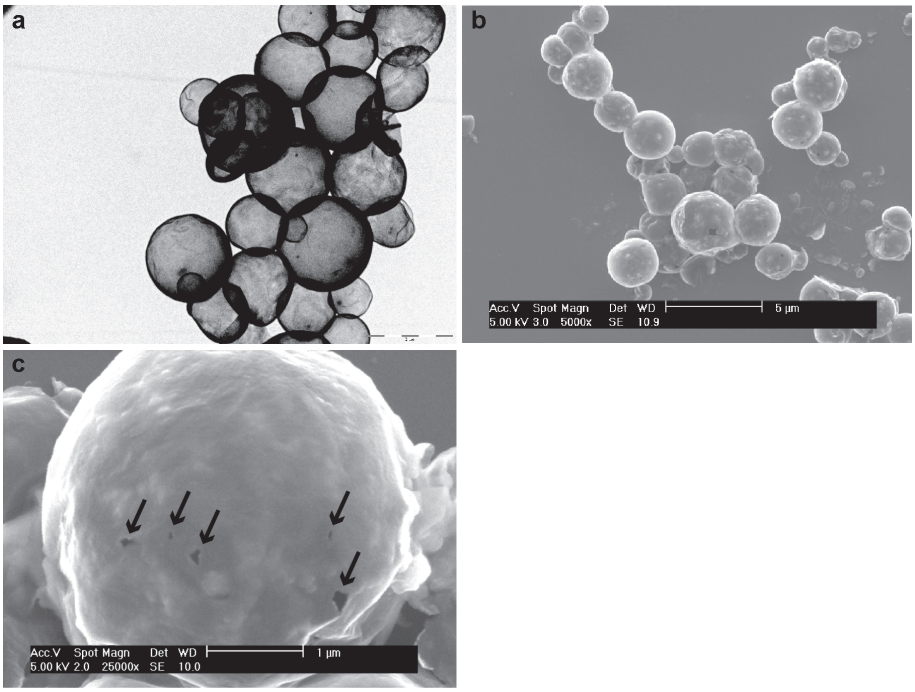

Fig. 7.3. Electron micrographs of lyophilised S_c microcapsules. a) TEM at 5,000 magnification, bar is 2 µm; the microcapsules are hollow and have a thin shell. b) SEM at 5,000 magnification, bar is 5 µm; the microcapsules are spherical and have an uneven surface. c) Higher magnification of the microcapsules (SEM at 25,000 magnification, bar is 1 µm), reveals pores in the shell (arrows), ranging from 30 to 210 nm.

and an uneven surface (Fig. 7.3.b), which contained pores (Fig. 7.3.c) ranging from 30 to 210 nm. Morphology of S_{ch} and S_h microcapsules could not be studied with TEM and SEM since these microcapsules broke upon introducing them in the vacuum column of the microscopes.

7.3.2. Acoustic properties of the microcapsules

Attenuation as a function of frequency is presented in Fig. 7.4.a for the S_c, S_{ch}, and S_h microcapsules as well as the solid polymer particles. Attenuation increased with increasing frequency from 0.3 MHz to 15 MHz for the S_c microcapsules and from 0.3 MHz to 10 MHz for the S_{ch} and S_h microcapsules. For each differently loaded microcapsule, the attenuation reached a maximum. For the S_c microcapsules, the maximum attenuation was 0.7 dB/cm at a frequency > 15 MHz. The maximum attenuation was 0.4 dB/cm for the S_{ch} microcapsules, and 0.1 dB/cm for the S_h microcapsules at a frequency between 10 and 15 MHz. These maxima show resonant behaviour of these microcapsules and indicate the resonant frequencies, which appeared to decrease with oil encapsulation. The attenuation of the solid

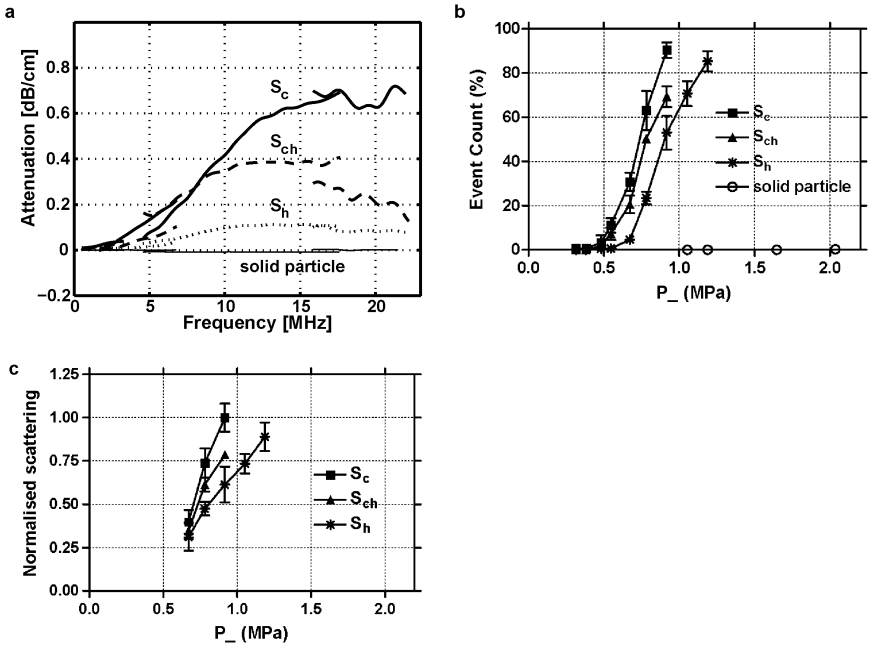

Fig. 7.4. a) Attenuation (in dB/cm) as function of frequency (0.3-22 MHz) for microcapsules and solid polymer particles. For each differently loaded microcapsule, attenuation reached a maximum. Attenuation of the solid polymer particles was ~ 0 dB/cm over the entire frequency range. b) Percentile event counts of individual microcapsules when insonified at 1 MHz (signal detected from 3-7 MHz). All three differently loaded microcapsules show a threshold followed by a sharp increase in event count for increasing P_. The solid polymer particles do not show any event counts. c) Normalised scattering of individual microcapsules when insonified at 1 MHz (signal detected from 3-7 MHz). All three differently loaded microcapsules scatter more with increasing P_.

polymer particles was ~ 0 dB/cm over the entire frequency range, indicating that they do not contain gas.

To further characterise the acoustic properties of the microcapsules, percentile event counts from single microcapsules were measured as a function of acoustic pressure. The microcapsules were insonified at a frequency of 1 MHz and the acoustic scattering was detected in the frequency range from 3 to 7 MHz. All three differently loaded microcapsules showed a threshold followed by a sharp increase in event count for increasing P_ (Fig. 7.4.b). To determine the event count threshold, a linear curve was fitted through the measurements having event counts greater than 4 %. The intercept with the x-axis was taken as the threshold. In this way the threshold for S_c was calculated to be 0.51 MPa, while the threshold of the S_{ch} showed only an insignificant increase to 0.52 MPa. For the S_h microcapsules the threshold was significantly higher, namely 0.65 MPa. The slope of the fitted linear curves above the threshold varied only slightly between the S_c, S_{ch}, and S_h microcapsules, indicating

that the activation rates were similar. The percentile event count is proportional to the microcapsule concentration, the confocal region volume, and microcapsule activation rate. Because both the microcapsule concentration and the confocal region volume remained unchanged among all the measurements with the same insonification condition, the percentile event counts therefore are a relative indicator of the percentage of activated microcapsules among all the particles flowing through the confocal region. For a high P_ of 0.8 MPa it can be concluded that about 25% of the S_h microcapsules were activated, while this increased up to 50% for the S_{ch} microcapsules, and up to 65% for the S_c microcapsules. As expected, no event count was shown for the solid polymer particles, suggesting that, although a hydrophobic polymer was used, no gas microbubbles spontaneously adhered to the surface.

Normalised scattering intensity (Fig. 7.4.c) showed that all three differently loaded microcapsules scattered more with increasing P_ when insonified at a frequency of 1 MHz and detected in the frequency range from 3 to 7 MHz. Scattering was highest for the S_c and lowest for the S_h microcapsules, suggesting that the S_c microcapsules contain more gas than the S_{ch} and S_h microcapsules.

7.3.3. Characterisation of microcapsule behaviour and drug release

Brandaris-128 high-speed camera recordings enabled us to optically observe how individual microcapsules behaved when insonified at a frequency of 1 MHz. At a low MI (P_ of 0.24 MPa; MI = 0.24), oil-filled microcapsules typically compressed without shell cracking. An area-time curve of a recording of an S_h microcapsule, 1.6 μm in diameter, is given in Fig. 7.5.a (top panel). During insonification, the area of the microcapsule decreased and hardly increased. Compression of the microcapsule was clearly visible in frame #41 and #80 of the bottom panel, and correlated with a positive pressure of the acoustic cycle. The compression was not symmetrical, and can be described as indenting from one side of the microcapsule, which for this particular microcapsule was at the top right corner. Indenting was more pronounced later in the US burst than in the beginning of the US burst. In between compressions, the microcapsule returned to its original spherical shape. These compressions did not crack the microcapsule, as it was still intact in the next recording which was recorded 80 ms later. However, in this next recording, in which the P_ was increased to 0.30 MPa (MI = 0.30), this microcapsule did crack after a few more compressions since we observed gas escaping from it at the location where it had indented (data not shown). Similar recordings were made for S_c and S_{ch} microcapsules with indenting occurring at a random place on the microcapsules. Although compression behaviour was identical for the three differently loaded microcapsules, the onset was at different acoustic pressures. About seven times more S_c microcapsules compressed at the lowest P_ of 170 kPa than S_{ch} and S_h microcapsules (n = 16-19). Also, about four times more S_c microcapsules cracked at a lower P_ than did S_{ch} and S_h, which is in agreement with the event count measurements shown in Fig. 7.4.b.

When the microcapsules were insonified at a high MI, (P_ of 0.51 MPa; MI = 0.51), the microcapsules typically indented only once, leading to cracking or at least weakening of the shell of the microcapsule since in the following negative pressure of the acoustic cycle we

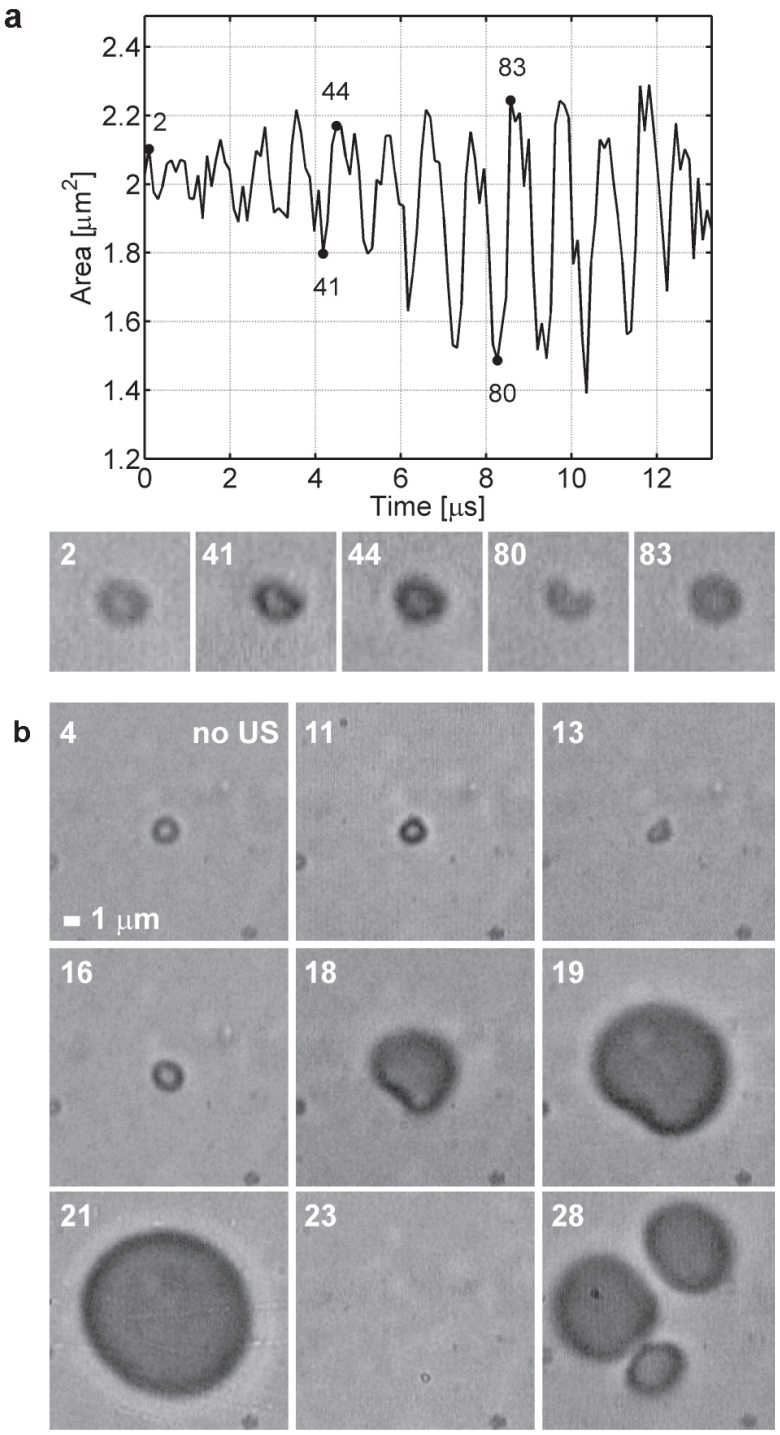
a
2.4
2.2
2
1.8
1.6
1.4
1.2
Area [μm²]
0
2
4
6
8
10
12
Time [μs]
2
44
83
41
80
2
41
44
80
83
b
4
no US
11
13
1 μm
16
18
19
21
23
28

observed gas escaping from the microcapsules. Fig. 7.5.b shows nine frames selected out of 128 frames from a typical recording of an S_h microcapsule with a diameter of 1.8 μm (see frame #4). The microcapsule indented (frame #11-13) at a positive pressure and returned to its original spherical shape (frame #16) when the pressure was zero. This was followed by gas escaping from the microcapsule (frame #18-21; negative pressure). The escaped free gas bubble expanded (frame #18-21), collapsed, and expanded again into three free gas bubbles (frame #28). At the peak positive pressures, the free gas bubbles were so compressed that they were no longer visible (frame #23). During the following US cycles, the free gas bubbles continued to expand, collapse, and coalesce. The free gas bubbles were no longer visible in the successive recording which was taken 80 ms later, indicating that they had dissolved. At high MI, the behaviour of the S_c and S_{ch} microcapsules was similar as described for S_h.

For drug release studies, we used microcapsules loaded with Sudan Black. Compressing the microcapsules by applying pressure resulted in a Sudan Black release relative to the amount encapsulated of 38 ± 17% for S_c and 75 ± 6% for S_{ch} microcapsules. MDSC indicated that for S_{ch} microcapsules no pLA-pFO was present in the released top fraction, while the melting peak of hexadecane was detected (data not shown), indicating that this fraction contained the encapsulated material and no intact or fragmented microcapsules. For S_c microcapsules, 64 ± 9 % of Sudan Black relative to the amount encapsulated was detected in the bottom fraction while this was 20 ± 10 % for S_{ch} microcapsules. Drug release was also triggered using US of 1 MHz at P_ of 0.51 MPa (MI = 0.51). Typical video recordings of an S_{ch} and S_h microcapsule showed that the shell of the drug-loaded microcapsules cracked upon insonification, thereby releasing the encapsulated drug (Fig. 7.6.d, Fig. 7.6.f). Shell fragments were identified as wrinkled non-spherical objects. When S_c microcapsules were sonocracked, only the fragmented shell was observed (Fig. 7.6.b).

7.3.4. Ultrasound Imaging

Fig. 7.7 shows fundamental B-mode images generated by a 2.5 MHz transducer connected to the VingMed System 5. For all suspensions, scattering of the microcapsules was observed when the applied power was 0.03 MPa (MI = 0.02) as demonstrated on the left panels of Fig. 7.7. However, the S_c microcapsules scattered more than the oil-filled microcapsules, which can be attributed to the larger amount of gas in these microcapsules. At

Fig. 7.5. Brandaris-128 high-speed camera recordings of microcapsules insonified with a 1 MHz transducer. a) Recording at frame rate of 9.56 MHz of an S_h microcapsule, 1.6 μm in diameter, insonified at P_ 0.24 MPa (MI = 0.24). Top panel: Area-time curve. Bottom panel: five selected cropped frames (4.5 by 4.5 μm) out of a total of 128 frames showing the microcapsule before insonification (frame #2) and during insonification (frame #41, 43, 81, and 83). Compression but no cracking is observed. b) Recording at frame rate of 9.41 MHz; nine selected cropped frames out of a total of 128 frames of recording of an S_h microcapsule, 1.8 μm in diameter, insonified at P_ of 0.51 MHz (MI = 0.51). Frame #4: no ultrasound. Frame #11-13: upon insonification the microcapsule compresses. Frame # 16: microcapsule returns to spherical shape. Frame #18-21: gas escapes from the microcapsule. Frame #23: at the highest pressure of the acoustic cycle the free gas bubble is compressed and not visible. Frame #28: when pressure becomes lower, 3 free gas bubbles are formed.

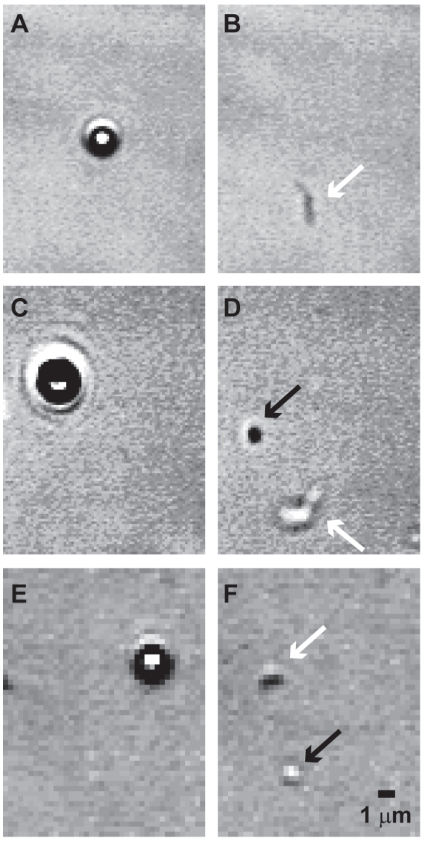

Fig. 7.6. Selected cropped frames out of typical video recordings of an S_c (a+b; 1.09 μm in diameter), S_{ch} (c+d; 2.08 μm in diameter), and S_h (e+f; 1.76 μm in diameter) microcapsule, loaded with the model lipophilic molecule Sudan Black. a, c, e: microcapsules before insonification. b, d, f: upon insonification at P_ of 0.51 MPa (MI = 0.51), the shell fragments (white arrows) and drug is released (black arrows). The selected frames are between 33 and 830 msec after insonification. The shell fragments and released oil droplets have different colours due to the different focal planes.

this low P_, no microcapsule destruction is expected since we observed, in both the event count measurements as well as optical observations with the Brandaris-128 high-speed camera, that a much higher P_ was needed to destroy the microcapsules. The right panels of Fig. 7.7 show B-mode images of the suspensions at a P_ of 0.53 MPa (MI = 0.34). The intensities of these images were scaled such that the tissue-mimicking phantom at both acoustic pressures had on average the same intensity. In this way, it can be appreciated that the backscattering at 0.53 MPa was much higher than at 0.03 MPa. At 0.53 MPa (MI = 0.34), the microcapsules, independent of their composition, were destroyed and their gas content was released, which resulted in an enhanced backscattering. For all samples, a clear contrast between the microcapsule suspension and the tissue-mimicking phantom was obtained. Fundamental B-mode images made at a centre frequency of 20 MHz, using the Vevo 770 machine (VisualSonics), gave comparable results (data not shown).

7.4. Discussion

In this study, novel polymer-shelled microcapsules were developed and characterised. The emulsification process used for the synthesis of partly oil-filled microcapsules allowed lipophilic compounds to be incorporated in a straightforward manner by dissolving them in hexadecane. By changing the ratio of cyclodecane to hexadecane, we could make gas-filled (S_c), half-oil filled (S_{ch}), and almost completely oil-filled microcapsules (S_h). The S_h microcapsules were not completely oil-filled and also contained 11 ± 1% gas. Since no cyclodecane was used during emulsification of the S_h microcapsules, the gas must have been incorporated into the microcapsules during another production step. It is likely that this occurred during the freeze-drying process. We found distinct differences between the amount of oil and gas between the

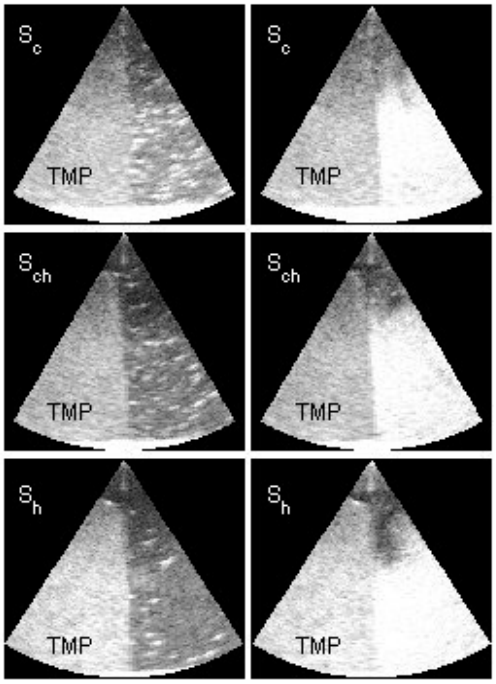

Fig. 7.7. Fundamental B-mode images recorded with the GE/VingMed System 5 using a 2.5 MHz transducer at a P_ of 0.03 MPa (MI = 0.02; panels on left) and 0.53 MPa (MI = 0.34; panels on right). Tissue-mimicking phantom (TMP) is located on the left of the scan; microcapsule suspension is located to the right of the scan. On the lower end of the scans, the lighter region represents the acoustic absorbing pad. Scanconverted image is 9 by 9 cm.

S_c, S_{ch}, and S_h microcapsules. Summing the amount of oil and gas for the S_c, S_{ch}, and S_h microcapsules resulted in values rather close to 100% (79-111%).

Although the S_{ch} and S_h microcapsules contained less gas than the S_c microcapsules, the resonance frequency of the S_{ch} and S_h microcapsules was lower than for the S_c microcapsules. This was unexpected since it is known that smaller gas bubbles have higher resonance frequencies than larger gas bubbles [36]. The discrepancy may be explained by the presence of oil and a relatively higher shell to gas ratio which may have increased damping which would result in a lower resonance frequency [37]. In addition, hexadecane may have influenced the pLA-pFO shell as we observed in the MDSC thermogram that the shell was less crystalline when only hexadecane was loaded in the microcapsules. This may have made the shell less rigid which may also have contributed to the lower resonance frequency. Further studies are needed to elucidate this.

As with every drug delivery system, it is important that the system incorporates an efficient payload of therapeutic agent. The pharmaceutical payload per microbubble is limited when drugs are attached to or incorporated into the shell of microbubbles [2]. Hydrophobic drug-carrier reservoirs can be distinctly improved by encapsulation of a liquid oil, for example soybean oil [16] or triacetin oil [38], as reported for acoustically active lipospheres (AALs). Although the S_{ch} and S_h microcapsules described in this study have even larger drug-carrier reservoirs than the AALs, the therapeutic significance of this needs to be investigated and will depend on the amount of drug that can be dissolved in oil and the therapeutic dose that is required. AALs have a relatively wide size range of 1-10 μm in diameter [38], while the S_c, S_{ch}, and S_h have a much narrower size distribution, which is beneficial for controlled drug delivery since a narrower size distribution equals a more defined payload. The near-

micrometer size of the pLA-pFO microcapsules also prevents trapping in pulmonary capillaries as well as other capillaries in the body [39]. In addition, AALs have a phospholipid shell and are therefore not believed to be as stable *in vivo* as polymer-shelled UCA [2].

A drug that is not released in the non-target areas of the body, unless the microbubble-drug complex is activated by US, represents the most desirable UCA-based drug delivery system. In addition, US-triggered drug release should be feasible using diagnostic US [2, 14, 40]. The oil-loaded microcapsules used in this study were typically cracked, thereby triggering drug release, at an MI of 0.34 and 0.51, which is within the clinically safe dose of diagnostic US and can be generated by regular US diagnostic imaging equipment. In comparison, US-triggered drug release from AALs loaded with triacetin is at higher MI's, as values of 0.67 to 2.0 have been reported [17, 38, 41]. Moreover, AALs loaded with soybean oil were even more difficult to fragment [38]. It is striking that much lower MI's are required to crack our polymer-shelled microcapsules in comparison to most other polymer-shelled microbubbles [42-45]. However, somewhat higher powers were needed to crack S_{ch} and S_h microcapsules compared to S_c microcapsules as illustrated in both the Brandaris-128 high-speed camera studies as well as the event count measurements. Compressing the microcapsules by applying static pressure showed that Sudan Black release is especially efficient for half oil-filled microcapsules since 75 ± 6% of the amount encapsulated was released with the oil. The remaining Sudan Black was retrieved from the bottom fraction, suggesting that it stayed associated with the shell. It needs to be investigated whether this also applies to US-triggered release.

For UCA-based drug delivery systems, it is also important that they can be imaged under non-destructive conditions so that diagnostic US can be used for guidance and monitoring of therapy [4, 7]. Our polymer-shelled microcapsules are suited for low MI imaging under non-destructive conditions, which is an important finding. Leong-Poi et al. [46] reported that non-drug loaded microbubbles with a polymer shell made of low molecular weight polylactide could also be used for low-pressure imaging under non-destructive conditions, although they did not investigate how these microcapsules oscillated under non-destructive conditions. How our pLA-pFO microcapsules oscillated under non-destructive conditions was clearly illustrated in the Brandaris-128 high-speed camera studies. At low acoustic pressures, compression-only behaviour was found, which was comparable to behaviour found for the polymer-shelled microsphere PB127 [45].

Unlike other imaging modalities, US can be used to perform triggered, controlled, and local interventions, such as the release of pharmaceutical agents. The minimally invasive nature of US may also permit multiple treatments. Since US systems are portable, bedside treatment is even possible. On the other hand, there are some limitations as US treatment is only possible in sonographically accessible tissues [1, 2, 14]. There are also limitations to the novel UCA-based drug delivery system we developed in this study as it can only be used for lipophilic drugs. However, it would be interesting to develop a system with large hydrophilic drug-reservoirs.

Although we have demonstrated US-triggered release with our partially oil-filled microcapsules loaded with Sudan Black, incorporating actual drugs and quantifying their release need to be investigated and will be the focus of our future research. At the same time, preliminary *in vivo* studies with S_{ch} microcapsules loaded with the chemotherapeutic drug paclitaxel were encouraging [24], but further studies also need to be done to demonstrate the therapeutic effect of this novel UCA-based drug delivery system *in vitro* as well as *in vivo*. The biodistribution of the drug-loaded microcapsules as well as the long-term fate of the loaded drug should also be investigated. It is expected that the microcapsules will be taken up by the reticulo-endothelial system (lung, liver, spleen), like reported for polymer microspheres, microparticles, and US contrast agent [47, 48]. The possibility therefore exists for increased toxicities to these tissues if the microcapsules contain a toxic drug.

In conclusion, we have made and characterised a novel UCA-based drug delivery system, based on polymer-shelled microcapsules filled with a mixture of gas and oil. Using diagnostic US, we demonstrated the ability to crack the oil-filled microcapsules, thereby releasing the encapsulated gas and drug. In addition, non-destructive imaging of the microcapsules was demonstrated indicating that guidance and monitoring of therapy will be possible. Of the microcapsules studied, the S_h microcapsules had the highest lipophilic drug-reservoir whilst diagnostic US could still be used to trigger drug release. These microcapsules therefore have great potential for US-triggered local delivery of lipophilic drugs.

Acknowledgements

This project is supported by innovation subsidies collaborative projects by the Dutch ministry of economic affairs under nr IS042035. The authors would like to thank Marcel Verheijen (TEM), Hugo Knobel (GC/MS), and Hetty de Barse and Monique Vervest (SEM) from Philips and Ing. Miranda Foppen-Harteveld (Coulter Counter) from the Dept. of Biomedical Engineering, Erasmus MC, for the material analysis. The authors are grateful to Dr. Leonard M. Sagis and Ing. Harry Baptist from the Food Physics Group at Wageningen University for assisting us with the densitometer measurements, and for valuable discussions.

References

[1] W.G. Pitt, G.A. Husseini, B.J. Staples, Ultrasonic drug delivery - A general review, Expert. Opin. Drug. Deliv. 1(1) (2004) 37-56.

[2] A.L. Klibanov, Microbubble contrast agents: targeted ultrasound imaging and ultrasound-assisted drug-delivery applications, Invest. Radiol. 41(3) (2006) 354-362.

[3] P.A. Dijkmans, L.J. Juffermans, R.J. Musters, A. van Wamel, F.J. ten Cate, W. van Gilst, C.A. Visser, N. de Jong, O. Kamp, Microbubbles and ultrasound: from diagnosis to therapy, Eur. J. Echocardiogr. 5(4) (2004) 245-256.

[4] E.C. Unger, T.O. Matsunaga, T. McCreery, P. Schumann, R. Sweitzer, R. Quigley, Therapeutic applications of microbubbles, Eur. J. Radiol. 42(2) (2002) 160-168.

[5] L.J. Juffermans, P.A. Dijkmans, R.J. Musters, A. van Wamel, A. Bouakaz, F.J. ten Cate, L. Deelman, C.A. Visser, N. de Jong, O. Kamp, Local drug and gene delivery through

microbubbles and ultrasound: a safe and efficient alternative for viral vectors?, Neth. Heart J. 12(9) (2004) 398-403.
[6] Y. Liu, H. Miyoshi, M. Nakamura, Encapsulated ultrasound microbubbles: therapeutic application in drug/gene delivery, J. Control. Release 114(1) (2006) 89-99.
[7] K. Ferrara, R. Pollard, M. Borden, Ultrasound microbubble contrast agents: fundamentals and application to gene and drug delivery, Annu. Rev. Biomed. Eng. 9 (2007) 415-447.
[8] M. Postema, G. Schmitz, Bubble dynamics involved in ultrasonic imaging, Expert Rev. Mol. Diagn. 6(3) (2006) 493-502.
[9] S. Muro, M. Koval, V. Muzykantov, Endothelial endocytic pathways: gates for vascular drug delivery, Curr. Vasc. Pharmacol. 2(3) (2004) 281-299.
[10] C.A. Kavanagh, Y.A. Rochev, W.M. Gallagher, K.A. Dawson, A.K. Keenan, Local drug delivery in restenosis injury: thermoresponsive co-polymers as potential drug delivery systems, Pharmacol. Ther. 102(1) (2004) 1-15.
[11] V.P. Torchilin, Drug targeting, Eur. J. Pharm. Sci. 11 Suppl 2 (2000) S81-91.
[12] L.H. Reddy, Drug delivery to tumours: recent strategies, J. Pharm. Pharmacol. 57(10) (2005) 1231-1242.
[13] A. van Wamel, K. Kooiman, M. Harteveld, M. Emmer, F.J. ten Cate, M. Versluis, N. de Jong, Vibrating microbubbles poking individual cells: drug transfer into cells via sonoporation, J. Control. Release 112(2) (2006) 149-155.
[14] J.C. Chappell, R.J. Price, Targeted therapeutic applications of acoustically active microspheres in the microcirculation, Microcirculation 13(1) (2006) 57-70.
[15] R. Bekeredjian, P.A. Grayburn, R.V. Shohet, Use of ultrasound contrast agents for gene or drug delivery in cardiovascular medicine, J. Am. Coll. Cardiol. 45(3) (2005) 329-335.
[16] E.C. Unger, T.P. McCreery, R.H. Sweitzer, V.E. Caldwell, Y. Wu, Acoustically active lipospheres containing paclitaxel: a new therapeutic ultrasound contrast agent, Invest. Radiol. 33(12) (1998) 886-892.
[17] M.S. Tartis, J. McCallan, A.F.H. Lum, R. LaBell, S.M. Stieger, T.O. Matsunaga, K.W. Ferrara, Therapeutic effects of paclitaxel-containing ultrasound contrast agents, Ultrasound Med. Biol. 32(11) (2006) 1771-1780.
[18] M.R. Böhmer, R. Schroeders, J.A.M. Steenbakkers, S.H.P.M. de Winter, P.A. Duineveld, J. Lub, W.P.M. Nijssen, J.A. Pikkemaat, H.R. Stapert, Preparation of monodisperse polymer particles and capsules by ink-jet printing, Colloids and Surf. A Physicochem. Eng. Aspects 289 (2006) 96-114.
[19] W.K. Lee, I. Losito, J.A. Gardella, W.L. Hicks, Synthesis and surface properties of fluorocarbon end-capped biodegradable polyesters, Macromolecules 34(9) (2001) 3000-3006.
[20] D.C. Bloedow, W.L. Hayton, Effects of lipids on bioavailability of sulfisoxazole acetyl, dicumarol, and griseofulvin in rats, J. Pharm. Sci. 65(3) (1976) 328-334.
[21] P.J. Dowding, R. Atkin, B. Vincent, P. Bouillot, Oil core/polymer shell microcapsules by internal phase separation from emulsion droplets. II: Controlling the release profile of active molecules, Langmuir 21(12) (2005) 5278-5284.
[22] G.H. Ma, Preparation of uniform poly(lactide) microspheres by employing the Shirasu Porous Glass (SPG) emulsification technique, Colloids Surf. A Physicochem. Eng. Aspects 153 (1999) 383-394.
[23] M.S. Romero-Cano, B. Vincent, Controlled release of 4-nitroanisole from poly(lactic acid) nanoparticles, J. Control. Release 82(1) (2002) 127-135.
[24] W.T. Shi, M. Bohmer, A. van Wamel, M. Celebi, A.L. Klibanov, C.T. Chin, C. Chlon, M. Emmer, K. Kooiman, N. de Jong, C.S. Hall, Ultrasound Therapy with Drug Loaded Microcapsules, IEEE Ultrasonics Symposium Proceedings (2007) pp. 773-776.
[25] J.F. Nijsen, M.J. van Steenbergen, H. Kooijman, H. Talsma, L.M. Kroon-Batenburg, M. van De Weert, P.P. van Rijk, A. De Witte, A.D. Van Schip, W.E. Hennink, Characterization of poly(L-lactic acid) microspheres loaded with holmium acetylacetonate, Biomaterials 22(22) (2001) 3073-3081.

[26] J.F. Nijsen, A.D. van Het Schip, M.J. van Steenbergen, S.W. Zielhuis, L.M. Kroon-Batenburg, M. van de Weert, P.P. van Rijk, W.E. Hennink, Influence of neutron irradiation on holmium acetylacetonate loaded poly(L-lactic acid) microspheres, Biomaterials 23(8) (2002) 1831-1839.
[27] S. Solarski, M. Ferreira, E. Devaux, Characterization of the thermal properties of PLA fibers by modulated differential scanning calorimetry, Polymer 46(25) (2005) 11187-11192.
[28] K. Bjerknes, P.C. Sontum, G. Smistad, I. Agerkvist, Preparation of polymeric microbubbles: formulation studies and product characterisation, Int. J. Pharm. 158(2) (1997) 129-136.
[29] M. Schneider, P. Bussat, M.B. Barrau, M. Arditi, F. Yan, E. Hybl, Polymeric Microballoons as Ultrasound Contrast Agents - Physical and Ultrasonic Properties Compared with Sonicated Albumin, Invest. Radiol. 27(2) (1992) 134-139.
[30] N. de Jong, L. Hoff, T. Skotland, N. Bom, Absorption and scatter of encapsulated gas filled microspheres: theoretical considerations and some measurements, Ultrasonics 30(2) (1992) 95-103.
[31] W. Shi, M. Bohmer, S. de Winter, J. Steenbakkers, M. Emmer, A. van Wamel, N. de Jong, C.S. Hall, Ultrasonic Characterization of Novel Monodispersed Contrast Agents, IEEE Ultrasonics Symposium Proceedings (2006) pp. 301-304.
[32] C.T. Chin, C. Lancee, J. Borsboom, F. Mastik, M. Frijlink, N. de Jong, M. Versluis, D. Lohse, Brandaris 128: a 25 million frames per second digital camera with 128 highly sensitive frames, Rev. Sci. Instru. 74(12) (2003) 5026-5034.
[33] M. Emmer, A. van Wamel, D.E. Goertz, N. de Jong, The onset of microbubble vibration, Ultrasound Med. Biol. 33(6) (2007) 941-949.
[34] S.M. van der Meer, B. Dollet, M.M. Voormolen, C.T. Chin, A. Bouakaz, N. de Jong, M. Versluis, D. Lohse, Microbubble spectroscopy of ultrasound contrast agents, J. Acoust. Soc. Am. 121(1) (2007) 648-656.
[35] M. Emmer, H.J. Vos, A. van Wamel, D.E. Goertz, M. Versluis, N. de Jong, Clinical relevance of pressure-dependent scattering at low acoustic pressures, Ultrasonics 47(1-4) (2007) 74-77.
[36] L. Hoff, P.C. Sontum, J.M. Hovem, Oscillations of polymeric microbubbles: effect of the encapsulating shell, J. Acoust. Soc. Am. 107(4) (2000) 2272-2280.
[37] T.G. Leighton, The acoustic bubble, Academic Press, London (1994).
[38] D.J. May, J.S. Allen, K.W. Ferrara, Dynamics and fragmentation of thick-shelled microbubbles, IEEE Trans. Ultrason. Ferroelectr. Freq. Control 49(10) (2002) 1400-1410.
[39] R.S. Meltzer, E.G. Tickner, R.L. Popp, Why do the lungs clear ultrasonic contrast?, Ultrasound Med. Biol. 6(3) (1980) 263-269.
[40] S.B. Barnett, G.R. Ter Haar, M.C. Ziskin, H.D. Rott, F.A. Duck, K. Maeda, International recommendations and guidelines for the safe use of diagnostic ultrasound in medicine, Ultrasound Med. Biol. 26(3) (2000) 355-366.
[41] M.J. Shortencarier, P.A. Dayton, S.H. Bloch, P.A. Schumann, T.O. Matsunaga, K.W. Ferrara, A method for radiation-force localized drug delivery using gas-filled lipospheres, IEEE Trans. Ultrason. Ferroelectr. Freq. Control 51(7) (2004) 822-831.
[42] S. Seemann, P. Hauff, M. Schultze-Mosgau, C. Lehmann, R. Reszka, Pharmaceutical evaluation of gas-filled microparticles as gene delivery system, Pharm. Res. 19(3) (2002) 250-257.
[43] S.H. Bloch, M. Wan, P.A. Dayton, K. Ferrara, Optical observation of lipid- and polymer-shelled ultrasound microbubble contrast agents, Appl. Phys. Lett. 84(4) (2004) 631-633.
[44] P.D. Bevan, R. Karshafian, E.G. Tickner, P.N. Burns, Quantitative measurement of ultrasound disruption of polymer-shelled microbubbles, Ultrasound Med. Biol. 33(11) (2007) 1777-1786.
[45] A. Bouakaz, M. Versluis, N. de Jong, High-speed optical observations of contrast agent destruction, Ultrasound Med. Biol. 31(3) (2005) 391-399.
[46] H. Leong-Poi, J. Song, S.J. Rim, J. Christiansen, S. Kaul, J.R. Lindner, Influence of microbubble shell properties on ultrasound signal: Implications for low-power perfusion imaging, J. Am. Soc. Echocardiogr. 15(10 Pt 2) (2002) 1269-1276.
[47] J.M. Anderson, M.S. Shive, Biodegradation and biocompatibility of PLA and PLGA microspheres, Adv. Drug Deliv. Rev. 28(1) (1997) 5-24.

[48] J.A. Straub, D.E. Chickering, T.G. Hartman, C.A. Gloff, H. Bernstein, AI-700 pharmacokinetics, tissue distribution and exhaled elimination kinetics in rats, Int. J. Pharm. 328(1) (2007) 35-41.

Therapy with oil-filled polymer microcapsules

Based on

Unpublished Results

Klazina Kooiman[1], Ceciel H.T. Chlon[2], Marcel R. Böhmer[2], Nico de Jong[1,3,4]

IEEE Ultrasonics Symposium Proceedings 2007, pp. 773-776

William T. Shi[5], Marcel R. Böhmer[2], Annemieke van Wamel[1,6], Muzaffer Celebi[6], Alexander L. Klibanov[6] , Chien T. Chin[5], Ceciel H.T. Chlon[2], Marcia Emmer[1,3], Klazina Kooiman[1], Nico de Jong[1,3,4], Christopher S. Hall[5]

[1] Dept. Biomedical Engineering, Thoraxcenter, Erasmus MC, Rotterdam, the Netherlands
[2] Philips Research Eindhoven, Eindhoven, the Netherlands
[3] Interuniversity Cardiology Institute of the Netherlands, Utrecht, the Netherlands
[4] Physics of Fluids Group, University of Twente, Enschede, the Netherlands
[5] Philips Research North America, Briarcliff Manor, NY, USA
[6] Health System-Cardiovascular Medicine, University of Virginia, Charlottesville, VA, USA

Lipid distribution and viscosity of coated microbubbles

Klazina Kooiman[1], Marcia Emmer[1,2], Tom J.A. Kokhuis[1,2], Johan G. Bosch[1], H. Martijn de Gruiter[3], Martin E. van Royen[3], Wiggert A. van Cappellen[4], Adriaan B. Houtsmuller[3], Antonius F.W. van der Steen[1,2], Nico de Jong[1,2,5]

[1] Dept. of Biomedical Engineering, Thoraxcenter, Erasmus MC, Rotterdam, the Netherlands
[2] Interuniversity Cardiology Institute of the Netherlands, Utrecht, the Netherlands
[3] Dept. of Pathology, Josephine Nefkens Institute, Erasmus MC, Rotterdam, the Netherlands
[4] Dept. of Reproduction and Development, Erasmus MC, Rotterdam, the Netherlands
[5] Physics of Fluids Group, University of Twente, Enschede, the Netherlands

Based on IEEE Ultrasonics Symposium Proceedings 2010

General discussion and conclusion

10.1 Discussion

Small gas bubbles for drug delivery triggered by ultrasound? It sounds futuristic and complicated because how can sound and gas be used for drug delivery? But at the same time is it simple because ultrasound is a widely used diagnostic imaging modality and ultrasound contrast agents (i.e. gas microbubbles) are already used in hospital worldwide to improve diagnostic ultrasound imaging for more than a decade? The answers to these questions will be covered in this chapter as well as the future of therapeutic bubbles.

10.1.1. Therapeutic bubbles

The physicians that accidentally discovered that small gas pockets improved ultrasound imaging [1] could probably not have predicted that forty-three years later the use of gas for therapy would be such an emerging field. Physicians are now even predicting that the therapeutic applications of microbubbles will have more impact on human health than the diagnostic applications [2].

One of the first papers on therapy with bubbles was published 16 years ago, which was just a few years after bubbles had become commercially available. In this paper, Tachibana et al showed that ultrasound-activated bubbles accelerated thrombolysis *in vitro* [3]. The mechanism was not clear and it was thought that the cavitation or collapse of the microbubbles induced microstreaming which drove the fibrinolytic agents into the fibrin network of the thrombus. Since then, many more papers followed on the administration of a bubble and a drug for therapy, which is now classed as co-administration [4-7]. Although many papers showed therapeutic efficacy, the mechanism was still not known at the start of the studies presented in this thesis. Elucidating this mechanism was one of the aims of this thesis.

Papers showing that drugs can be incorporated into or attached to bubbles started to be published about 13 years ago. One of the first papers was by Unger et al [8] who demonstrated ultrasound-triggered release of a drug that was incorporated in the lipid-coating of microbubbles. Since then more strategies of incorporating drugs into bubbles have been published [4-7]. Loading a sufficient amount of drug onto or into a bubble as well as its efficient release remained a limitation for these bubble-based drug delivery systems [9, 10]. Producing a novel bubble-based drug delivery system was an important aim during this thesis.

10.1.2. Co-administration of bubble and drug

A class of therapeutic bubbles is co-administration of bubbles with drugs. As already clinically approved bubbles and clinically approved drugs can be used for this approach, this technique could therefore be brought to the clinic much faster than a novel bubble in which a drug is incorporated into or attached to. In a co-administration setting, bubbles in an ultrasound field induce a transient increase in permeability of cells membrane and/or tissues.

The microbubble-induced increase in cell membrane permeability in an ultrasound field is also referred to as sonoporation [4-7]. One of the first papers reporting this effect was published in 1998 by Greenleaf et al [11] who showed that ultrasound-activated microbubbles markedly enhanced transfection of cells. At the start of this thesis, the mechanism of sonoporation was still unclear. In **Chapters 2 – 5** we describe co-administration experiments that were designed to unravel this mechanism. For this we used high-speed optical imaging approaches (Chapter 2, 5) as well as cell electrophysiological and morphological evaluations (Chapter 3, 4, 5). In Chapter 2, Brandaris-128 high-speed imaging recordings (~ 10 million frames per second) are described which for the first time revealed that the vibration of a microbubble against a cell is the key factor for inducing sonoporation. We observed that not only pores are created during sonoporation, but endocytosis is also increased (Chapter 3). Following sonoporation, smaller molecules (in our case dextrans of 4.4 and 70 kDa) were shown to be taken up throughout the cytosol by transient pores created in the endothelial cells. However, larger dextrans (155 and 500 kDa) were found in distinct vesicles after sonoporation. These vesicles were endocytotic vesicles so therefore in addition to pore formation, endocytosis was found to be a key mechanism of sonoporation. Chapter 3 was published in Circulation Research, volume 104. In the same issue, an editorial by Walton and Shohet was published entitled 'Tiny bubbles and endocytosis?' [12]. In this editorial, a need for a deeper mechanistic explanation was raised. Since endocytosis upregulation was observed *in vitro* as well as *in vivo*, our findings were certainly not an *in vitro* artefact. Other studies not involving bubbles have shown a direct correlation of endocytosis with intracellular calcium ions $[Ca^{2+}]_i$, and reactive oxygen species (ROS) [13-15]. Both $[Ca^{2+}]_i$ and ROS were previously reported to be induced by vibrating microbubbles [16-20]. A mechanistic explanation was therefore already proposed in our study namely that vibrating bubbles upregulate endocytosis through an increase in $[Ca^{2+}]_i$ and/or (ROS). In Chapter 4 and 5 we describe that vibrating microbubbles can also be used to increase endothelial layer permeability. An increased cell membrane permeability was also observed, but in addition to this the involvement of $[Ca^{2+}]_i$, and ROS. So in all, in endothelial cells tiny vibrating bubbles are capable of inducing pores and activating signalling cascades which can result in upregulation of endocytosis or an increase in endothelial layer permeability. Formation of pores and an increase in endocytosis were observed within the same study, as were formation of pores and an increase in endothelial layer permeability. It needs to be further investigated whether different ultrasound parameters favour one over the other mechanism or both occur at the same time.

Table 10.1 shows an overview of several studies in which the sonoporation-induced cell membrane pore size was reported. The induced cell membrane pores sizes ranged from ~ < 75 nm to ~ 5 µm and were investigated using different cell types and different ultrasound parameters (see Table 10.1). On the other hand, others suggested that pore-like structures represent depression in the membrane rather than actual pores [21, 22] (see Table 10.1). Further studies will have to elucidate this, but pores of > 1 µm seem very large to allow cell survival. Resealing times of sonoporation-induced permeability have also been reported and

range from milliseconds to several seconds [23, 24], which is in line with what we found in Chapter 2.

Table 10.1. Sonoporation-induced cell membrane pores; SEM = scanning electron microscopy, AFM = atomic force microscopy; DC = duty cycle, PRF = pulse repetition frequency.

Cell	Bubble	Pore size	Determined by	Ultrasound settings		1st author and Ref.
MAT B III [1] Erythrocyte (both in suspension)	BG1766 (soft lipid) BG1766 (hard polymer)	~100 nm ~ < 75 nm	SEM and uptake molecules of different sizes	BG1766: 1.15 MHz 0.4 MPa 20% DC PRF 100 Hz 10 sec	BG1766: 1.15 MHz 0.4 MPa 20% DC PRF 100 Hz 10 sec	Mehier-Humbert [23]
MCF7 [2] (in suspension)	SonoVue	150 nm – 1 µm	SEM	1 MHz 0.3-3 MPa 20 cycles PRF 20 Hz – 1 kHz 5 – 60 sec		Qiu [25]
MCF7 [2] (in suspension)	Lipid (made by them)	1 nm – 4.3 µm	SEM	1 MHz 0.19+0.25+0.38+0.48 MPa 20 cycles PRF 10 kHz 40 sec		Yang [26]
BEC [3] (adhered)	Levovist	~ 1 µm	SEM	1 MHz 1.1 MPa 3 cycles 3 µsec		Kudo [24]
SK-BR-3 [4] (adhered)	Lipid (made by them)	0.9 – 2.4 µm [5]	AFM	1.3 MHz 1.4 MPa continuous 30 sec		Zhao [27]
SK-BR-3 [4] (adhered)	Lipid (made by them) with air (a), C_3F_8 (c), SF_6 (s) gas core	a: no change c+s: 1 – 5 µm [6]	AFM	1.3 MHz 1400 kPa continuous 30 sec		Zhao [28]
HAEC [7] VSMC [8] (both adhered)	Optison	small holes (size not given)	SEM	MHz not specified 2.5 W/cm^2 (~ 0.2 MPa) 8× 1 min		Taniyama [29]
BHK-21 [9] (adhered)	Optison	no pores but smoother cell membrane, less microvilli	SEM	1 MHz 2 W/cm^2 (0.159 MPa) 30% DC 30 min		Duvshani-Eshet [30]
BHK-21 [9] (adhered)	Optison	less rough cell membrane	AFM	1 MHz 2 W/cm^2 (0.159 MPa) 30% DC 30 min		Duvshani-Eshet [22]

[1] rat mammary carcinoma cell; [2] human breast cancer cell; [3] Bovine endothelial cell; [4] breast cancer cell; [5] pores of 0.8µm already existed before ultrasound exposure; [6] pores < 1 µm already existed before ultrasound-exposure; [7] human aortic endothelial cell; [8] vascular smooth muscle cell; [9] baby hamster kidney cells.

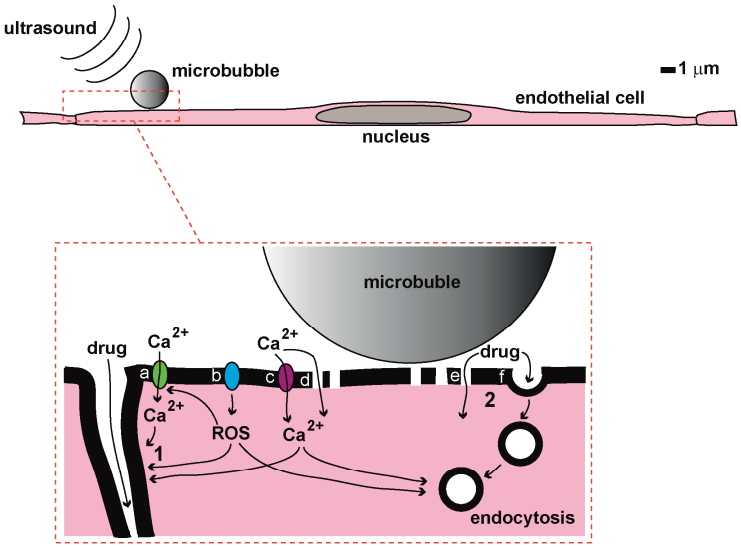

Fig. 10.1. Schematic overview vibrating bubble-induced bio-effects in endothelial cells. Bio-effect 1: drug delivery through endothelial layer via Ca^{2+} influx through pore formation (d) or mechanotransduction-induced Ca^{2+} channel activation (c), or ROS production (b). ROS can directly and indirectly (a; via Ca^{2+} channel activation) influence endothelial layer permeability [31, 32]. Bio-effect 2: drug uptake through pore formation (e) or endocytosis (f). Endocytosis is influenced by Ca^{2+} influx and ROS [13-15]. Upper overview schematic is drawn to scale; inset is not drawn to scale.

The experiments described in Chapter 2 – 5 contribute to the field of unravelling the mechanism of sonoporation but are by no means the answer to the question: *what is the mechanism of sonoporation?* Even though our experiments were set out to answer this exciting mechanism, our findings may even raise more questions because how do vibrating microbubbles activate signalling cascades in endothelial cells? Is it solely through the formation of pores or is there another mechanism involved? To answer the initial question 'why does an endothelial cell respond to vibrating microbubbles by increasing its cell permeability', more (optical high-speed) studies are certainly needed. This will hopefully reveal more about the microbubble-cell behaviour and give the answers to fully elucidate the mechanism. It is however striking that so many of the observed bio-effects in endothelial cells after poking these cells with vibrating microbubbles [16-20] are also observed in these cells after mechanotransduction [33]. These effects include hyperpolarization, a rise in $[Ca^{2+}]_i$, ROS generation, stimulated pinocytosis and F-actin cytoskeletal rearrangement. Mechanotransduction itself can trigger a rise in $[Ca^{2+}]_i$ by activation of mechanosensitive ion channels on the cell membrane and / or stimulation of the release of intracellular calcium

storage pools [33, 34]. It needs further investigation whether vibrating microbubbles also increase $[Ca^{2+}]_i$ via mechanotransduction and / or that a different mechanism leads to an increase in $[Ca^{2+}]_i$, namely the induction of cell membrane pores. The induction of cell membrane pores is observed in Chapter 2, 3, 5, and 6 and these alone could already result in a rise in $[Ca^{2+}]_i$ as $[Ca^{2+}]_i$ is much lower than $[Ca^{2+}]$ outside the cell [35]. Diffusion of Ca^{2+} is therefore expected during the existence of the pores. A schematic of these bioeffects is given in Fig. 10.1.

The most obvious target tissue for co-administration is the endothelium since bubbles come into contact with endothelial cells after intravenous injection [36, 37]. In experimental animals, bubbles and ultrasound have also shown therapeutic effect beyond the endothelium, for example in underlying tumours and muscles [38, 39]. It is possible that all these therapeutic effects have a common mechanism, as illustrated in Fig. 10.1.

For the co-administration studies described in Chapter 2 – 6 lipid-coated non-targeted bubbles were used. In **Chapter 6** we investigated whether targeted lipid-coated microbubbles could also be used to induce sonoporation in endothelial cells. Induction of sonoporation was also investigated for non-targeted polymer-shelled microcapsules in **Chapter 9**. Both targeted lipid-coated and non-targeted polymer-shelled bubbles were observed to induce sonoporation in endothelial cells. Because sonoporation is not restricted to non-targeted lipid-coated (Chapter 2 - 6; [40, 41]) or even albumin-coated microbubbles [42-44] in an ultrasound field, there is plenty of choice in bubbles for co-administration. For each specific bubble a specific ultrasound setting is required, for example polymeric microbubbles induce sonoporation at a much higher peak negative acoustic pressure than lipid-coated microbubbles, namely 500 kPa (Chapter 8) versus 80-400 kPa (Chapter 2 – 6).

Bubbles have to be close to cells for sonoporation to occur, as was already demonstrated in Chapter 2 with non-targeted bubbles. *In vivo,* the advantage of using targeted microbubbles versus non-targeted microbubbles is not expected in small capillaries as in these small

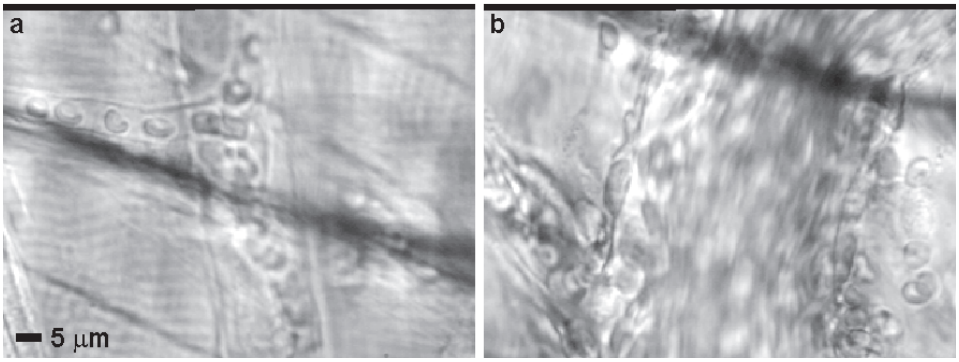

Fig. 10.2. Selected frames out of a video recording (25 frames per second) of blood cells flowing through vessels of a mouse cremaster muscle. The animal study was approved by the Animal Research Committee at Erasmus MC. Assistance of Miranda Foppen-Harteveld during this study is gratefully acknowledged. a) small vessel (~ 5 μm); b) larger vessel (~ 40 μm).

capillaries non-targeted microbubbles will automatically be close to the endothelial cells that line the vessel wall (see Fig. 10.2.a). However, in larger vessels the chance of a non-targeted microbubble being close to the endothelial cells will decrease as the vessel size increases (see Fig. 10.2.b). A targeted microbubble will overcome this because it can adhere to endothelial cells. Critical appraisal has already been shown for the adherence of targeted microbubbles in larger vessels [45]. However, what is not known is how many microbubbles have to adhere and induce sonoporation in a vessel to obtain a therapeutic effect. This needs further investigation. The first article about targeted microbubbles was already published in 1997 by Klibanov et al [46]. Microbubbles are ideally suited for molecular imaging, i.e. to image intravascular molecular changes associated with cardiovascular diseases or cancer [5, 47]. With the current knowledge that targeted microbubbles induce sonoporation (Chapter 6), you have a dual therapeutic bubble that can be used to diagnose and treat a disease.

10.1.3. Incorporation of drugs into microbubbles

The advantage of using microbubbles as drug carriers is a local triggered release of the drug at the site of disease [4-7], thereby making it possible to reduce administered drug dosages. In **Chapter 7** we describe and characterise a novel polymer microcapsule for drug delivery of lipophilic drugs. The aim was to design a microbubble that could incorporate a higher payload than previously reported by others. This was done by incorporating an oil reservoir inside the microcapsule and thus replacing part of the gas core. A remaining gas core of just 10% of the microcapsule was shown to still leave the microcapsules responsive to ultrasound. Even though these novel oil-filled microcapsules have a higher drug carrier reservoir compared to bubbles that have drugs incorporated in their shell [48] or lipid-coated bubbles that have an oil-reservoir [49, 50], the limiting factor will be the amount of bubbles that is currently allowed per examination. At the moment the amount of microbubbles that are typically injected in humans are ~ 1×10^{9} – 1×10^{10} microbubbles per examination [51]. This corresponds to ~ 8 – 80 µl of gas [37] and thus this will be the maximum amount of drug carrier reservoir. Hopefully higher amounts will be allowed for drug-loaded microbubbles. In the mean time, novel approaches to increase the drug carrier reservoir of microbubbles even further are under development and include for example attaching liposomes to the bubbles [52]. Although the drug payload of therapeutic bubbles is a concern, therapeutic efficacy of therapeutic bubbles is undoubtedly present. For the oil-filled microcapsules we designed and describe in Chapter 7, therapeutic efficacy is shown in **Chapter 8**. In a preliminary study, tumours treated with paclitaxel-containing microcapsules in the presence of ultrasound showed a marked slower tumour growth compared to the tumours not treated with ultrasound. Even though this was a preliminary study, the potential to treat tumours is shown.

10.1.4. In vitro research therapeutic bubbles

All *in vitro* research performed within this thesis on therapeutic bubbles was done with endothelial cells. We specifically chose endothelial cells because ultrasound contrast agents

are blood pool agents [2, 36, 37] and therefore will only be able to come into contact with cells within a vessel, i.e. endothelial cells and circulating blood cells. However, to the best of our knowledge, the amount of papers published on therapeutic efficacy of bubbles that use endothelial cells for their *in vitro* studies is sadly very limited, namely ten [17, 24, 29, 53-59]. This does not include the six studies described in Chapter 2-6 and 8 of this thesis or studies including targeted bubbles. These ten studies are described in Table 10.2. All focus on co-administration of a lipid or protein-coated microbubble and a drug or gene. Even though all these studies were done using endothelial cells, it is still difficult to compare these studies because of the differences in ultrasound parameters, used microbubbles, and type of endothelial cells. Nonetheless, several of these studies have reported interesting bio-effects of ultrasound and microbubble treatment, such as the displacement of the cell membrane, an increase in intracellular calcium ions, $[Ca^{2+}]_i$, and $[H_2O_2]_i$, and disruption of cell-cell interaction (Table 10.2, column results).

A tremendous amount more articles have been published using non-endothelial cells as the *in vitro* model. Although these studies will certainly aid to our understanding of the therapeutic efficacy of therapeutic bubbles, other cells will by no means be able to mimic an endothelial cell as endothelial cells are highly specialised cells. They are able to withstand pressures and shear stresses, are able to respond to changes in blood pressures, maintain the vascular barrier and play a key role in maintaining vascular homeostasis [60-62].

10.1.5. Bubble behaviour

For both co-administration and bubble-based drug delivery systems, ultrasound is needed to trigger drug delivery. In an ultrasound field, bubbles start to vibrate, emitting a very specific signal containing nonlinear and harmonic components [2, 36, 37]. In fact, it is the vibration of the bubbles in response to ultrasound that triggers drug delivery. Triggering of drug delivery is preferably done using diagnostic ultrasound [63]. Bubbles vibrate most prominent around their resonance frequency [64]. The size of commercially available microbubbles is 1 – 10 µm in diameter [36, 37]. Microbubbles of this size happened to have a resonance frequency within the range of frequencies (1 – 10 MHz) used for medical ultrasound imaging from outside the body [64, 65]. For cardiac imaging, ultrasound of 2.5 MHz is often used and is widely available on current ultrasound machines [66]. This is the reason why within this thesis ultrasound frequencies between 1.0 and 2.5 MHz were used. In addition, ultrasound of ~ 1 – 2.5 MHz can penetrate deep into the body allowing optimal insonification of even the deeper structures [67].

Table 10.2: Overview of *in vitro* experiments on endothelial cells with therapeutic bubbles. All studies are on co-administration. PAEC = pig aortic endothelial cell; HUVEC = human umbilical vein endothelial cell; bEnd.3 = immortalized mouse brain capillary endotheel cell; HAEC = human aortic endothelial cell; BAEC = bovine aortic endothelial cell; BEC = bovine endothelial cell; LDH = lactate dehydrogenase; SEM = scanning electron microscopy.

Cell	Aim study	Ultrasound settings	Results	1st author + Ref.
PAEC	SonoVue-cell interaction	1 MHz 0.9 MPa 6 cycles 6 µsec	Deformation of cell membrane up to 2.3 µm.	Van Wamel [55]
HUVEC	Intra- and inter-cellular bioeffects SonoVue	1 MHz 0.1 MPa 0.2% duty cycle 20 Hz burst 10 sec	- $[Ca^{2+}]_i$ ↑ (significantly blocked by catalase, an extracellular H_2O_2 scavenger - $[H_2O_2]_i$ ↑ - protein nitrosylation ↑ - F-actin: rearrangement and stress fibers ↑ - disruption cell-cell interaction (restored by 30 min)	Juffermans [17]
bEnd.3	Effects ultrasound-stimulated Definity	1.25 MHz 0.24 MPa 10 cycles 8 µs	Cells adjacent to bubble: - $[Ca^{2+}']_i$ changes with and without PI uptake - $[Ca^{2+}']_i$ changes 2× larger in cells with PI uptake Cells near sonoporated cell (no bubble): - delayed $[Ca^{2+}']_i$ changes, no PI uptake	Park [58]
HUVEC	Disintegration cells by Levovist	1.8 MHz 0.5-2.1 MPa 3 min	Gap formation at highest P_, increasing with higher microbubble concen-trations.	Nixdorff [56]
HUVEC	Mechanism interaction Definitiy and cells	2.25 MHz 0.6 MPa Continuous or 10 µs burst at 75 ms interval 1 – 5 min	For continuous US: - disruption monolayer - 0.6 fold decreased TEER - 5.7 fold increased permeability albumin - no difference between 1 or 5 min treatment - 52% reduction of cell viability For pulsed US: no changes	Soman [57]
BEC	Mechanism membrane damage and repair by Levovist	1 MHz 1.1 MPa 3 cycles 3 µsec	- micron-sized membrane perforations (SEM) - liquid microjet production of bubbles - Ca^{2+} dependent and independent resealing mechanism - 25% cell damage and 16% (60% of damaged cells) resealed within 5 sec.	Kudo [24]
HAEC	Gene therapy of Optison + luciferase plasmid	MHz not specified 2.5 W/cm^2 (~0.2 MPa) 8× 1 min	- small pores (size not specified) in cell surface (restored by 24 hr) - no toxicity (LDH activity) - 8000-fold increase luciferase activity than plasmid alone	Taniyama [29]
HUVEC#	Effects of cellular uptake and delivery of drugs/genes with SonoVue	0.02 MHz 3.77 W/m^2 (~0.2 MPa) 10% duty cycle 6 sec	- EGFP gene transfection efficiency 0.2-2% - TO-PRO(R)-1 maximum delivery efficiency 34% - 70 kDa dextran maximum delivery efficiency 0.5% - lower migration ability	Yang [59]
HUVEC#	Gene therapy of lipid-coated microbubbles + luciferase plasmid	2 MHz 2.5 W/cm^2 (~0.2 MPa) 50% duty cycle 2 Hz burst 10 sec	about 1000-fold increase luciferease activity than plasmid and ultrasound	Suzuki [53]
BAEC	Optimisation gene therapy of SonoVue + luciferase and EGFP plasmid	1 + 2 MHz 0.33 MPa 1000-10,000 cycles 20 Hz burst 30-120 sec	optimal settings were 1 MHz, 20 µg/ml plasmid, 3111 cycles for 30 sec; this gave 3-fold increase of number of transfected cells and 1.7-fold level of transgene expression per cell	Meijering [54]

cells treated in suspension

The interaction between microbubbles and the ultrasound field is already complex [68]. It becomes even more complex for the interplay between the therapeutic agent, microbubble characteristics and target tissue. As pointed out well by the review by Pua and Zhong about ultrasound-mediated drug delivery [7], the multitude of cell models, ultrasound systems, and experimental environments has made the organization and acquired knowledge of therapeutic effects by bubbles difficult. Microbubble behaviour is key to the therapeutic effect. The behaviour of microbubbles in an ultrasound field is being studied by several investigators [69-71], both experimentally as well as by modelling [72-74]. Within an ultrasound field, the reported experimentally observed high differences in responses of similar sized microbubbles cannot be explained by the models [75, 76]. Heterogeneous coating properties have been suggested to be the underlying cause. One of these properties is the microbubble shell viscosity. Until now, viscosity was mostly studied dynamically using a set-up of vibrating microbubbles in an ultrasound field [77, 78]. In **Chapter 9** we describe a novel method to determine the bubble shell viscosity of non-vibrating bubbles. This method is based on fluorescence recovery after photobleaching (FRAP). This chapter is a good example of where biology meets physics as techniques already used for decades in biology [79] were used to elucidate a physical parameter of the lipid microbubble coating. The experimentally determined viscosity of the microbubble coating of this preliminary study could change the way microbubble behaviour is described and modelled in the sense that it will more closely resemble the actual viscosity of the bubbles. This will both aid our understanding of microbubble behaviour and ultimately understand what kind of ultrasound parameters will give the microbubble behaviour we desire for drug delivery.

10.1.6. Safety of therapeutic bubbles

Currently available microbubbles for diagnostic imaging have passed numerous stringent safety tests. Although serious adverse events are rare, they do occur (1/10,000). Most of these are allergic reactions to the microbubble components. In the USA alone, about two million examinations have been done using microbubbles for cardiac studies. The mortality rate is 1/500,000 which is far lower than for example the mortality rate of 1/1,000 for coronary angiography [2].

When introducing a new drug or novel drug delivery approach, safety remains paramount. On top of the safety of the drug and microbubble components of the UCA-based drug delivery system, the effects induced by insonification also need to be taken into account [2]. The induction of an increased endothelial cell membrane for co-administration is not always reversible and can lead to cell death or even rupture of capillaries [80-82]. When treating a tumour this may not be such an unwanted side-effect. However, for the treatment of atherosclerosis this will be a severely unwanted side-effect. The risk of plaque rupture is higher when there are more neovessels in the plaque because these neovessels are fragile and red blood cells are leaking out which increase the lipid pool of the plaque [83]. Disrupting these neovessels by vibrating microbubbles will increase the red blood cell leakiness even

more and could further increase the risk of plaque rupture causing severe side-effects such as myocardial infarction or stroke [83]. It is therefore paramount that bubble treatment for atherosclerosis does not lead to rupture of capillaries.

When using drug-loaded bubbles the fate of the bubbles also has to be taken into consideration. Bubble circulation times are about 5 minutes [84, 85]. By then, most of the bubbles are cleared by the reticuloendothelial system (RES) [86, 87]. The RES is comprised of monocytes, mobile macrophages, fixed tissue macrophages, and a few specialised endothelial cells in the bone marrow, spleen and lymph nodes [35]. When highly toxic drugs are incorporated into bubbles, the drugs will undergo the same fate as the bubbles after administration and thus are also cleared by the RES. Toxicity to these cells has to be considered.

10.2 Conclusion and future

In this thesis therapeutic bubbles were evaluated. Both classes of therapeutic bubbles were studied, namely co-administration of a drug and a bubble, and bubbles in which a drug was incorporated in the bubble. Co-administration is associated with an increased cell membrane permeability and / or endothelial layer permeability so that the co-injected drug will be delivered more into the cell or tissue. From the studies described in this thesis we have taken steps forward in understanding the mechanism involved. Not only answers but also more questions were raised. The described studies will definitely form a stepping stone for further studies to fully elucidate the mechanism. A complete understanding of the mechanism will give us more control to tune the bioeffects that are needed to increase drug uptake by cells and / or tissue. Within this thesis a new polymeric therapeutic bubble was also produced and characterised for local drug delivery of lipophilic drugs. Therapeutic potential was shown *in vivo*. These polymeric bubbles also showed potential for co-administration *in vitro*.

The design and/or mechanism of action of therapeutic bubbles remains complex. It is therefore not that simple to go from an already clinically approved bubble to a clinically approved therapeutic bubble. Although the number of articles that demonstrate feasibility of therapeutic microbubbles in animals keeps on increasing, many technical and pharmaceutical issues still have to be resolved before microbubble-mediated treatments in humans will become widely available [37]. At the moment there are already a few trials with therapeutic bubbles in the clinic. An example is the Sonolysis study [88] which is a multicenter, randomised, placebo controlled clinical trial. The effect of ultrasound in combination with a clinically approved bubble in enhancing the effectiveness of thrombolytic agents in patients with ST-elevation myocardial infarction is studied. This could well become the golden standard for treatment of myocardial infarction in the distant future. Ultrasound machines are become smaller and smaller [89] and it likely that treatment can already be given by ambulance personal with a small hand-held ultrasound machine. The sooner the coronary arteries will be unblocked, the better which is also reflected in the phrase “time is muscle” [90] that cardiologists use.

Therapeutic efficacy of drug-loaded bubbles for the treatment of cancer is likely to increase if multiple treatments can be given. Instead of having to come back to the hospital for repeated intravenous administration of the therapeutic bubbles and application of ultrasound, devices could be designed that would not make this necessary anymore. A device that is surgically implanted and gives off a specific dose of therapeutic bubbles would be ideal. If this device can still be accessed minimally invasive, it can be refilled with new therapeutic bubbles so treatment can be given for longer periods of time. A specifically designed miniature ultrasound machine would make it possible for patients to do the treatment at home after a training period. The importance of the ultrasound being applied to the area where drug delivery is needed could be addressed with a brace or vest that is tailored for each patient. This may well be justified for the treatment of cancer.

Cinical trials are underway for molecular imaging using targeted bubbles. The pre-clinically used targeted bubbles to which ligands were conjugated via biotin-(strept)avidin bridging had to be replaced by a conjugation without the use of (strept)avidin because this is associated with immunogenicity [91]. A Phase 0 trial is currently running for BR55 for molecular imaging of prostate cancer. Phase 0 trials are conducted early in the development process of novel therapeutics and are designed to assist the go versus no-go process of the fate of the studied therapeutic [92]. BR55 is a lipid-coated microbubble designed to target the vascular endothelial growth factor receptor 2 (VEGFR2). The bubble is manufactured by Bracco Suisse SA and a peptide that recognises the VEGFR2 is covalently linked to the lipids that form the coating of the microbubble. Pre-clinical molecular imaging efficiency for BR55 was recently shown in a rat-tumour model [93]. In the clinical, the use of BR55 for the detection of prostate cancer is expected to fill a much needed gap in the detection of prostate cancer. Currently, the disease is confirmed based on biopsies that are taken randomly and hence there is a high risk that the tumour will be missed [94].

Targeted bubbles will certainly be very powerful in the diagnosis of for example cancer or atherosclerosis when specific biomarkers are found that are more disease specific. These specific biomarkers are needed because at the moment the adherence of for example a P-selectin targeted microbubble can indicate inflammation [95], ischemia [96], atherosclerosis [97], or cancer [98].

So what makes a bubble a good therapeutic bubble that can outcompete other imaging modalities and drug delivery systems? *The* therapeutic bubble most likely does not exist. In the future, hospital pharmacies are expected to have a stock of several different therapeutic bubbles, ranging from bubbles purely for diagnostic imaging to drug-loaded bubbles. When someone for example is expected to have cancer, molecular imaging bubbles will be used to confirm this after which therapy can straight away be started with drug-loaded bubbles or co-administration of a bubble with a drug. The choice of the drug-loaded bubble versus co-administration of a bubble with a drug will be the result of clinical trials in which the two types are compared for treatment of types of cancer. During the course of treatment the molecular imaging bubbles will be used to monitor the progress of the treatment.

In the future therapeutic bubbles deserve a strong place in the treatment of diseases like cancer, stroke and myocardial infarction that are in the top 10 of leading causes of death in the western world. For now, therapeutic bubbles are excitingly vibrant and bursting of great potential!

References

[1] R. Gramiak, P.M. Shah, Echocardiography of the aortic root. Invest. Radiol. 3(5) (1968) 356-366.

[2] D. Cosgrove, C. Harvey, Clinical uses of microbubbles in diagnosis and treatment. Med. Biol. Eng. Comput. 47(8) (2009) 813-826.

[3] K.M.D. Tachibana, S.M.D.P. Tachibana, Albumin Microbubble Echo-Contrast Material as an Enhancer for Ultrasound Accelerated Thrombolysis. Circulation 92(5) (1995) 1148-1150.

[4] M.R. Böhmer, A.L. Klibanov, K. Tiemann, C.S. Hall, H. Gruell, O.C. Steinbach, Ultrasound triggered image-guided drug delivery. Eur. J. Radiol. 70(2) (2009) 242-253.

[5] M. Schneider, Molecular imaging and ultrasound-assisted drug delivery. J. Endourol. 22(4) (2008) 795-802.

[6] S. Hernot, A.L. Klibanov, Microbubbles in ultrasound-triggered drug and gene delivery. Adv. Drug Deliver. Rev. 60(10) (2008) 1153-1166.

[7] E.C. Pua, P. Zhong, Ultrasound-mediated drug delivery. IEEE Eng. Med. Biol. 28(1) (2009) 64-75.

[8] E.C. Unger, T. McCreery, R. Sweitzer, G. Vielhauer, G. Wu, D. Shen, D. Yellowhair, MRX 501: a novel ultrasound contrast agent with therapeutic properties. Acad. Radiol. 5 Suppl 1 (1998) S247-249.

[9] R. Bekeredjian, P.A. Grayburn, R.V. Shohet, Use of ultrasound contrast agents for gene or drug delivery in cardiovascular medicine. J. Am. Coll. Cardiol. 45(3) (2005) 329-335.

[10] K. Ferrara, R. Pollard, M. Borden, Ultrasound microbubble contrast agents: fundamentals and application to gene and drug delivery. Annu. Rev. Biomed. Eng. 9 (2007) 415-447.

[11] W.J. Greenleaf, M.E. Bolander, G. Sarkar, M.B. Goldring, J.F. Greenleaf, Artificial cavitation nuclei significantly enhance acoustically induced cell transfection. Ultrasound Med. Biol. 24(4) (1998) 587-595.

[12] C.B. Walton, R.V. Shohet, Tiny bubbles and endocytosis? Circ. Res. 104(5) (2009) 563-565.

[13] T. Sundqvist, S.M. Liu, Hydrogen peroxide stimulates endocytosis in cultured bovine aortic endothelial cells. Acta Physiol. Scand. 149(2) (1993) 127-131.

[14] P.E. MacDonald, L. Eliasson, P. Rorsman, Calcium increases endocytotic vesicle size and accelerates membrane fission in insulin-secreting INS-1 cells. J. Cell Sci. 118(Pt 24) (2005) 5911-5920.

[15] J. Saliez, C. Bouzin, G. Rath, P. Ghisdal, F. Desjardins, R. Rezzani, L.F. Rodella, J. Vriens, B. Nilius, O. Feron, J.L. Balligand, C. Dessy, Role of caveolar compartmentation in endothelium-derived hyperpolarizing factor-mediated relaxation: Ca2+ signals and gap junction function are regulated by caveolin in endothelial cells. Circulation 117(8) (2008) 1065-1074.

[16] Z. Fan, R.E. Kumon, J. Park, C.X. Deng, Intracellular delivery and calcium transients generated in sonoporation facilitated by microbubbles. J. Control. Release 142(1) (2010) 31-39.

[17] L.J. Juffermans, A. van Dijk, C.A. Jongenelen, B. Drukarch, A. Reijerkerk, H.E. de Vries, O. Kamp, R.J. Musters, Ultrasound and microbubble-induced intra- and intercellular bioeffects in primary endothelial cells. Ultrasound Med. Biol. 35(11) (2009) 1917-1927.

[18] L.J. Juffermans, P.A. Dijkmans, R.J. Musters, C.A. Visser, O. Kamp, Transient permeabilization of cell membranes by ultrasound-exposed microbubbles is related to formation of hydrogen peroxide. Am. J. Physiol. Heart Circ. Physiol. 291(4) (2006) H1595-1601.

[19] T.A. Tran, J.Y. Le Guennec, P. Bougnoux, F. Tranquart, A. Bouakaz, Characterization of cell membrane response to ultrasound activated microbubbles. IEEE T. Ultrason. Ferr. 55(1) (2008) 44-49.
[20] L.J. Juffermans, O. Kamp, P.A. Dijkmans, C.A. Visser, R.J. Musters, Low-intensity ultrasound-exposed microbubbles provoke local hyperpolarization of the cell membrane via activation of BK(Ca) channels. Ultrasound Med. Biol. 34(3) (2008) 502-508.
[21] M. Duvshani-Eshet, M. Machluf, Therapeutic ultrasound optimization for gene delivery: a key factor achieving nuclear DNA localization. J. Control. Release 108(2-3) (2005) 513-528.
[22] M. Duvshani-Eshet, L. Baruch, E. Kesselman, E. Shimoni, M. Machluf, Therapeutic ultrasound-mediated DNA to cell and nucleus: bioeffects revealed by confocal and atomic force microscopy. Gene Ther. 13(2) (2006) 163-172.
[23] S. Mehier-Humbert, T. Bettinger, F. Yan, R.H. Guy, Plasma membrane poration induced by ultrasound exposure: Implication for drug delivery. J. Control. Release 104(1) (2005) 213-222.
[24] N. Kudo, K. Okada, K. Yamamoto, Sonoporation by Single-Shot Pulsed Ultrasound with Microbubbles Adjacent to Cells. Biophys. J. 96(12) (2009) 4866-4876.
[25] Y. Qiu, Y. Luo, Y. Zhang, W. Cui, D. Zhang, J. Wu, J. Zhang, J. Tu, The correlation between acoustic cavitation and sonoporation involved in ultrasound-mediated DNA transfection with polyethylenimine (PEI) in vitro. J. Control. Release 145(1) (2010) 40-48.
[26] F. Yang, N. Gu, D. Chen, X. Xi, D. Zhang, Y. Li, J. Wu, Experimental study on cell self-sealing during sonoporation. J. Control. Release 131(3) (2008) 205-210.
[27] Y.Z. Zhao, Y.K. Luo, H.D. Liang, X.G. Mei, J. Tang, C.T. Lu, Y. Zhang, Q. Lin, Comparing transfection efficiency and safety for antisense oligodeoxyribonucleotide between phospholipids-based microbubbles and liposomes. J. Drug Target. 14(10) (2006) 687-693.
[28] Y.Z. Zhao, Y.K. Luo, C.T. Lu, J.F. Xu, J. Tang, M. Zhang, Y. Zhang, H.D. Liang, Phospholipids-based microbubbles sonoporation pore size and reseal of cell membrane cultured in vitro. J. Drug Target. 16(1) (2008) 18-25.
[29] Y. Taniyama, K. Tachibana, K. Hiraoka, T. Namba, K. Yamasaki, N. Hashiya, M. Aoki, T. Ogihara, K. Yasufumi, R. Morishita, Local delivery of plasmid DNA into rat carotid artery using ultrasound. Circulation 105(10) (2002) 1233-1239.
[30] M. Duvshani-Eshet, D. Adam, M. Machluf, The effects of albumin-coated microbubbles in DNA delivery mediated by therapeutic ultrasound. J. Control. Release 112(2) (2006) 156-166.
[31] K.G. Birukov, Cyclic stretch, reactive oxygen species, and vascular remodeling. Antioxid. Redox Signal. 11(7) (2009) 1651-1667.
[32] M. Ushio-Fukai, R.S. Frey, T. Fukai, A.B. Malik, Free Radical Effects on Membranes, Vol. 61, Elsevier Academic Press Inc, San Diego (2008) pp. 147-189.
[33] P.F. Davies, Flow-mediated endothelial mechanotransduction. Physiol. Rev. 75(3) (1995) 519-560.
[34] B. Nilius, G. Droogmans, R. Wondergem, Transient receptor potential channels in endothelium: solving the calcium entry puzzle? Endothelium 10(1) (2003) 5-15.
[35] A.C. Guyton, J.E. Hall, Medical Physiology, Elsevier Saunders, London (2006).
[36] J.M. Correas, O. Helenon, L. Pourcelot, J.F. Moreau, Ultrasound contrast agents. Examples of blood pool agents. Acta Radiol. Suppl. 412 (1997) 101-112.
[37] C. Greis, Ultrasound contrast agents as markers of vascularity and microcirculation. Clin. Hemorheol. Microcirc. 43(1) (2009) 1-9.
[38] P. Hauff, S. Seemann, R. Reszka, M. Schultze-Mosgau, M. Reinhardt, T. Buzasi, T. Plath, S. Rosewicz, M. Schirner, Evaluation of gas-filled microparticles and sonoporation as gene delivery system: feasibility study in rodent tumor models. Radiology 236(2) (2005) 572-578.
[39] M.R. Böhmer, C.H.T. Chlon, B.I. Raju, C.T. Chin, T. Shevchenko, A.L. Klibanov, Focused ultrasound and microbubbles for enhanced extravasation. J. Control. Release 148(1) (2010) 18-24.
[40] R. Karshafian, P.D. Bevan, R. Williams, S. Samac, P.N. Burns, Sonoporation by ultrasound-activated microbubble contrast agents: effect of acoustic exposure parameters on cell membrane permeability and cell viability. Ultrasound Med. Biol. 35(5) (2009) 847-860.

[41] Y. Zhou, J.M. Cui, C.X. Deng, Dynamics of sonoporation correlated with acoustic cavitation activities. Biophys. J. 94(7) (2008) L51-L53.
[42] M.M. Forbes, R.L. Steinberg, W.D. O'Brien, Jr., Examination of inertial cavitation of Optison in producing sonoporation of chinese hamster ovary cells. Ultrasound Med. Biol. 34(12) (2008) 2009-2018.
[43] D.M. Hallow, A.D. Mahajan, T.E. McCutchen, M.R. Prausnitz, Measurement and correlation of acoustic cavitation with cellular bioeffects. Ultrasound Med. Biol. 32(7) (2006) 1111-1122.
[44] C.X. Deng, F. Sieling, H. Pan, J. Cui, Ultrasound-induced cell membrane porosity. Ultrasound Med. Biol. 30(4) (2004) 519-526.
[45] L.M. Kornmann, K.D. Reesink, R.S. Reneman, A.P. Hoeks, Critical appraisal of targeted ultrasound contrast agents for molecular imaging in large arteries. Ultrasound Med. Biol. 36(2) (2010) 181-191.
[46] A.L. Klibanov, M.S. Hughes, J.N. Marsh, C.S. Hall, J.G. Miller, J.H. Wible, G.H. Brandenburger, Targeting of ultrasound contrast material. An in vitro feasibility study. Acta Radiol. Suppl. 412 (1997) 113-120.
[47] J.R. Lindner, Molecular imaging of cardiovascular disease with contrast-enhanced ultrasonography. Nat. Rev. Cardiol. 6(7) (2009) 475-481.
[48] J.R. Eisenbrey, P. Huang, J. Hsu, M.A. Wheatley, Ultrasound triggered cell death in vitro with doxorubicin loaded poly lactic-acid contrast agents. Ultrasonics 49(8) (2009) 628-633.
[49] E.C. Unger, T.P. McCreery, R.H. Sweitzer, V.E. Caldwell, Y. Wu, Acoustically active lipospheres containing paclitaxel: a new therapeutic ultrasound contrast agent. Invest. Radiol. 33(12) (1998) 886-892.
[50] M.S. Tartis, J. McCallan, A.F.H. Lum, R. LaBell, S.M. Stieger, T.O. Matsunaga, K.W. Ferrara, Therapeutic effects of paclitaxel-containing ultrasound contrast agents. Ultrasound Med. Biol. 32(11) (2006) 1771-1780.
[51] K.W. Ferrara, M.A. Borden, H. Zhang, Lipid-Shelled Vehicles: Engineering for Ultrasound Molecular Imaging and Drug Delivery. Accounts Chem. Res. 42(7) (2009) 881-892.
[52] I. Lentacker, B. Geers, J. Demeester, S.C. De Smedt, N.N. Sanders, Design and Evaluation of Doxorubicin-containing Microbubbles for Ultrasound-triggered Doxorubicin Delivery: Cytotoxicity and Mechanisms Involved. Mol. Ther. 18(1) (2010) 101-108.
[53] R. Suzuki, T. Takizawa, Y. Negishi, N. Utoguchi, K. Maruyama, Effective gene delivery with liposomal bubbles and ultrasound as novel non-viral system. J. Drug Target. 15(7-8) (2007) 531-537.
[54] B.D.M. Meijering, R.H. Henning, W.H. Van Gilst, I. Gavrilovic, A. Van Wamel, L.E. Deelman, Optimization of ultrasound and microbubbles targeted gene delivery to cultured primary endothelial cells. J. Drug Target. 15(10) (2007) 664-671.
[55] A. van Wamel, A. Bouakaz, M. Versluis, N. de Jong, Micromanipulation of endothelial cells: ultrasound-microbubble-cell interaction. Ultrasound Med. Biol. 30(9) (2004) 1255-1258.
[56] U. Nixdorff, A. Schmidt, T. Morant, N. Stilianakis, J.U. Voigt, F.A. Flachskampf, W.G. Daniel, C.D. Garlichs, Dose-dependent disintegration of human endothelial monolayers by contrast echocardiography. Life Sci. 77(13) (2005) 1493-1501.
[57] N.R. Soman, J.N. Marsh, M.S. Hughes, G.M. Lanza, S.A. Wickline, Acoustic activation of targeted liquid perfluorocarbon nanoparticles does not compromise endothelial integrity. IEEE T. Nanobiosci. 5(2) (2006) 69-75.
[58] J. Park, Z. Fan, R.E. Kumon, M.E. El-Sayed, C.X. Deng, Modulation of intracellular Ca2+ concentration in brain microvascular endothelial cells in vitro by acoustic cavitation. Ultrasound Med. Biol. 36(7) (2010) 1176-1187.
[59] H. Yang, Z.H. Liu, Y.Y. Liu, C.C. Lou, Z.L. Ren, H. Miyoshi, Vascular gene transfer and drug delivery in vitro using low-frequency ultrasound and microbubbles. Acta Pharm. Sinica 31(4) (2010) 515-522.
[60] A.A. Quyyumi, Endothelial function in health and disease: new insights into the genesis of cardiovascular disease. Am. J. Med. 105(1A) (1998) 32S-39S.

[61] H. Lum, A.B. Malik, Regulation of vascular endothelial barrier function. Am. J. Physiol. 267(3 Pt 1) (1994) L223-241.
[62] D. Mehta, A.B. Malik, Signaling mechanisms regulating endothelial permeability. Physiol. Rev. 86(1) (2006) 279-367.
[63] S.B. Barnett, F. Duck, M. Ziskin, Recommendations on the safe use of ultrasound contrast agents. Ultrasound Med. Biol. 33(2) (2007) 173-174.
[64] T.G. Leighton, The acoustic bubble, Academic Press, London (1994).
[65] T. Wagai, Studies on the foundation and development of diagnostic ultrasound. P. Jap. Acac. B-Phys. 83(8) (2007) 256-265.
[66] J.D. Kasprzak, B. Paelinck, F.J. Ten Cate, W.B. Vletter, N. de Jong, D. Poldermans, A. Elhendy, A. Bouakaz, J.R. Roelandt, Comparison of native and contrast-enhanced harmonic echocardiography for visualization of left ventricular endocardial border. Am. J. Cardiol. 83(2) (1999) 211-217.
[67] R.S.C. Cobbold, Foundations of biomedical ultrasound, Oxford University Press, New York (2007).
[68] J.M. Tsutsui, F. Xie, R.T. Porter, The use of microbubbles to target drug delivery. Cardiovasc. Ultrasound 2(1) (2004) 23.
[69] E. Stride, Physical principles of microbubbles for ultrasound imaging and therapy. Cerebrovasc. Dis. 27 Suppl 2 (2009) 1-13.
[70] N. de Jong, M. Emmer, A. van Wamel, M. Versluis, Ultrasonic characterization of ultrasound contrast agents. Med. Biol. Eng. Comput. 47(8) (2009) 861-873.
[71] S. Qin, C.F. Caskey, K.W. Ferrara, Ultrasound contrast microbubbles in imaging and therapy: physical principles and engineering. Phys. Med. Biol. 54(6) (2009) R27-57.
[72] P. Marmottant, S. van der Meer, M. Emmer, M. Versluis, N. de Jong, S. Hilgenfeldt, D. Lohse, A model for large amplitude oscillations of coated bubbles accounting for buckling and rupture. J. Acoust. Soc. Am. 118(6) (2005) 3499-3505.
[73] E. Stride, The influence of surface adsorption on microbubble dynamics. Phil. Trans. R. Soc. A 366 (2008) 2103-2115.
[74] A.A. Doinikov, J.F. Haac, P.A. Dayton, Modeling of nonlinear viscous stress in encapsulating shells of lipid-coated contrast agent microbubbles. Ultrasonics 49(2) (2009) 269-275.
[75] M. Emmer, The onset of bubble vibration. PhD thesis, Erasmus MC, Biomedical Engineering (Thoraxcenter), Rotterdam, the Netherlands (2009).
[76] T. Faez, M. Emmer, M. Doctor, J. Sijl, M. Versluis, N. de Jong, Subharmonic spectroscopy of ultrasound contrast agents. IEEE Ultrasonics Symposium Proceedings, 2010.
[77] S.M. van der Meer, B. Dollet, M.M. Voormolen, C.T. Chin, A. Bouakaz, N. de Jong, M. Versluis, D. Lohse, Microbubble spectroscopy of ultrasound contrast agents. J. Acoust. Soc. Am. 121(1) (2007) 648-656.
[78] J. Tu, J.F. Guan, Y.Y. Qiu, T.J. Matula, Estimating the shell parameters of SonoVue® microbubbles using light scattering. J. Acoust. Soc. Am. 126(6) (2009) 2954-2962.
[79] M.E. van Royen, P. Farla, K.A. Mattern, B. Geverts, J. Trapman, A.B. Houtsmuller, Fluorescence Recovery After Photobleaching (FRAP) to Study Nuclear Protein Dynamics in Living Cells. Methods Mol. Biol. 464 (2009) 363-385.
[80] H.D. Liang, J. Tang, M. Halliwell, Sonoporation, drug delivery, and gene therapy. Proc. Inst. Mech. Eng. 224(2) (2010) 343-361.
[81] D.L. Miller, J. Quddus, Diagnostic ultrasound activation of contrast agent gas bodies induces capillary rupture in mice. Proc. Natl. Acad. Sci. USA 97(18) (2000) 10179-10184.
[82] S.M. Stieger, C.F. Caskey, R.H. Adamson, S. Qin, F.R. Curry, E.R. Wisner, K.W. Ferrara, Enhancement of vascular permeability with low-frequency contrast-enhanced ultrasound in the chorioallantoic membrane model. Radiology 243(1) (2007) 112-121.
[83] R. Virmani, F.D. Kolodgie, A.P. Burke, A.V. Finn, H.K. Gold, T.N. Tulenko, S.P. Wrenn, J. Narula, Atherosclerotic plaque progression and vulnerability to rupture: angiogenesis as a source of intraplaque hemorrhage. Arterioscl. Thromb. Vas. 25(10) (2005) 2054-2061.
[84] M. Schneider, Characteristics of SonoVue (TM). Echocardiogr.-J. Card. 16(7) (1999) 743-746.

[85] S. Kaul, Myocardial contrast echocardiography: a 25-year retrospective. Circulation 118(3) (2008) 291-308.
[86] J.M. Anderson, M.S. Shive, Biodegradation and biocompatibility of PLA and PLGA microspheres. Adv. Drug Deliver. Rev. 28(1) (1997) 5-24.
[87] J.A. Straub, D.E. Chickering, T.G. Hartman, C.A. Gloff, H. Bernstein, AI-700 pharmacokinetics, tissue distribution and exhaled elimination kinetics in rats. Int. J. Pharm. 328(1) (2007) 35-41.
[88] J. Slikkerveer, P.A. Dijkmans, G.T. Sieswerda, P. Doevendans, A.P.J. van Dijk, F.W.A. Verheugt, T.R. Porter, O. Kamp, Ultrasound enhanced prehospital thrombolysis using microbubbles infusion in patients with acute ST elevation myocardial infarction: Rationale and design of the Sonolysis study. Trials 9 (2008) 7.
[89] A.E. Weyman, Future directions in echocardiography. Rev. Cardiovasc. Med. 10(1) (2009) 4-13.
[90] C.M. Gibson, J.A. de Lemos, E.M. Antman, Time is muscle in primary PCI: the strength of the evidence grows. Eur. Heart J. 25(12) (2004) 1001-1002.
[91] M. Chinol, P. Casalini, M. Maggiolo, S. Canevari, E.S. Omodeo, P. Caliceti, F.M. Veronese, M. Cremonesi, F. Chiolerio, E. Nardone, A.G. Siccardi, G. Paganelli, Biochemical modifications of avidin improve pharmacokinetics and biodistribution, and reduce immunogenicity. Br. J. Cancer 78(2) (1998) 189-197.
[92] P.M. LoRusso, Phase 0 clinical trials: an answer to drug development stagnation? J. Clin. Oncol. 27(16) (2009) 2586-2588.
[93] S. Pochon, I. Tardy, P. Bussat, T. Bettinger, J. Brochot, M. von Wronski, L. Passantino, M. Schneider, BR55: a lipopeptide-based VEGFR2-targeted ultrasound contrast agent for molecular imaging of angiogenesis. Invest. Radiol. 45(2) (2010) 89-95.
[94] N.B. Delongchamps, G.P. Haas, Saturation biopsies for prostate cancer: current uses and future prospects. Nat. Rev. Urol. 6(12) (2009) 645-652.
[95] J.R. Lindner, J. Song, J. Christiansen, A.L. Klibanov, F. Xu, K. Ley, Ultrasound assessment of inflammation and renal tissue injury with microbubbles targeted to P-selectin. Circulation 104(17) (2001) 2107-2112.
[96] F.S. Villanueva, E. Lu, S. Bowry, S. Kilic, E. Tom, J. Wang, J. Gretton, J.J. Pacella, W.R. Wagner, Myocardial ischemic memory imaging with molecular echocardiography. Circulation 115(3) (2007) 345-352.
[97] B.A. Kaufmann, C.L. Carr, J.T. Belcik, A. Xie, Q. Yue, S. Chadderdon, E.S. Caplan, J. Khangura, S. Bullens, S. Bunting, J.R. Lindner, Molecular imaging of the initial inflammatory response in atherosclerosis: implications for early detection of disease. Arterioscl. Thromb. Vas. 30(1) (2010) 54-59.
[98] A. van Wamel, M. Celebi, J.A. Hossack, J.M. Backer, M.V. Backer, K. Ley, N. De Jong, A.L. Klibanov, Molecular mapping of murine tumor vasculature biomarkers using targeted contrast high-frequency ultrasound imaging. European Symposium on Ultrasound Contrast Imaging, Rotterdam, the Netherlands, 2008, pp. 89-90 abstract book.

Summary

The high scattering of gas microbubbles was accidentally discovered in 1968 when agitated saline was injected during an examination. This formed the basis of the current commercially available ultrasound contrast agents. The agents all consist of gas microbubbles (1 – 10 μm) that are coated by either a protein, lipid or polymer. Without them, diagnostic ultrasound imaging of the blood circulation would not be possible because blood is two to three orders of magnitude less echogenic than tissue. Microbubbles are very effective ultrasound scatterers due to their high compressibility. Upon insonification, they start to vibrate as the gas responds to the pressure change of the ultrasound by volume pulsations. Amongst contrast agents for imaging, microbubbles are unique in that the imaging process changes the agent and even destroys it. **Chapter 1** introduces microbubbles for diagnostic imaging, and also the potential to use microbubbles for therapeutic applications. Over the last decades, microbubbles as local drug delivery systems have continued to expand. Generally, two classes of therapeutic bubbles are distinguished. The first class is when drugs and microbubbles are simultaneously applied, also referred to as co-administration. The second class is when a therapeutic is attached to or incorporated into the microbubble. For both co-administration and bubble-based drug delivery systems, ultrasound is needed to trigger drug delivery.

The aim of co-administration is to use ultrasound-activated microbubbles to induce a transient increase in permeability of cell membranes and/or tissues. Although it is already known for several decades that vibrating microbubbles can induce a transient increase in cell membrane permeability, the mechanism was still not known at the start of this thesis. Elucidating this mechanism was one of the aims of this thesis. In the *in vitro* study described in **Chapter 2** we studied whether there was a direct correlation between the vibration of microbubbles and enhanced cell membrane permeability. BR14 microbubbles (lipid-coated microbubbles) were insonified at 1 MHz at a peak negative acoustic pressure of 400 kPa. Propidium iodide was used as a membrane integrity probe. From the optical Brandaris-128 high-speed camera recordings (~ 10 million frames per second) of vibrating microbubbles together with fluorescent recordings of propidium iodide uptake by the cells, we observed a direct correlation between cell deformation by vibrating microbubbles and cell membrane permeability. The membrane permeabilisation lasted for a short period (< 30 seconds) without affecting endothelial cell viability. This study identified that the vibration of microbubbles are crucial for transiently enhancing cell membrane permeability. Since propidium iodide is a small (~ 1 nm) molecule, we also investigated whether larger molecules could be taken up by endothelial cells using vibrating microbubbles. The much larger fluorescent dextrans were chosen as marker drugs. Their uptake in endothelial cells via vibrating microbubbles is described in the *in vitro* study in **Chapter 3**. SonoVue microbubbles (lipid-coated microbubbles) were insonified at 1 MHz at 220 kPa peak negative acoustic pressure. Fluorescence microscopy showed homogeneous distribution of 4.4 and 70-kDa dextrans through the cytosol, and localisation of 155 and 500-kDa dextrans in distinct vesicles. After ATP depletion a reduced uptake of the 4.4-kDa dextran and no uptake of the 500-kDa dextran was observed. Independently inhibiting clathrin- and caveolae-mediated endocytosis, as well

as macropinocytosis significantly decreased intracellular delivery of 4.4 to 500-kDa dextrans. Furthermore, fluorescence microscopy demonstrated co-localisation of dextran vesicles (500-kDa) with caveolin-1 and especially clathrin. In addition to triggering endocytosis, vibrating microbubbles also induced transient pore formation, as demonstrated by the influx of calcium ions and cellular release of pre-loaded dextrans. *In vivo* uptake of 500-kDa dextran into rat femoral artery endothelium was also demonstrated after ultrasound in combination with microbubble treatment. The dextran molecules again localised in vesicles that partially co-localised with caveolin-1 and clathrin. Together, these data indicate that vibrating microbubbles induce transient pore formation, but also an increase in endocytosis. The contribution of endocytosis was found to be dependent on molecular size.

In Chapter 2 and 3 we observed that vibrating microbubbles can be used to induce an enhanced cell membrane permeability and / or induce an increase in endocytosis. This would allow uptake of drugs that have difficulty crossing the endothelial cell membrane. However, there are also several drugs that have difficulty crossing the endothelial cell layer because their extravasation is restricted by the endothelial cells. **Chapter 4** describes *in vitro* experiments to investigate whether vibrating microbubbles could increase the permeability of an endothelial layer in the absence of cell damage. Monolayers of endothelial cells were treated with ultrasound of 1 MHz and 210 kPa peak negative acoustic pressure and the contrast agent BR14. Endothelial layer integrity was assessed by measuring transendothelial electrical resistance (TEER). Ultrasound-activated BR14 significantly decreased TEER by 40.3 ± 3.7 % ($p < 0.01$). After treatment, no cell detachment or damage was observed. In **Chapter 5** the mechanism of increased endothelial layer permeability by ultrasound-activated BR14 microbubbles was investigated. Reported bioeffects of others following ultrasound treatment in combination with a contrast agent are a rise in intracellular calcium ions, $[Ca^{2+}]_i$, and reactive oxygen species (ROS). From mechanotransduction studies it is known that both $[Ca^{2+}]_i$, and ROS can lead to an increase in endothelial layer permeability. The aim of the *in vitro* studies in Chapter 5 was to elucidate whether $[Ca^{2+}]_i$, and ROS are part of the mechanism that leads to an increased endothelial layer permeability following ultrasound and BR14 treatment. Endothelial cells treated with ultrasound-activated BR14 had an increased permeability that lasted up to two hours. Recovery of permeability after two hours was only found when the endothelial cells were preincubated with the $[Ca^{2+}]_i$ chelator BAPTA-AM or the antioxidant BHT. This suggests that both $[Ca^{2+}]_i$ and ROS play an important role in the mechanism of increased permeability following ultrasound in combination with BR14 treatment. The mechanism could therefore involve the activation of signalling mechanisms that induce endothelial layer permeability. This is more likely than an actual opening or disruption of the cell-cell contacts by the vibrating microbubbles as we did not observe such events in the optical studies. In fact, we observed propidium iodide uptake indicating a local increase in cell membrane permeability in line with the study described in Chapter 2.

Lately, a lot of attention has also been on using microbubbles for molecular imaging. Molecular imaging is the visualisation of biological processes at the cellular and molecular level in living systems, with the aim to image molecular changes associated with diseases.

Molecular imaging using ultrasound makes use of targeted microbubbles. In **Chapter 6** we investigated whether these targeted microbubbles could also be used to induce an increase in cell membrane permeability in endothelial cells. Lipid-coated microbubbles were targeted to CD31 and insonified at 1 MHz at low peak negative acoustic pressures of 80 to 200 kPa. Vibration of the targeted microbubbles was recorded with the Brandaris-128 high-speed camera (~ 13 million frames per second). In total, 31 cells were studied that all had one microbubble (1.2 – 4.2 micron in diameter) attached per cell. After insonification at 80 kPa, 30% of the cells (n = 6) had taken up propidium iodide, while this was 20% (n = 1) at 120 kPa and 83% (n = 5) at 200 kPa. Irrespective of used acoustic pressure, uptake of propidium iodide was observed when the relative vibration amplitude of the targeted microbubbles was larger than 0.5. No relationship was found between the position of the microbubble on the cell and an increase in cell membrane permeability. This study shows that targeted microbubbles can also be used to induce an increase in cell membrane permeability, thus making it possible to combine molecular imaging and drug delivery.

Microbubbles can also be used as drug delivery system by attachment to or incorporation of drugs into the microbubbles. Limitations of microbubbles as drug delivery systems were the amount of drug that could be incorporated as well as the efficiency of drug release upon insonification. Producing a novel bubble-based drug delivery system was an important aim during this thesis. **Chapter 7** focuses on the synthesis and characterisation of novel polymeric microcapsules for ultrasound-triggered delivery of lipophilic drugs. Microcapsules with a polymer shell of fluorinated end-capped poly(L-lactic acid) were made through pre-mix membrane emulsification and contained, apart from a gaseous phase, different amounts of hexadecane oil as drug-carrier reservoir. Microcapsule diameters were between 1.22 μm and 1.31 μm. Brandaris-128 high-speed recordings at ~10 million fames per second showed that for low peak negative acoustic pressures of 240 kPa at 1 MHz, microcapsules compressed but remained intact. At higher but still diagnostic peak negative acoustic pressures of 510 kPa, microcapsules cracked, thereby releasing the encapsulated gas and model lipophilic drug. Using conventional ultrasound B-mode imaging at a frequency of 2.5 MHz, a marked enhancement of scatter intensity over a tissue-mimicking phantom was observed for the microcapsules. The half and almost completely oil-filled microcapsules with high drug loads and well-defined acoustic activation thresholds were expected to have great potential for ultrasound-triggered local delivery of lipophilic drugs under ultrasound image-guidance. This potential was studied in **Chapter 8** where murine tumours were treated with half oil-loaded microcapsules loaded with the anti-cancer drug paclitaxel. This drug is commonly used to treat ovarian and breast cancer. Because of its poor water solubility, paclitaxel needs to be administered in a vehicle which itself is toxic. Studies are ongoing to find alternative less toxic formulations for paclitaxel delivery. By incorporating paclitaxel into the oil-reservoir of the pLA-pFO-shelled microcapsules, a vehicle will not be needed anymore and the systemic side effects of paclitaxel are also expected to be markedly reduced since it is incorporated in the microcapsules and will only be released upon application of ultrasound. The *in vivo* tumour growth suppression of paclitaxel-loaded pLA-pFO-shelled microcapsules was studied

in mice. Our preliminary study showed that tumour growth in mice was suppressed after treatment with paclitaxel-loaded microcapsules and ultrasound.

In the *in vitro* study described in Chapter 8 the potential of the polymeric microcapsules to induce an increase in endothelial cell membrane permeability was studied. Upon insonification at 1 MHz and peak negative acoustic pressure of 500 kPa, the microcapsules cracked after which the encapsulated gas escaped. Vibration of the escaped gas microbubbles was recorded with the Brandaris-128 high-speed camera (~ 12 million frames per second). When the relative vibration of the escaped gas microbubble was above 4.0, cell membrane permeability was increased as uptake of the impermeable dye propidium iodide was observed.

The *in vitro* and *in vivo* pilot studies in Chapter 8 show that the polymeric microcapsules have great potential for therapeutic applications as co-administration and local drug delivery of an encapsulated drug and are worth to be investigated further. The microcapsules also offer other options for drug delivery as mixing the pLA-pFO polymer with a biotin-pegylated pLA polymer, gives biotinylated microcapsules. Via avidin-biotin bridging, drug-loaded liposomes can for example be conjugated, similar to what has already been reported for a lipid-coated microbubble. In this respect the polymer microcapsules show promise to be a very diverse microbubble-based drug delivery system.

For both co-administration and bubble-based drug delivery systems, ultrasound is needed to trigger drug delivery. In an ultrasound field, bubbles start to vibrate. It is this vibration of the bubbles in response to ultrasound that actually triggers drug delivery. The interaction between microbubbles and the ultrasound field is complex. The behaviour of lipid-coated microbubbles in an ultrasound field is being studied by several investigators. Besides experimental research, microbubble modelling is also performed. Within an ultrasound field, the reported experimentally observed high differences in responses of similar sized microbubbles cannot be explained by the models. Heterogeneous coating properties have been suggested to be the underlying cause. One of these properties is the microbubble shell viscosity. Until now, viscosity was mostly studied dynamically using a set-up of vibrating microbubbles in an ultrasound field. In **Chapter 9** we describe a novel method to determine the bubble shell viscosity of non-vibrating lipid-coated microbubbles. This method is based on Fluorescence Recovery After Photobleaching (FRAP). The viscosity of the lipid coating was determined by measuring the mobility of the fluorescent lipid using FRAP. We found a surface shear viscosity of 8×10^{-6} kg/s that was independent of the microbubble size. The value of the surface shear viscosity is in line with previously reported values by others which are based on completely different methods using microbubble dynamics. The method described in Chapter 9 can now be used to determine the surface shear viscosity of microbubble coatings of non-vibrating microbubbles and thereby aid the microbubble dynamic studies. In addition, we observed that the lipid distributions in the coating were heterogeneous and varied from microbubble to microbubble.

All *in vitro* research performed within this thesis on therapeutic bubbles was done with endothelial cells. We specifically chose endothelial cells because microbubbles are blood pool agents and therefore will only be in contact with cells within a vessel, i.e. endothelial cells

and circulating blood cells. As described in **Chapter 10**, the amount of papers published on therapeutic efficacy of microbubbles (not including targeted microbubbles) that use endothelial cells for their *in vitro* studies are very limited, namely ten. The multitude of cell models, ultrasound systems, and experimental environments has made the organisation and acquired knowledge difficult. The complex interplay between the therapeutic agent, microbubble characteristics and target tissue has made designing or understanding the actions of a therapeutic bubble challenging. The research described in this thesis aids in understanding how to utilise bubbles for therapy in the most optimal way. However, many technical and pharmaceutical issues still need to be resolved before microbubble-mediated treatments in humans become available. For now, therapeutic bubbles are excitingly vibrant and bursting of great potential!

Nederlandse samenvatting

De eigenschap van gas om effectief ultrageluid te weerkaatsen werd per abuis ontdekt in 1986 middels een zoutinjectie tijdens een echografisch onderzoek. Dit vormde de basis van de tegenwoordig commercieel verkrijgbare ultrageluid contrast middelen. Deze bestaan allemaal uit gasbellen (1 – 10 μm) die een eiwit, lipiden of polymeer coating hebben. Microbellen verbeteren diagnostische ultrageluid beeldvorming van de bloedcirculatie. Zonder deze contrast middelen zou dit niet mogelijk zijn omdat bloed twee tot drie orders minder te zien is met echo dan weefsel. Microbellen zijn erg effectieve ultrageluid weerkaatsers vanwege hun hoge compressibiliteit. Onder invloed van ultrageluid gaan ze vibreren als gevolg van het gas dat reageert op de drukveranderingen van het ultrageluid. Onder de contrastmiddelen zijn microbellen uniek omdat het beeldvormende proces ze verandert en zelfs vernietigd. In **Hoofdstuk 1** worden de microbellen geïntroduceerd voor diagnostiche toepassing, als ook de potentie die ze hebben voor therapeutische toepassingen. Sinds enkele tientallen jaren zijn de mogelijkheden voor het gebruik van microbellen voor het lokaal afgeven van geneesmiddelen enorm gegroeid. Over het algemeen worden er twee typen therapeutische bellen onderscheiden. Bij het eerste type worden geneesmiddelen en microbellen tegelijkertijd apart toegediend. Deze methode wordt ook wel co-administratie genoemd. Bij het tweede type worden geneesmiddelen aan de bel vastgekoppeld of worden ze in de bel geïncorporeerd.

Het doel van co-administratie is het gebruik van ultrageluid-geactiveerde microbellen om een tijdelijke permeabiliteitverhoging te induceren van de cel membraan en / of het weefsel. Hoewel al tientallen jaren bekend is dat vibrerende microbellen een tijdelijke verhoging van de celmembraan kunnen induceren, was het mechanisme waarmee dit gebeurt nog niet bekend bij aanvang van het onderzoek beschreven in dit proefschrift. Het ophelderen van dit mechanisme was één van de doelen van dit proefschrift. In de *in vitro* studie beschreven in **Hoofdstuk 2** bestudeerden we of er een directe relatie was tussen de vibratie van microbellen en een verhoogde celmembraan permeabiliteit. De BR14 microbellen (lipiden-gecoate microbellen) werden geïnsonificeerd bij 1 MHz bij een piek negatieve akoestische druk van 400 kPa. Het model geneesmiddel propidium jodide werd gebruikt om de membraanpermeabiliteit te bepalen. Hoge snelheidsopnamen (~ 10 miljoen beelden per seconde) van vibrerende bellen tegen endotheelcellen werden gecombineerd met fluorescente opnames (20 beelden per seconde) van propidium jodide opname. Hierdoor werd een directe relatie tussen cel deformatie en celmembraan permeabiliteit gevonden. De celmembraan permeabilisatie hield korte tijd aan (< 30 seconden) zonder invloed te hebben op de endotheelcel viabiliteit. We bepaalden dat de vibraties van de microbellen cruciaal zijn bij het tijdelijk verhogen van de celmembraan permeabiliteit. Omdat propidium jodide een klein molekuul is (~ 1 nm), onderzochten we ook of grotere moleculen door endotheelcellen kunnen worden opgenomen door vibrerende microbellen. Hiervoor werden de veel grotere dextraan moleculen gekozen als model geneesmiddelen. Hun opname in endotheelcellen onder invloed van vibrerende bellen is beschreven in de *in vitro* studie in **Hoofdstuk 3**. SonoVue microbellen (lipden-gecoate microbellen) werden gedurende 30 seconden geïnsonificeerd bij 1 MHz en een piek negatief akoestische druk van 220 kPa. Fluorescentie microscopie liet een homogene verdeling van de 4.4 en 70-kDa dextranen zien in het

cytoplasma van de endotheelcellen, terwijl lokalisatie van de 155 en 500-kDa dextranen in blaasjes was. Na ATP depletie was de opname van de 4.4-kDa dextranen verlaagd terwijl er geen opname van de 500-kDa dextran meer was. Onafhankelijke inhibitie van clathrine- en caveolae-gemedieerde endocytose, als ook macropinocytose verlaagde significant de opname van de 4.4 tot 500-kDa dextranen. Driedimensionale microscopie liet zien dat de dextraan blaasjes (500-kDa) deels co-lokaliseerden met caveolin-1 en met name clathrine. Naast een activatie van endocytose, induceerden vibrerende microbellen ook een tijdelijke porie formatie. Porie formatie door ultrageluid en microbellen werd aangetoond door de influx van calcium ionen en het uit de cel vrijkomen van dextranen waarmee de cellen eerder waren opgeladen. *In vivo* opname van 500-kDa dextraan in endotheelcellen van de femoralis slagader van een rat werd ook aangetoond. Net als bij de *in vitro* experimenten, lokaliseerden de dextraan moleculen zich in blaasjes die deels co-lokaliseerden met caveolin-1 en clathrine. Deze data lieten zien dat vibrerende bellen een tijdelijke porie formatie kunnen induceren als ook endocytose kunnen verhogen. De contributie van endocytose bleek afhankelijk te zijn van de grootte van het model geneesmiddel.

In Hoofdstuk 2 en 3 werden vibrerende microbellen gebruikt om een tijdelijke verhoging van de permeabiliteit van de celmembraan van endotheelcellen te induceren. Hierdoor kunnen geneesmiddelen door de cel opgenomen worden die moeite hebben met het passeren van de celmembraan. Er zijn echter ook geneesmiddelen die moeite hebben de endotheel cellaag te passeren omdat de extravasatie van deze geneesmiddelen wordt geblokkeerd door de endotheelcellen. **Hoofdstuk 4** beschrijft *in vitro* experimenten waarin onderzocht werd of vibrerende microbellen de permeabiliteit van een endotheellaag kunnen verhogen zonder celschade aan te richten. Om de mogelijkheid te onderzoeken of het gecontroleerd verhogen van de permeabiliteit van de endotheellaag mogelijk is, werden monolagen van endotheelcellen behandeld met ultrageluid (1 MHz, 210 kPa piek negatieve akoustische druk) en het contrast middel BR14. De permeabiliteit van de endotheellaag werd bepaald door het meten van de transendotheliale elektrische weerstand (TEER). Ultrageluid-geactiveerde BR14 microbellen verlaagden de TEER significant met 40.3 ± 3.7 % ($p < 0.01$). Na behandeling werd geen celschade of het loslaten van cellen waargenomen. In **Hoofdstuk 5** werd het mechanisme verantwoordelijk voor deze verhoogde endotheellaag permeabiliteit onderzocht. De door anderen beschreven bio-effecten van ultrageluid in combinatie met microbellen zijn een verhoging van de calcium concentratie in de cel, $[Ca^{2+}]_i$, en de vorming van reactieve zuurstof deeltjes (ROS). Mechanotransductie studies hebben aangetoond dat zowel $[Ca^{2+}]_i$ en ROS kunnen leiden tot een verhoging van de endotheellaag permeabiliteit. Het doel van de in Hoofdstuk 5 beschreven *in vitro* studies was het bepalen of $[Ca^{2+}]_i$ en ROS deel uitmaken van het mechanisme waarmee ultrageluid-geactiveerde microbellen de endotheellaag permeabiliteit verhogen. Monolagen van endotheelcellen behandeld met ultrageluid-geactiveerde BR14 microbellen hadden een verhoogde endotheellaag permeabiliteit die ten minste 2 uur aanhield. Herstel van de verhoogde permeabiliteit 2 uur na behandeling werd alleen gevonden als de endotheelcellen werden voorbehandeld met de $[Ca^{2+}]_i$ chelator BAPTA-AM of de antioxidant BHT. Dit suggereert dat na een ultrageluid en microbellen

behandeling zowel $[Ca^{2+}]_i$ als ROS een belangrijke rol spelen in het mechanisme van de verhoogde endotheellaag permeabiliteit. Het mechanisme zou dus kunnen bestaan uit het activeren van signaalmechanismen die leiden tot een verhoging van de endotheellaag permeabiliteit. Het activeren van signaalmechanismen is meer waarschijnlijk dan het door de vibrerende microbellen daadwerkelijk openen of verbreken van de cell-cell contacten. In onze optische studies zagen we namelijk dergelijk belgedrag niet. Wel zagen we propidium jodide opname wat een lokaal verhoogde celmembraan permeabiliteit betekent en in overeenstemming is met wat we vonden in de in Hoofdstuk 2 beschreven studie.

Recentelijk is er veel aandacht voor het gebruik van microbellen voor moleculaire beeldvorming. Moleculaire beeldvorming is het visualiseren van biologische processen op het cellulaire en moleculaire niveau in levende organismen met als doel het visualiseren van de moleculaire veranderingen die gepaard gaan met ziektebeelden. Moleculaire beeldvorming met ultrageluid berust op het gebruik van getargete microbellen. In **Hoofdstuk 6** hebben we onderzocht of deze getargete microbellen (lipiden gecoat) ook gebruikt konden worden voor het induceren van een verhoogde celmembraan permeabiliteit in endotheelcellen. Lipiden-gecoate microbellen werden getarget naar CD31 en geïnsonificeerd bij 1 MHz en lage piek negatieve akoestische drukken van 80 tot 200 kPa. De vibraties van de getargete microbellen werden opgenomen met de Brandaris-128 hoge snelheids camera (~ 13 miljoen frames per seconde). In totaal werden 31 cellen onderzocht. Aan alle cellen was één microbel gehecht (1.2 – 4.2 micron in diameter). Na insonificatie bij 80 kPa, hadden 30% van de cellen (n = 6) propidium jodide opgenomen, terwijl dit 20% (n = 1) was bij 120 kPa en 83% (n = 5) bij 200 kPa. Onafhankelijk van de akoestische druk waarbij de microbellen werden geïnsonificeerd, werd opname van propidium jodide alleen gezien wanneer de relatieve vibratie amplitude van de getargete bellen groter was dan 0.5. Er werd geen relatie gevonden tussen de positie van de bel op de cel en de celmembraan permeabiliteitverhoging. Deze studie toont aan dat getargete bellen ook gebruikt kunnen worden voor het verhogen van de celmembraan permeabiliteit, waardoor het dus mogelijk is om moleculaire beeldvorming met geneesmiddelafgifte te combineren.

Microbellen kunnen ook gebruikt worden als geneesmiddel afgifte systeem door geneesmiddelen aan de bel vast te koppelen of in de bel te incorporeren. Tekortkomingen van microbellen als geneesmiddel afgifte systeem waren de hoeveelheid geneesmiddel dat kon worden ingebouwd en de efficiëntie waarmee het geneesmiddel onder invloed van ultrageluid vrij kon komen. Het maken van een nieuw op microbellen gebaseerd geneesmiddel afgifte systeem was een belangrijk doel van dit proefschrift. **Hoofdstuk 7** beschrijft de productie en karakterisatie van een nieuwe microcapsule voor ultrageluid getriggerde afgifte van lipofiele geneesmiddelen. Deze microcapsules met een schil van het polymeer poly(L-melkzuur) met eindstandige fluorgroepen (pLA-pFO) werden gemaakt met een pre-mix membraan emulsificatie techniek. De microcapsules bevatten, afgezien van een gasfase, verschillende hoeveelheden hexadecaan olie dat dient als geneesmiddel reservoir. De microcapsules waren tussen de 1.22 µm en 1.31 µm in diameter. Hoge snelheids opnames (~ 10 miljoen beelden per seconde) lieten zien dat de microcapsules gecomprimeerd werden, maar intact bleven bij

lage akoestische drukken van 240 kPa bij 1 MHz. Bij hogere, maar nog steeds diagnostiche drukken van 510 kPa, braken de microcapsules waarbij het geëncapsuleerde gas en model lipofiele geneesmiddel vrijkwamen. Met conventioneel ultrageluid B-mode beeldvorming bij een frequentie van 2.5 MHz lieten de microcapsules een beduidend hogere weerkaatsing van het ultrageluid zien ten op zichten van een weefsel-imiterend fantoom. De half en bijna geheel olie-gevulde microcapsules met hoge geneesmiddel capaciteiten en goed gedefinieerde akoestische activatie drempels hebben grote potententie voor ultrageluid-geactiveerde lokale afgifte van lipofiele geneesmiddelen. Daarbij komt nog dat de therapie te volgen is met ultrageluidbeeldvorming omdat de microcapsules ook een ultrageluid contrastmiddel zijn. Deze potentie was verder gedemonstreerd in **Hoofdstuk 8** waarin muizen met tumoren werden behandeld met de half olie-gevulde microcapsules. Het geïncorporeerde anti-tumor geneesmiddel was het lipofiele paclitaxel, een geneesmiddel dat vaak gebruikt wordt in de behandeling van eierstok- en borstkanker. Vanwege de slechte wateroplosbaarheid van paclitaxel, moet het worden toegediend in een oplosmiddel dat van zichzelf als toxisch is. Er zijn verschillende studies gaande naar het vinden van minder toxische manieren om paclitaxel toe te dienen. Door paclitaxel te incorporeren in het olie-reservoir van de pLA-pFO microcapsules zal een oplosmiddel niet meer nodig zijn. De verwachting is ook dat de systemische bijwerkingen van paclitaxel minder zullen zijn doordat paclitaxel verpakt zit in de microcapsules en alleen vrij zal komen door middel van ultrageluid. Suppressie van *in vivo* tumor groei met paclitaxel-geladen microcapsules werd onderzocht in muizen. Onze initiële studie toonde aan dat de tumor groei onderdrukt werd na behandeling met paclitaxel-geladen microcapsules en ultrageluid.

In de *in vitro* studie in Hoofdstuk 8 werd onderzocht of de pLA-pFO microcapsules geschikt zijn om een verhoging van de celmembraan permeabiliteit te induceren. De microcapsules gingen kapot bij ultrageluid van 1 MHz en 500 kPa piek negatieve akoestische druk. De vibratie van het vrijgekomen geëncapsuleerde gas werd opgenomen met de Brandaris-128 hoge snelheidscamera (~ 12 miljoen beelden per seconde). Als de relatieve vibratie amplitude van het vrijgekomen gasbelletje groter was dan 4.0, dan werd opname van het model geneesmiddel propidium jodide waargenomen wat een verhoging van de celmembraan permeabiliteit betekent.

De initiële *in vitro* en *in vivo* studies beschreven in Hoofdstuk 8 tonen aan dat de pLA-pFO microcapsules potentie hebben voor therapeutische toepassingen als co-administratie en lokale geneesmiddel afgifte van een geëncapsuleerd geneesmiddel. Ze verdienen het daarom om verder onderzocht te worden. De microcapsules bieden ook andere therapeutische mogelijkheden aangezien het pLA-pFO polymeer gemixt kan worden met een gebiotinyleerd pLA polymeer waardoor gebiotinyleerde microcapsules gemaakt kunnen worden. Via de linker avidine kunnen bijvoorbeeld geneesmiddel-geladen gebiotinyleerde liposomen aan de microcapsules worden gekoppeld, net als al beschreven is voor lipiden-gecoate microbellen. Vanwege deze veelzijdigheid, hebben de pLA-pFO microcapsules de potentie om een erg divers microbel-gebaseerd geneesmiddel afgifte systeem te zijn.

Voor zowel co-administratie als microbel-gebaseerde geneesmiddel afgifte systemen is ultrageluid nodig voor het bewerkstelligen van geneesmiddel afgifte. Microbellen gaan vibreren in een ultrageluid veld. Het is eigenlijk deze vibratie van de bellen als respons op het ultrageluid dat zorgt voor geneesmiddel afgifte. De interactie tussen microbellen en het ultrageluid veld is complex. Het gedrag van lipiden-gecoate microbellen in een ultrageluid veld wordt door verschillende onderzoekers onderzocht. Naast experimenteel onderzoek, wordt belgedrag ook gemodelleerd. De huidige modellen kunnen echter niet verklaren waarom bellen van gelijke grootte heel verschillend reageren in een ultrageluid veld. Er wordt gedacht dat niet-homogene coating eigenschappen hieraan ten grondslag liggen. Eén van die eigenschappen is de viscositeit van de coating. Tot nu toe werd de viscositeit voornamelijk bepaald aan de hand van het gedrag van vibrerende bellen in een ultrageluid veld. In **Hoofdstuk 9** beschrijven we een nieuwe methode om de viscositeit van de coating van niet-vibrerende bellen te bepalen. Deze methode is gebaseerd op fluorescentie herstel na photobleken (FRAP). De viscositeit van de lipiden coating werd bepaald door het meten van de mobiliteit van een fluorescent lipide door middel van FRAP. We vonden een viscositeit van 3×10^{-6} kg/s. Deze waarde is in overeenstemming met eerder gepubliceerde waarden van anderen die gebaseerd zijn op compleet verschillende methodes, gebruik makend van de microbel dynamiek. De methode beschreven in Hoofdstuk 9 kan vanaf nu worden toegepast voor het bepalen van de viscositeit van de coating van niet-vibrerende bellen en zo bijdragen aan belgedrag studies. Tevens observeerden wij bij alle bestudeerde microbellen een niet-homogene lipiden distributie die varieerde van bel tot bel. Dit duidt op een niet-uniforme lipiden verdeling in de belcoating.

Al het *in vitro* onderzoek dat in dit proefschrift is beschreven over therapeutische efficientie van microbellen werd gedaan met endotheelcellen. Hiervoor werd bewust gekozen aangezien microbellen bloed compartiment middelen zijn. Ze zullen daarom alleen in contact komen met cellen in een vat, zoals endotheelcellen en circulerende bloedcellen. Zoals beschreven in **Hoofdstuk 10**, is het aantal artikelen dat gepubliceerd is over de therapeutische effectiviteit van microbellen (hierbij de getargete microbellen niet meegerekend) erg gelimiteerd, namelijk tien. Het veelvoud aan cel modellen, ultrageluid systemen, en experimentele condities heeft de organisatie van de opgedane kennis bemoeilijkt. Bovenop de complexe interactie tussen geneesmiddelen, microbellen en het weefsel van bestemming, is de interactie tussen microbellen en het ultrageluid veld ook complex. Het bewerkstelligen en het begrijpen van de werking van therapeutische bellen is daarom niet simpel. Het onderzoek beschreven in dit proefschrift draagt bij aan het begrip hoe therapeutische microbellen optimaal gebruikt kunnen worden. Veel technische en farmaceutische vraagstukken zullen echter nog moeten worden opgelost eer microbel-gemedieerde behandelingen voor mensen beschikbaar kunnen komen. Voor alsnog zitten therapeutische bellen barstensvol potentie!

Dankwoord

Van iedereen hoor ik altijd dat het dankwoord het laatste is dat je schrijft van al je proefschrift hoofdstukken. Het klopt helemaal. Het betekent ook dat mijn aio-periode er nu echt bijna op zit, iets dat ik op een bepaald moment niet meer voor mogelijk achtte. Erop terug kijkende kan ik alleen maar zeggen dat ik een fantastische tijd gehad heb.

Het begon allemaal met mijn sollicitatie in december 2004. Nico en Ton, jullie weten nog niet half hoe dankbaar ik ben dat jullie mij de biologische aio-positie gaven binnen het BURST project. Er komt namelijk niet iedere dag iemand rollend op gesprek. Tijdens mijn aio-periode heb ik heel veel van jullie geleerd en jullie begeleiding heb ik zeer gewaardeerd. Ik kan me geen betere promotoren voorstellen! Nico, ik snap nu dat jij je “hele leven” al onderzoek doet naar belletjes. Ik hoop dat dit voor mij ook is weggelegd. Bedankt ook voor je praktische hulp bij de Brandaris-experimenten.

Als je de eerste biologische aio binnen de vakgroep bent, dan valt dat nog niet mee. Denk maar aan een opmerking als “een bioloog moet niet aan knoppen van elektrische apparaten zitten” (hè Martijn!). Gelukkig kan ik nu zeggen dat ik afgezien van dat ene moment in mijn derde werkweek geen schade heb aangericht. Ook ik kan/mag nu met elektrische apparaten werken en dat zelfs in combinatie met water.

Dat ik zo’n fantastische tijd heb gehad, heb ik zeker ook te danken aan alle mensen binnen de vakgroep. Ik heb genoten van de sfeer in de vakgroep, zowel tijdens het werk als tijdens de buiten-het-werk activiteiten zoals het labuitje en de congressen. Ik heb mezelf kunnen en mogen zijn, iets dat echt niet overal mogelijk is. Bedankt ook voor het letterlijke duwtje in de rug daar waar het nodig was; velen van jullie zijn hiervoor geslaagd. Graag wil ik een aantal van jullie persoonlijk bedanken.
Marcia en Rik, jullie waren net als ik bellen-aio’s. Jullie promotie zit er al op, nu de mijne nog. Bedankt dat jullie me wegwijs hebben willen maken in de wondere wereld van de bel. Ook heel erg bedankt voor al jullie hulp bij mijn experimenten. Marcia, tijdens jouw aio-periode stonden onze bureaus tegenover elkaar. Ik heb me wat keertjes omgedraaid met de vraag of jij je ook even wilde omdraaien als het weer eens rood werd op mijn computer. Altijd wist jij het dan weer werkend te krijgen. Ook onze gesprekken over niet-werk-dingen waren enorm gezellig. Ik vind het super dat we heel nauw samen hebben gewerkt aan hoofdstuk 9 van mijn proefschrift. Hierdoor is het toch gelukt om samen onderzoek te doen, iets dat we al lang wilden. De verdieping die nu tussen ons in zit, maakt gelukkig niets uit. Marcia, ik vind het super dat jij mijn paranimf wilt zijn.
Miranda, onze tijd bij de vakgroep begon op het zelfde moment. De samenwerking met jou, maar zeker ook de gezellig niet-werk gesprekken heb ik zeer gewaardeerd. Tegenwoordig kunnen we ook katten-verhalen uitwisselen. Vanaf januari zullen we niet meer samen zijn, succes met vinden van iets nieuws.
Annemieke, bedankt dat jij me als bioloog hebt ingewerkt en laten kennis maken met de bellen-cellen wereld. Het ga je goed.
Martijn, Antoinette, Radj, Marijn, Egon, Esther, Alina, Paul, Mirza, Harald, Guillaume M., ook jullie promotie zit er al op en velen van jullie zijn niet meer bij de vakgroep. Bedankt voor de fantastische tijd samen (hierbij de aio-weekenden niet te vergeten) en ook heel erg bedankt dat ik altijd voor ultrageluid vragen bij jullie aan kon kloppen. Paul, jij ook heel erg bedankt voor je inside-promotie-

tips, het koffer-zitten, het beklimmen van bergen, en de fantastische manier waarop jij ultrageluid-dingen kunt uitleggen.
Ali, David, Krista, Telli, and Sandra, good luck with your research and finishing your thesis (jij hopelijk ook Sandra)! Tom, Ying, Ilya, Zeynettin, Verya, Alexander, and Pieter, you have all recently started your PhD-project. I hope you research will go well and you will have a lot of fun doing it as well. Ilya, you remind me of me when I just started. I hope you will find your biological way in the bubble world and I hope I can be to you what others have been to me. Sorry for not being there enough whilst finishing my thesis.
Hans B., Guillaume R., Zeynettin, and Verya, I look forward to working more closely with you on the PARISK project. The subject is close to my heart.
Cees, Frits, Geert, Gerard, Hans V., Jan, Leo, Michiel, Robert, Wim, het onderzoek dat ik heb gedaan zou niets zijn zonder jullie. Ik heb bewondering voor jullie werk van elektriciteit tot computerprogramma tot ontwerp tot datgene maken wat in iemands zit. Bedankt! Robert, jij ook heel erg bedankt voor de fijne gesprekken en je altijd helpende hand.
Kim, werken op het lab is met jou erbij altijd gezellig. Bedankt daarvoor en ook voor je helpende hand.
Een afdeling kan niet zonder secretariaat. Mieke, Riekje, Monique, Marianne, Anja, Gracia, jullie vorm(d)en het secretariaat. Mieke, ik heb bewondering hoe jij je hart en ziel in de afdeling en het bellencongres stopt. Er is fysiek bewijs dat ik vaak bij je langs ben geweest. Promoveren is met jou aan boord een stuk minder roerig. Bedankt voor alles van de afgelopen jaren. Ik hoop dat je gezondheid en die van je familie jullie niet meer zullen plagen. Riekje, bedankt dat jij letterlijk deuren voor me open hebt gemaakt.

Aan de andere kant van het land (Enschede) wil ik graag Michel, Benjamin, Marlies, Anne en Erik bedanken. Mijn samenwerking met jullie begon in het BURST-project. Marlies (en Anne), we waren heel dichtbij het combineren van ons beider onderzoek. Jammer genoeg was één celexperiment net niet genoeg, maar hopelijk wel een springplank voor verder onderzoek. Erik, jij veel succes met je fluorescerende aio-periode.

Hassan, Jos en Karin, jullie vormden de Wageningse tak van het BURST-team. Bedankt voor de fijne samenwerking. Jullie hebben ook het contact gelegd met Leonard zodat we dichtheidsmetingen op de “BURST-microcapsules” konden doen. Leonard en Harry, bedankt voor de hulp bij de metingen en de analyse ervan. Yul, good luck with your PhD thesis research.

Ceciel, Marcel, Suzanne, jullie vormden onder andere de Eindhovense tak van het BURST-team. Wat hebben jullie een bellen gemaakt die ik allemaal weer kapot mocht maken. Bedankt voor de heel fijne samenwerking! Nu werken we weer fijn samen, maar dan in het Sonodrugs project.

Sasha, it is always a joy to talk to you about bubbles. Thank you for learning us how to make our own bubbles.

Lynda en Bernadet, jullie waren net zo onbekend met bellen als ik toen we met onze aio-projecten begonnen. Samen hebben we veel geleerd. Lynda, ik kijk uit naar het samen verder gaan met bel-cel experimenten. Bedankt ook voor al je promotie-tips en het lekker samen kletsen over bellen.

Het OIC wil ik bedanken voor het gebruik van de microscopen. Adriaan en Gert, de hulp bij en interesse in mijn onderzoek heb ik zeer gewaardeerd. Ik vind het super dat we jullie eigen onderzoekstechnieken hebben kunnen combineren met de bellen. Alex, Martin, Martijn, jullie bedankt voor de hulp daarbij. Ik kan bijna niet wachten om met jullie hulp verder te gaan met FRAPpen en 4Pi-en.

Geerten en Victor, bedankt voor jullie interesse in en bijdrage aan het bel-cel onderzoek. Ik kijk uit naar een verdere samenwerking met jullie.

Op de 23ste zitten meerdere afdelingen waar ik ook vaak te vinden was. Zo heb ik heel wat emmertjes water in vloeibare, dan wel vaste vorm bij de afdeling Eperimentele Cardiologie gehaald (om maar niet te zwijgen van al die andere dingen). Iedereen van de Cardio wil ik bedanken voor de gastvrijheid, het altijd klaar staan met raad en daad en de gezellige gesprekken. In het bijzonder wil ik daarbij André, Caroline, Dennie, Elza, Esther, Lau, Liz, Marcel, Martine, Remco, Rob, Stefan en Vincent noemen. Een aantal jullie heb ik zelfs met het TEER-virus kunnen besmetten. Voor diegenen die nog aan het promoveren zijn: heel veel succes! Marcel, Stefan en alle studenten van de Cardio wil ik in het bijzonder bedanken voor de supertijd in het celkweeklab.
Een andere afdeling op de 23ste is de Radiologie. Monique, bedankt voor je presentatie van mijn poster in Montreal. Gaby en Sandra, ook jullie bedankt voor de supertijd in het celkweeklab. Ik hoop dat er mooie dingen uit het gezamenlijke project gaan komen.
Ann en Timo, onze ontmoeting begon met mijn zoektocht naar een fluorescentie-meter op de 1ste verdieping. Sindsdien kan ik altijd bij jullie terecht voor endotheelcelvragen en vele andere dingen. Bedankt daarvoor. Ann, heel veel succes nog in Münster!

Paul, bedankt dat ik ook altijd welkom was op de 24ste bij de afdeling Klinische Genetica. De fluorescentie- en absorbantiemetingen zijn dan wel niet in het proefschrift terecht gekomen, maar ze hebben wel veel opgeleverd.

Goran, onze auto's hebben tijdens onze aio-periodes meer van elkaar gezien dan wij van elkaar. Als we elkaar tegen kwamen, waren de gesprekken superfijn. Ik heb bewondering hoe jij als onderzoeker bent. Veel succes voor je verdere loopbaan.

Aukje, Cobie, Debora, Femke, Leo, Petra, wat heb ik jullie verwaarloosd de afgelopen tijd. Bedankt voor jullie begrip. Ik ga het na mijn promotie goedmaken! Cobie, bedankt dat jouw apotheek model mocht staan voor mijn proefschrift.

Anne, al meerdere jaren vormen wij samen een danspaar. Daarnaast zijn we ook goede vriendinnen geworden. Er is niets fijner dan met jou over de vloer te zwieren. Eén van de hoogtepunten was in 2008 toen wij Nederlands Kampioen Latin werden. Tegenwoordig moet je het stellen met jetlegs en een hoofd vol met proefschrift, alhoewel een jetleg wonderen doet voor mijn ballroom-prestaties. Ik hoop nog heel lang samen met jou van het dansen te kunnen genieten. Naast je drukke dansleven heb je de tijd gevonden om de omslag voor mijn proefschrift te maken. Dat was niet gemakkelijk want ik

wist niet zo goed wat ik wilde. Mijn vage ideeën heb je omgezet in een prachtige omslag. Heel, heel veel dank daarvoor.
Peter en Euvgenia, bedankt dat jullie ons dansen op een hoger niveau brengen. Elke les met jullie is een cadeautje. Peter, ook bedankt dat ik bij jou terecht kon voor de stof van mijn jurk.

Lieve Wendy, jij geloofde zo dat ik het ging halen. En nu ben ik er inderdaad bijna. Ook al weet ik dat je altijd in mijn hart zit en bij me bent, ik mis je toch. Dikke knuf.

Meneer Laman, heel erg bedankt dat u tijdens mijn gehele opleiding iedere week weer voor me klaar stond om me letterlijk op de been te houden. Zonder uw gouden handen had ik dit allemaal nooit kunnen doen. Ook bedankt voor uw wijze raad en alle moestuintips. Veel sterkte.

De familie Kooiman wil ik bedanken voor de altijd gezellige familieweekenden en jullie interesse in mijn onderzoek. Ik kijk uit naar het volgende familieweekend!

Tineke en Gerard, jullie zijn een superfijne tante en oom, ook al noem ik jullie nooit zo. Bedankt hiervoor!

Oma, samen met u zijn is altijd gezellig. Bedankt voor uw interesse in en steun bij mijn onderzoek. Ook bedankt voor het begrip dat ik daardoor ook u verwaarloosd heb. Ik heb zin om samen weer eens te gaan frutselen.

Marjo, lieve zus, ik ben er trots op dat jij mijn zusje bent. Ik vind het super dat jij mijn paranimf wilt zijn want ik had echt niet anders gewild na al je steun en begrip van de afgelopen jaren. Samen met je man Michel heb jij ervoor gezorgd dat ik er al een titel bij heb, die van tante. Al voor Lisa geboren was, hebben we samen tussen de schroevendraaiers in een o zo opgeruimd lab (ahum!) al kennis met haar kunnen maken. Een blijvende herinnering daaraan staat in het introductie hoofdstuk van mijn proefschrift. Lisa, jij doet mijn hart smelten en ik kan niet wachten totdat je echt tante Klazina kunt zeggen. Ik hoop met jullie alledrie veel meer tijd te kunnen gaan doorbrengen na mijn promotie want ook jullie heb ik flink verwaarloosd.

Lieve papa en mama, een grote droom van mij gaat uitkomen. Ik kan niet in woorden beschrijven hoe ontzettend dankbaar ik jullie ben dat jullie daaraan zo veel bijgedragen hebben. Jullie hebben er altijd voor gezorgd dat ik een toekomst op kon bouwen. Het maakte niet uit wat ik daarbij op mijn pad tegenkwam. Altijd weer stonden jullie klaar met jullie liefde en steun, ook op de momenten dat ik het niet meer zag zitten. Zelfs jullie bezorgdheid waardeer ik zeer. Sinds twee jaar kan ik ook vol trots zeggen dat jullie mijn buren zijn. Ik draag dan ook graag dit proefschrift aan jullie op want ik weet zeker dat ik dit zonder jullie niet had kunnen volbrengen.

Klazina
Januari 2011

Curriculum vitae (Nederlands)

Klazina Kooiman werd op 5 september 1977 geboren te Dordrecht. In 1995 behaalde ze haar vwo diplima aan het Develstein College te Zwijndrecht waarna ze aan de studie Bio-Farmaceutische Wetenschappen (BFW) aan de Universiteit Leiden begon. Haar afstudeerstage liep ze in 1999-2000 bij de afdeling Farmaceutische Technologie van het Leiden/Amsterdam Center for Drug Research (LACDR) onder begeleiding van Dr. B.I. Florea, Dr. G. Borchard en Prof. Dr. H.E. Junginger. Haar onderzoek richtte zich op het ophelderen van het transportmechanisme van flunisolide (een medicijn gebruikt bij asthma) door humane long epitheelcellen (Calu-3). Dit transport bleek P-glycoproteïne gemedieerd. Met het verslag van deze stage won ze in 2000 de Suzanne Hovinga prijs, een prijs die door de Suzanne Hovinga Stichting ieder studiejaar wordt uitgereikt aan het beste MSc verslag binnen de BFW-studie. Na een korte moleculair biologische stage bij de afdeling Medische Farmacologie van het LACDR onder leiding van Ing. T.G. Schouten en Dr. E. Vreugdenhil, studeerde ze in 2000 *cum laude* af. Aansluitend begon ze als promovenda te werken aan organische anion transporterende eiwitten in de nier bij het Nijmegen Centre for Molecular Life Sciences (NLMS) van het Universitair Medisch Centrum St Radboud. Vanwege de ziekte van Pfeiffer kon zij dit project niet afronden. Van januari 2005 tot december 2010 was zij werkzaam als promovenda bij de afdeling Biomedische Technologie van het Erasmus MC op het project Bubbles for UltRaSound and Therapy (BURST). Het in dit proefschrift beschreven onderzoek is verricht onder leiding van Prof. Dr. Ir. N. de Jong en Prof. Dr. Ir. A.F.W. van der Steen. Per 1 januari 2011 zal zij als postdoc haar onderzoek naar therapeutische bellen voortzetten binnen het Plaque At RISK (PARISK) project. Binnen dit project zal zij zich richten op moleculaire beeldvorming van aderverkalking, een samenwerkingsproject tussen de afdeling Biomedische Technologie van het Erasmus MC en de afdeling Pathologie van het Maastricht UMC. Vanwege een chronische ziekte die ze in haar kinderjaren opliep heeft ze haar stages en promotiewerk parttime gedaan (vier dagen in de week).

Curriculum vitae (English)

Klazina Kooiman was born on September 5th, 1977 in Dordrecht. In 1995 she graduated from Develstein College in Zwijndrecht, after which she started to study Bio-Pharmaceutical Sciences (BPS) at the University of Leiden. From 1999 to 2000, she did her main traineeship at the department of Pharmaceutical Technology of the Leiden/Amsterdam Center for Drug Research (LACDR) under supervision of Dr. B.I. Florea, Dr. G. Borchard and Prof. Dr. H.E. Junginger. Her research topic was to elucidate the transport mechanism of flunisolide, a drug used in asthma treatment, by human lung epithelial cells (Calu-3). The transport proved to be P-glycoprotein mediated. With the thesis of this traineeship she won the Suzanne Hoving prize in 2000, a prize that is awarded to the best MSc thesis within the BPS study each year. After a short molecular biology traineeship at the Department of Medical Pharmacology of the LACDR under the supervision of Ing. T.G. Schouten and Dr. E. Vreugdenhil, she graduated *cum laude* in 2000. Subsequently, she started to work as a PhD student at the Nijmegen Centre for Molecular Life Sciences (NLMS) at the Radboud University Nijmegen Medical Centre. Her project focused on organic anion transport proteins in the kidney. Due to the Epstein Barr virus she could not finish the project. From January 2005 till December 2010 she worked as a PhD student at the Department of Biomedical Technology of the Erasmus MC on the project entitled Bubbles for UltRaSound and Therapy (BURST). The research described in this thesis was performed under the supervision of Prof. Dr. Ir. N. de Jong and Prof. Dr. Ir. A.F.W. van der Steen. Starting January 1st 2011 she will continue her research on therapeutic bubbles as a postdoc within the Plaque At RISK (PARISK) project. Within this project she will focus on molecular imaging of atherosclerosis. This will be a collaboration between the Department of Biomedical Technology of Erasmus MC and the Department of Pathology of Maastricht UMC. Due to an underlying chronic illness since childhood she conducted her traineeships and PhD thesis work parttime (four days a week).

Publications and presentations

Papers in preparation

Kooiman, K., Foppen-Harteveld, M., and de Jong, N., "Sonoporation of endothelial cells by vibrating targeted microbubbles," – submitted.

Emmer, M., Faez, T., **Kooiman, K.**, van der Steen, A.F.W., de Jong, N., "20 years of ultrasound contrast agent modeling," – submitted.

Kooiman, K., van Hinsbergh, V.W.M., van Nieuw Amerongen, G.P., de Jong, N., "Mechanism of increased Endothelial Layer Permeability through Ultrasound-Activated Microbubbles," – in preparation.

Kooiman, K., Emmer, M., Kokhuis, T.J.A., Bosch, J.G., de Gruiter, H.M., van Royen, M.E., van Cappellen, W.A., Houtsmuller, A.B., van der Steen, A.F.W., de Jong, N., "Lipid distribution and viscosity of coated microbubbles," – in preparation.

Peer-reviewed papers

Kooiman, K., Emmer, M., Foppen-Harteveld, M., van Wamel, A., de Jong, N., "Increasing the endothelial layer permeability through ultrasound-activated microbubbles," IEEE Transactions on Biomedical Engineering; 57(1): p. 29-32, 2010.

Kooiman, K., Bohmer, M.R., Emmer, M., Vos, H.J., Chlon, C., Shi, W.T., Hall, C.S., de Winter, S. H., Schroen, K., Versluis, M., de Jong, N., van Wamel, A., "Oil-filled polymer microcapsules for ultrasound-mediated delivery of lipophilic drugs," Journal of Controlled Release; 133 (2): p. 109-118, 2009.

Juffermans, L. J., Meijering, D. B., van Wamel, A., Henning, R. H., **Kooiman, K.**, Emmer, M., de Jong, N., van Gilst, W. H., Musters, R., Paulus, W. J., van Rossum, A. C., Deelman, L. E., Kamp, O., "Ultrasound and microbubble-targeted delivery of therapeutic compounds: ICIN Report Project 49: Drug and gene delivery through ultrasound and microbubbles," Netherlands Heart Journal; 17(2): p. 82-86, 2009.

Meijering, B. D., Juffermans, L. J., van Wamel, A., Henning, R. H., Zuhorn, I. S., Emmer, M., Versteilen, A. M., Paulus, W., van Gilst, W. H., **Kooiman, K.**, de Jong, N., Musters, R. J., Deelman, L. E., Kamp, O., "Ultrasound and Microbubble-Targeted Delivery of Macromolecules Is Regulated by Induction of Endocytosis and Pore Formation,"Circulation Research; 104(5): p. 679-87, 2009.

Van Wamel, A., **Kooiman, K.**, Harteveld, M., Emmer, M., ten Cate, F.J., Versluis, M., de Jong, N., "Vibrating microbubbles poking individual cells: drug transfer into cells via sonoporation," Journal of Controlled Release; 112(2): p. 149-55, 2006.

Florea, B.I., van der Sandt, I.C., Schrier, S.M., **Kooiman, K.**, Deryckere, K., de Boer, A.G., Junginger, H.E., Borchard, G., "Evidence of P-glycoprotein mediated apical to basolateral transport of flunisolide in human broncho-tracheal epithelial cells (Calu-3)," Brithish Journal of Pharmacology; 134(7): p. 1555-63, 2001.

Conference papers

Kooiman, K., Emmer, M., Kokhuis, T.J.A., Bosch, J.G., de Gruiter, H.M., van Royen, M.E., van Cappellen, W.A., Houtsmuller, A.B., van der Steen, A.F.W., de Jong, N., "Lipid distribution and viscosity of coated microbubbles," in proceedings IEEE International Ultrasonics Symposium, San Diego, USA, ref. 10A-3, 2010.

Kooiman, K., Foppen-Harteveld, M., de Jong, N., "Ultrasound-mediated targeted microbubble sonoporation of endothelial cells," European symposium on Controlled Drug Delivery, Egmond aan Zee, the Netherlands, published in Journal of Controlled Release; 148(1): p. e62-e63, 2010.

Gelderblom, E.C., **Kooiman, K.**, Böhmer, M.R., de Jong, N., Lohse, D., Versluis, M., "Ultra high-speed fluorescence imaging of ultrasound contrast agents for imaging and therapy," in proceedings 20th International Congress on Acoustics (ICA), Sydney, Australia, 2010.

Kooiman, K., Foppen-Harteveld, M., de Jong, N., "Sonoporation of endothelial cells with CD31-targeted microbubbles at low acoustic pressures," in proceedings IEEE International Ultrasonics Symposium, Rome, Italy, ref. 1B-1, 2009.

Sugiura, T., **Kooiman, K.**, Emmer, M., Vos, H.J., van Wamel, A., de Jong, N., "Evaluation of the Binding Force between a Biotinylated Microbubble and a Streptavidin-coated Surface by Ultrasound Radiation," in proceedings IEEE International Ultrasonics Symposium, Rome, Italy, ref. P1-B-02, 2009.

Kooiman, K., Böhmer, M.R., Emmer, M., Vos, H.J., Chlon, C., Shi, W.T., Hall, C.S., de Winter, S.H.P.M., Schroën, K., Versluis, M., de Jong, N., van Wamel, A., "Oil-filled polymeric ultrasound contrast agent as local drug delivery system for lipophilic drugs," in proceedings IEEE International Ultrasonics Symposium, Beijing, China, ref. 2D-1, 2008.

Kooiman, K., Böhmer, M.R., Emmer, M., Vos, H.J., Chlon, C., Foppen-Harteveld, M., Versluis, M., de Jong, N., van Wamel, A., "Ultrasound-triggered local release of lipophilic drugs from a novel polymeric ultrasound contrast agent," European symposium on Controlled Drug Delivery, Noordwijk aan Zee, the Netherlands, published in Journal of Controlled Release; 132: p. e41-42, 2008.

Shi, W.T., Böhmer, M.R., van Wamel, A., Celebi, M., Klibanov, A.L., Chin, C.T., Chlon, C., Emmer, M., **Kooiman, K.**, de Jong, N., Hall, C.S., "Ultrasound therapy with drug loaded microcapsules," in proceedings IEEE International Ultrasonics Symposium, New York, USA, ref. 9B-5, 2007.

Böhmer, M.R, Chlon, C., Constant, G., Shi, W.T., Hall, C.S., Schmidt, B., van Wamel, A., **Kooiman, K.**, Emmer, M., de Jong, N., "Polymer-shelled, gas containing capsules for ultrasound mediated drug deliver," in proceedings International congress on acoustics (ICA), Madrid, Spain, ref. ULT-16-004, 2007.

Kooiman, K. , Emmer, M., Harteveld, M., de Jong, N., van Wamel, A., "Ultrasound contrast agent mediated transendothelial drug delivery," in proceedings International Congress on Ultrasonics (ICU), Vienna, Austria, ref. 1400, 2007.

Kooiman, K., Harteveld, M., de Jong, N., van Wamel, A., "Transiently increased endothelial layer permeability by ultrasound-activated microbubbles," in proceedings IEEE International Ultrasonics Symposium, Vancouver, Canada, ref. 1F-6, 2006.

Van Wamel, A., **Kooiman, K.**, Emmer, M. ten Cate, F.J., Versluis, M., de Jong, N., "Ultrasound microbubble induced endothelial cell permeability," European Symposium on Controlled Drug

Delivery, Noordwijk aan Zee, the Netherlands, published in Journal of Controlled Release; 116(2): p. e100-102, 2006.

Oral and poster presentations

(presenter underlined)

Kooiman, K., Foppen-Harteveld, M., van der Steen, A.F.W., Verweij, M., de Jong, N., "Drug uptake by endothelial cells through targeted microbubble sonoporation," oral at 2nd Pan American/Iberian Meeting on Acoustics, Cancun, Mexico, 2010. Abstract published in: Journal of the Acoustical Society of America, 128(4): 2442 (2010).

Kooiman, K., Emmer, M., Kokhuis, T.J.A., Bosch, J.G., de Gruiter, H.M., van Royen, M.E., van Cappellen, W.A., Houtsmuller, A.B., van der Steen, A.F.W., de Jong, N., "Lipid distribution and viscosity of coated microbubbles," oral at 2010 IEEE International Ultrasonics Symposium, San Diego, USA, 2010.

Gelderblom, E.C., **Kooiman, K.**, Böhmer, M.R., de Jong, N., Lohse, D., Versluis, M., "Ultrasound contrast agent dynamics: ultra high-speed fluorescence imaging of shell morphology and local drug release," poster (student finalist) and oral at 2010 IEEE International Ultrasonics Symposium, San Diego, USA, 2010.

ten Cate, F.J., **Kooiman, K.**, "Ultrasound microbubbles: designer therapy," oral at 2010 ICUS Bubble Conference, Chicago, USA, 2010.

Gelderblom, E.C., **Kooiman, K.**, Böhmer, M.R., de Jong, N., Lohse, D., Versluis, M., "Ultra high-speed fluorescence imaging of ultrasound contrast agents for imaging and therapy," oral at 20th International Congress on Acoustics (ICA), Sydney, Australia, 2010.

Kooiman, K., Foppen-Harteveld, M., de Jong, N., "Ultrasound-mediated targeted microbubble sonoporation of endothelial cells," poster at 11th European symposium on Controlled Drug Delivery, Egmond aan Zee, the Netherlands, 2010.

Kooiman, K., Foppen-Harteveld, M., de Jong, N., "Drug uptake by endothelial cells through targeted microbubble sonoporation," oral at 15th European Symposium on Ultrasound Contrast Imaging, Rotterdam, the Netherlands, 2010.

Gelderblom, E.C., **Kooiman, K.**, Böhmer, M.R., de Jong, N., Lohse, D., Versluis, M., "Ultra high-speed fluorescence imaging of ultrasound triggered local drug release," oral at 15th European Symposium on Ultrasound Contrast Imaging, Rotterdam, the Netherlands, 2010.

Gelderblom, E.C., **Kooiman, K.**, Böhmer, M.R., de Jong, N., Lohse, D., Versluis, M., "Ultra high-speed fluorescence imaging," poster at FOMdagen, Veldhoven, the Netherlands, 2010.

Gelderblom, E.C., **Kooiman, K.**, Böhmer, M.R., de Jong, N., Lohse, D., Versluis, M., "Ultra high-speed fluorescence imaging," poster at Burgersdag, Enschede, the Netherlands, 2010.

Kooiman, K., Foppen-Harteveld, M., de Jong, N., "Sonoporation induced drug uptake by endothelial cells with ultrasound and CD31-targeted microbubbles," oral and poster at Vascular Biology PhD course under auspices of the Netherlands Platform for Cardiovascular Research of the Netherlands Heart Foundation, Papendal, the Netherlands, 2009.

Kooiman, K., Foppen-Harteveld, M., ten Cate, F.J., de Jong, N., "New "designer" bubbles," oral at

2009 ICUS Bubble Conference, Chicago, USA, 2009.

Kooiman, K., Foppen-Harteveld, M., Bernsen, M.R., de Jong, N., "Sonoporation induced drug uptake by endothelial cells with ultrasound and CD31-targeted microbubbles," poster at 2009 World Molecular Imaging Congress, Montreal, Canada, 2009.

Sugiura, T., **Kooiman, K.**, Emmer, M., Vos, H.J, Bernsen, M.R., van Wamel, A., de Jong, N., "Binding force of targeted microbubbles measured by ultrasound radiation force," poster at 2009 World Molecular Imaging Congress, Montreal, Canada, 2009.

Kooiman, K., Foppen-Harteveld, M., de Jong, N., "Sonoporation of endothelial cells with CD31-targeted microbubbles at low acoustic pressures," oral at 2009 IEEE International Ultrasonics Symposium, Rome, Italy, 2009.

Sugiura, T., **Kooiman, K.**, Emmer, M., Vos, H.J., van Wamel, A., de Jong, N., "Evaluation of the Binding Force between a Biotinylated Microbubble and a Streptavidin-coated Surface by Ultrasound Radiation," poster at 2009 IEEE International Ultrasonics Symposium, Rome, Italy, 2009.

van Wamel, A., **Kooiman, K.**, de Jong, N., "Ultrasound contrast agents for cardiovascular drug delivery," oral at 14th European Symposium on Ultrasound Contrast Imaging, Rotterdam, the Netherlands, 2009.

Juffermans, L.J.M., Meijering, B.D.M., **Kooiman, K.**, Deelman, L.E., van Gilst, W., van Wamel, A., de Jong, N., Visser, C.A., Musters, R.J.P., Kamp, O., "Targeted delivery of macromolecules using ultrasound and microbubbles is regulated by induction of endocytosis and pore formation," oral at American Heart Association, New Orleans, USA, 2008 (abstract published in *Circulation*, 118:S-643, 2008).

Kooiman, K., Böhmer, M.R., Emmer, M., Vos, H.J., Chlon, C., Shi, W.T., Hall, C.S., de Winter, S.H.P.M., Schroën, K., Versluis, M., de Jong, N., van Wamel, A., "Microcapsules for ultrasound-mediated delivery of lipophilic drugs," oral at workshop Microbubbles for Ultrasound Imaging and Drug Delivery: New Applications with BURSTing Bubbles, Eindhoven, the Netherlands, 2008.

Kooiman, K., Böhmer, M.R., Emmer, M., Vos, H.J., Chlon, C., Shi, W.T., Hall, C.S., de Winter, S.H.P.M., Schroën, K., Versluis, M., de Jong, N., van Wamel, A., "Oil-filled polymeric ultrasound contrast agent as local drug delivery system for lipophilic drugs," oral at 2008 IEEE International Ultrasonics Symposium, Beijing, China, 2008.

Chlon, C., **Kooiman, K.**, van Wamel, A., Shi, W.T, de Jong, N., Böhmer, M.R., "Delivery of a lipophilic model drug with a polymer-shelled ultrasound contrast agent," poster at 6th International Nanomedicine and Drug Delivery Symposium (NanoDDS'08), Toronto, Canada.

van Wamel, A., **Kooiman, K.**, de Jong, N., "Ultrasound contrast agents pushing drug delivery: high speed optical observations," presentation at Acoustics '08 Conference, Paris, France, 2008.

Shi, W.T., Böhmer, M.R., van Wamel, A., Celebi, M., Klibanov, A.L., Chin, C., Emmer, M., **Kooiman, K.**, de Jong, N., Hall, C.S., "Ultrasound therapy with drug loaded microcapsules," oral at Leading Edge Annual Ultrasound Conference 2008, Atlantic City, NJ, USA.

Kooiman, K., Böhmer, M.R., Emmer, M., Vos, H.J., Chlon, C., Foppen-Harteveld, M., Versluis, M., de Jong, N., van Wamel, A., "Ultrasound-triggered local release of lipophilic drugs from a novel polymeric ultrasound contrast agent," poster at 10th European symposium on Controlled Drug Delivery, Noordwijk aan Zee, the Netherlands, 2008.

Juffermans, L.J.M., Meijering, B.D.M., **Kooiman, K.**, Deelman, L.E., van Gilst, W., van Wamel, A., de Jong, N., Visser, C.A., Musters, R.J.P., Kamp, O., , "Enhanced uptake of macromolecules by endothelial cells using ultrasound and microbubbles: mechanisms and bioeffects," poster at International Vascular Biology Meeting, Sydney, Australia, 2008.

Meijering, B.D.M., Juffermans, L.J.M., **Kooiman, K.**, Deelman, L.E., van Gilst, W., Musters, R.J.P., Kamp, O., Visser, C.A., de Jong, N., van Wamel, A., "Mechanisms of delivery of therapeutic compounds by ultrasound and microbubbles," oral at 13th European Symposium on Ultrasound Contrast Imaging, Rotterdam, the Netherlands, 2008.

Kooiman, K., Böhmer, M.R., Emmer, M., Vos, H.J., Chlon, C., Foppen-Harteveld, M., de Jong, N., van Wamel, A., "A new drug delivery system for liphophilic drugs using polymeric ultrasound contrast agents," poster at 13th European Symposium on Ultrasound Contrast Imaging. Rotterdam, the Netherlands, 2008.

Meijering, B.D.M., Juffermans, L.J.M., **K. Kooiman**, Deelman, L.E., van Gilst, W., Musters, R.J.P., Kamp, O., Visser, C.A., de Jong, N., van Wamel, A., "Mechanisms of delivery of therapeutic compounds by ultrasound and microbubbles," poster at Euroecho, Lisbon, Portugal, 2007 (abstract published in *European Journal of Eurechocardiography*, 8:Suppl 1-S202, 2007).

Meijering, B.D.M., Juffermans, L.J.M., **K. Kooiman**, Musters, R.J.P., van Wamel, A., Kamp, O., Henning, R.H., Visser, C.A., van Gilst, W., de Jong, N., Deelman, L.E., "Ultrasound and microbubble targeted delivery of therapeutic compounds; mechanisms and cellular distribution," oral at Farmacologiedagen 2007, Lunteren, the Netherlands, 2007 (abstract published in Naunyn-Schmiedebergs Archives of Pharmacology, 379(2): 207, 2009).

Shi, W.T., Böhmer, M.R., van Wamel, A., Celebi, M., Klibanov, A.L., Chin, C.T., Chlon, C., Emmer, M., **Kooiman, K.**, de Jong, N., Hall, C.S., "Ultrasound therapy with drug loaded microcapsules," oral at 2008 IEEE International Ultrasonics Symposium, New York, USA, 2007.

Böhmer, M.R, Chlon, C., Constant, G., Shi, W.T., Hall, C.S., Schmidt, B., van Wamel, A., **Kooiman, K.**, Emmer, M., de Jong, N., "Polymer-shelled, gas containing capsules for ultrasound mediated drug deliver," oral at 19th International congress on acoustics (ICA), Madrid, Spain, 2007.

Kooiman, K., Emmer, M., Harteveld, M., de Jong, N., van Wamel, A., "Ultrasound contrast agent mediated transendothelial drug delivery," oral at International Congress on Ultrasonics (ICU), Vienna, Austria, 2007.

Meijering, B.D.M., Juffermans, L.J.M, **Kooiman, K.**, Deelman, L.E., van Gilst, W.H., Musters, R.J.P., Kamp, O., Visser, C.A., de Jong, N., van Wamel, A., "Unraveling the mechanisms of ultrasound microbubble targeted gene delivery," poster at 12th European Symposium on Ultrasound Contrast Imaging, Rotterdam, the Netherlands, 2007.

Kooiman, K., Harteveld, M., de Jong, N., van Wamel, A., "Transiently increased endothelial layer permeability by ultrasound-activated microbubbles," oral at 2006 IEEE International Ultrasonics Symposium, Vancouver, Canada, 2006.

Kooiman, K., Harteveld, M., de Jong, N., van Wamel, A., "Drug delivery to extravascular tissue by ultrasound-activated microbubbles," oral and poster at ISTU 2006 International Symposium on Therapeutic Ultrasound, Oxford, United Kingdom, 2006.

Kooiman, K., Harteveld, M., de Jong, N., van Wamel, A., "Regulation of endothelial layer permeability by ultrasound contrast agents," poster at 9th European Symposium on Controlled Drug Delivery, Noordwijk aan Zee, the Netherlands, 2006.

Kooiman, K., Harteveld, M., de Jong, N., van Wamel, A., "Bubbles for therapy: manipulation of endothelial layer permeability," poster at 11th European Symposium on Ultrasound Contrast Imaging, Rotterdam, the Netherlands, 2006.

Academic reports

Kooiman, K., "Therapeutic bubbles," PhD thesis, Erasmus MC, Rotterdam, the Netherlands, 2011.

Kooiman, K., "Elucidation of the transport mechanism of the glucocorticoid Flunisolide in an *in vitro* Calu-3 cell model for the treatment of asthma," M.Sc. thesis, Leiden University, the Netherlands, 2000.

Supervised academic reports

Bons, J., "Characterisation of the transport of organic anions by Oatp3 (*Slc21a7*) in *Xenopus laevis* oocytes," report of traineeship, Radboud University Nijmegen Medical Centre, the Netherlands, 2002.

Schaafsma, G., "Molecular aspects of the renal anion drug transporters, organic anion transporting polypeptides 1 (oatp1, *Slc21a1*) and 3 (oatp3, *Slc21a7*)," report of traineeship, Radboud University Nijmegen Medical Centre, the Netherlands, 2002.

Awards

First prize for best oral presentation during Vascular Biology PhD course under auspices of the Netherlands Platform for Cardiovascular Research of the Netherlands Heart Foundation. Papendal, the Netherlands, 2009 for presentation "Sonoporation induced drug uptake by endothelial cells with ultrasound and CD31-targeted microbubbles".

IEEE Student travel support to IEEE 2008 International Ultrasonics Symposium, Beijing, China.

Martin Blomley poster prize for best clinical poster during 13th European symposium on ultrasound contrast imaging. Rotterdam, the Netherlands, 2008, for poster "A new drug delivery system for liphophilic drugs using polymeric ultrasound contrast agents".

Martin Blomely prize for best student presentation during 7th ISTU International Symposium on Therapeutic Ultrasound, Oxford, United Kingdom, 2006, for presentation "Drug delivery to extravascular tissue by ultrasound-activated microbubbles".

Martin Blomley poster prize for best clinical poster during 11th European Symposium on Ultrasound Contrast Imaging, Rotterdam, the Netherlands, 2006, for poster "Bubbles for therapy: manipulation of endothelial layer permeability".

Suzanne Hovinga prize for best MSc report of Bio-pharmaceutical Sciences study at Leiden University, the Netherlands, 2000.

Erasmus MC
Universitair Medisch Centrum Rotterdam

PhD Portfolio Summary

Summary of PhD training and teaching activities

Name PhD student: Klazina Kooiman Erasmus MC Department: Biomedical Engineering, Thoraxcenter Research School: COEUR	PhD period: 2005-2010 Promotor(s): Prof.dr.ir. N. de Jong Prof.dr.ir. A.F.W. van der Steen Supervisor: Prof.dr.ir. N. de Jong

1. PhD training

	Year	Workload (ECTS)
General academic skills		
- Biomedical English Writing and Communication	2006	3.0
Research skills		
- Biomedical Research Techniques (Molmed)	2008	0.15
- Practical introduction to laser scanning microscopy (OIC)	2005	0.3
In-depth courses		
- Vascular biology (Netherlands Heart Foundation)	2009	1.5
- Peripheral and Intracranial Obstructive Vascular Disease (COEUR)	2009	1.5
- Animal Imaging workshop (AMIE)	2008	0.9
- Summer School Therapeutic Ultrasound (ESPCI, Corsica)	2007	1.5
- Cardiovascular imaging and diagnostics (COEUR)	2006	1.5
- In Vivo Imaging; from Cell to Organism (OIC)	2005	1.5
- Clinical Applications of Diagnostic Ultrasound (IEEE course, Rotterdam, the Netherlands)	2005	0.15
- Ultrasound Contrast Agents: Theory and Experimental Results (IEEE course, Rotterdam, The Netherlands)	2005	0.15
- Cardiovascular medicine (COEUR)	2005	1.5
- Cardiovascular pharmacology (COEUR)	2005	1.5
- Pathophysiology of ischemic heart disease (COEUR)	2005	1.5
- Molecular biology in cardiovascular research (COEUR)	2005	1.5
Presentations		
- IEEE International Ultrasonics Symposium, San Diego, USA (oral)	2010	1.0
- European Symposium on Controlled Drug Delivery, Egmond aan Zee, the Netherlands (poster)	2010	0.5
- European Symposium Ultrasound Contrast Imaging, Rotterdam, the Netherlands (oral)	2010	1.0

- IEEE International Ultrasonics Symposium, Rome, Italy (oral)	2009	1.0
- workshop Microbubbles for Ultrasound Imaging and Drug Delivery: New Applications with BURSTing Bubbles (oral)	2008	1.0
- IEEE International Ultrasonics Symposium, Beijing, China (oral)	2008	1.0
- European Symposium on Controlled Drug Delivery, Noordwijk aan Zee, the Netherlands (poster)	2008	0.5
- European Symposium Ultrasound Contrast Imaging, Rotterdam, The Netherlands (poster)	2008	0.5
- Presentation 'Ultrasound contrast agents for drug delivery' at Department Molecular Cell Biology Center for Electron Microscopy, LUMC, Leiden, the Netherlands.	2008	1.0
- IEEE International Ultrasonics Symposium, Vancouver, Canada (oral)	2006	1.0
- International Symposium on Therapeutic Ultrasound, Oxford, United Kingdom (poster + oral)	2006	1.5
- European Symposium on Controlled Drug Delivery, Noordwijk aan Zee, the Netherlands (poster)	2006	0.5
- European Symposium Ultrasound Contrast Imaging, Rotterdam, the Netherlands (poster)	2006	0.5
International conferences		
- IEEE International Ultrasonics Symposium, San Diego, USA	2010	0.9
- European Symposium on Controlled Drug Delivery, Egmond aan Zee, the Netherlands	2010	0.9
- European Symposium Ultrasound Contrast Imaging, Rotterdam, the Netherlands	2010	0.6
- IEEE International Ultrasonics Symposium, Rome, Italy	2009	0.9
- European Symposium Ultrasound Contrast Imaging, Rotterdam, the Netherlands	2009	0.6
- IEEE International Ultrasonics Symposium, Beijing, China	2008	0.9
- European Symposium on Controlled Drug Delivery, Noordwijk aan Zee, the Netherlands	2008	0.9
- European Symposium Ultrasound Contrast Imaging, Rotterdam, the Netherlands	2008	0.6
- European Symposium Ultrasound Contrast Imaging, Rotterdam, the Netherlands	2007	0.6
- IEEE International Ultrasonics Symposium, Vancouver, Canada	2006	0.9
- International Symposium on Therapeutic Ultrasound, Oxford, United Kingdom	2006	1.2
- European Symposium on Controlled Drug Delivery, Noordwijk aan Zee, the Netherlands	2006	0.9
- European Symposium Ultrasound Contrast Imaging, Rotterdam, the Netherlands	2006	0.6
- IEEE International Ultrasonics Symposium, Rotterdam, the Netherlands	2005	0.9
- European Symposium Ultrasound Contrast Imaging, Rotterdam, the Netherlands	2005	0.6
Seminars and lectures		
- Microbubbles for ultrasound imaging and drug delivery: new applications with bursting bubbles (Eindhoven, The Netherlands)	2008	0.3

- COEUR research seminars:		
- Cardiovascular imaging	2005	0.4
- Hypertension and stroke	2005	0.4
- Atherosclerosis, inflammation and vulnerable plaque	2005	0.4
- COEUR lecture:		
- Physical activity is effective in prevention and treatment of coronary artery disease: role of endothelial phenotype	2008	0.1
2. Teaching activities		
	Year	**Workload (ECTS)**
Lecturing		
- 'Nano-sized probes for ultrasound imaging,' AMIE workshop, Rotterdam, the Netherlands	2008	1.0
- 'Ultrasound molecular imaging: oncology & cardiology applications,' Biomedical Research Techniques Course, Molmed, Rotterdam, the Netherlands	2008	1.0
- 'Application of ultrasound for drug delivery and molecular imaging,' AMIE workshop, Rotterdam, the Netherlands	2008	1.0
Supervising practicals and excursions		
- AMIE workshop demonstrations	2010	0.3
- Brandaris-128 high-speed camera demonstration to students from Delft University of Technology	2009	0.3
- AMIE workshop demonstrations	2009	0.3
	Total	46.65 ECTS

Abbreviations and symbols

3D	3-Dimensional
AAL	acoustically active lipospheres
ATP	adenosine triphosphate
BAEC	Bovine aortic endothelial cell
BEC	Bovine endothelial cell
bpm	Beats per minute
BSA	Bovine serum albumin
BHT	butylated hydroxytoluene
$[Ca^{2+}]_i$	Intracellular calcium concentration
C_3F_8	Perfluoropropane
C_4F_{10}	Perfluorobutane
D	Diffusion coefficient ($m^2\ s^{-1}$)
D	Diameter
D_0	Diameter at resting size
d10	Microcapsule diameters below which 10% of the cumulative amount of microcapsules is found
d50	Microcapsule diameters below which 50% of the cumulative amount of microcapsules is found
d90	microcapsule diameters below which 90% of the cumulative amount of microcapsules is found
Da	Dalton
DAPI	4',6-diamidino-2-phenylindole
dB	Decibel
DCM	Dichloromethane
DLPC	1,2-dilauroyl-*sn*-glycero-3-phosphocholine / 12:0 phosphocholine
D_{max}	Diameter at maximum size
D_{min}	Diameter at minimum size
DMPC	1,2-dimyristoyl(d54)-*sn*-glycero-3-phosphocholine / 14:0 phosphocholine
DMSO	Dimethylsulfoxide
DNA	Deoxyribonucleic acid
DPPC	1,2-dipalmitoyl-*sn*-glycero-3-phosphocholine / 16:0 phosphocholine
DPPG	1,2-dipalmitoyl-*sn*-glycero-3-phospho-(1'-*rac*-glycerol) / 16:0 phosphoglycerol
DPPE	1,2-dipalmitoyl-sn-glycero-3-phosphoethanolamine / 16:0 phosphoethanolamine
DSPC	1,2-distearoyl-*sn*-glycero-3-phosphocholine / 18:0 phosphocholine
DSPE	1,2-distearoyl-sn-glycero-3-phosphoethanolamine / 18:0 phosphoethanolamine
Dt	Diameter-time
EDTA	Ethylenediaminetetraacetic acid
f	Frequency (Herz)
FBS	Fetal bovine serum
FITC	Fluorescein isothiocyanate
FRAP	Fluoresence recovery after photobleaching
GC/MS	Gas chromatography/mass spectrometry
HAEC	Human aortic endothelial cell
HUVEC	Human umbilical vein endothelial cell
Hz	Herz
ICAM-1	Intercellular adhesion molecule 1 / CD54
k	Boltzmann's constant (1.38×10^{-23} J K^{-1})
LDH	Lactate dehydrogenase
M	Molarity
MDSC	Modulated differential scanning calorimetry

MI	Mechanical index; $MI = \frac{P_-}{\sqrt{f}}$ with P_ in MPa and f in MHz
MIF	Mean intensity of fluorescene
MW	Molecular weight
P_	Peak negative acoustic pressure
Pa	Pascal
PAEC	Pig aortic endothelial cell
PBS	Phosphate-buffered saline
PC	Phosphocholine
PECAM-1	Platelet/endothelial cell adhesion molecule-1 / CD31
PEG(2000)	Polyethylene glycol with molecular weight of 2000
PI	Propidium iodide
pLA-pFO	poly(L-lactic acid) terminated with 1H-1H perfluoro-octan-1-ol
PLE	Polar lipid extract
PVA	Poly-vinylalcohol
r	Radius (m)
RES	Reticuloendothelial system
RNA	Ribonucleic acid
ROI	Region of interest
ROS	Reactive oxygen species
RP equation	Rayleigh-Plesset equation
rpm	Rotations per minute
S_c	Completely gas-filled microcapsules
S_{ch}	Half oil-filled microcapsules
SEM	Scanning electron microscopy
SEM	Standard error of the mean
S_h	Almost completely oil-filled microcapsules
SF_6	Sulphur hexafluoride
T	Temperature
TB-BSA	Trypan blue-labelled bovine serum albumin
TEER	Transendothelial electrical resistance
TEM	Transmission electron microscopy
TMP	Tissue-mimicking phantom
TRITC	Tetramethylrhodamine isothiocyanate
U	Unit
UMD	Ultrasound and microbubble treatment
UCA	Ultrasound contrast agent
US	Ultrasound
VEGFR	Vascular endothelial growth factor receptor 2
VCAM-1	Vascular cell adhesion molecule 1
v/v	Volume per volume
w/w	Weight per weight
γ	Euler's constant (0.58)
κ_s	Dilatation viscosity (kg s^{-1})
η_s	Surface shear viscosity (kg s^{-1})
μ	Bulk viscosity (kg m^{-1} s^{-1})
μ_w	Viscosity of embedding liquid (kg m^{-1} s^{-1})
ρ	Density (kg m^{-3})